Alma Mater Studiorum-Università di Bologna

DOTTORATO DI RICERCA IN

CHIMICA

Ciclo 33

Settore Concorsuale: 03/C1 CHIMICA ORGANICA

Settore Scientifico Disciplinare: CHIM/06 – CHIMICA ORGANICA

EXPLORING NEW ASPECTS OF RADICAL MOLECULAR MACHINERY: STUDIES AND PERSPECTIVES IN THE FIELD OF PARAMAGNETIC ARCHITECTURES.

Presentata da: Cecilia Poderi

Coordinatore Dottorato

Domenica Tonelli

Supervisore

Marco Lucarini

Co-supervisore

Elisabetta Mezzina

Esame finale anno 2021

It is not the researcher who pursues the truth, it is the truth that pursues the researcher
(Robert Musil)

Abstract

The challenge of achieving molecular devices able to reproduce the impressive features of biological nano-machines has been attracting the interest of many scientists during the last decades. At present, several examples of artificial molecular machines based on mechanically interlocked molecules (MIMs) have been reported, which are able to perform a wide set of highly complex motions. On the other hand, the increasing complexity of molecular machines designed by scientists requires also new analytical approaches capable to characterize the nanoscale processes affecting these kind of systems. To this aim, the covalent incorporation of stable paramagnetic moieties inside the structure of artificial MIMs enables to use Electronic Paramagnetic Resonance spectroscopy (EPR) for monitoring the dynamics of the target structures. Bis-alkyl nitroxide radicals ($R_2N\text{-}O\bullet$) are an important example of open-shell molecules largely employed in many fields of chemistry and related sciences, but their use in supramolecular assembly chemistry and in molecular machinery remains basically unexplored despite their intrinsic properties. In this scenario, this research focused on the design, synthesis and EPR study of novel supramolecular architectures containing persistent nitroxide groups and employable in the field of radical molecular machines.

The **Chapter 3** of this manuscript describes the design, synthesis and EPR investigation of two novel crown-ether macrocycles containing a persistent nitroxide group into their structure. The reduction kinetics of the compounds were investigated by registering the progressive decay of the nitroxide EPR signal in the presence of glutathione as reductant. The target macrocycles displayed a significantly high resistance against reduction in water, making them good candidates as spin probes employable for biological investigations.

In **Chapter 4** the use of 2-phenyl-2-cyanopropanoic acid as single fuel for promoting the full back and forth cycle of motions of an acid-base switchable nitroxide-labelled rotaxane was investigated. EPR spectroscopy was used to monitor the shuttling process of the paramagnetic ring over the dumbbell, because it allowed to distinguish the two possible co-conformations assumed by the rotaxane. In addition, examining the EPR behaviour of the paramagnetic MIM in the presence of some *para*-substituted derivatives of the fuel, the occurrence of an alternative process preventing the completion of cycle of motions of the rotaxane was detected and studied in detail.

Later on, a research study focusing on the aerobic oxidation of alcohols promoted by a synthetic nitroxide-based macrocycle and its rotaxane derivative was performed, which is illustrated in **Chapter 5**. The aim was to exploit and study the oxidation of the nitroxide group contained in the macrocycle to oxoammonium salt, which catalyze the cycle of aerobic oxidation of alcohols. In this

investigation, EPR studies combined with GC-MS analysis were performed for monitoring the *in situ* oxidation of the nitroxide moiety and for following the evolution of the catalytic cycle of oxidation.

Finally, **Chapter 6** describes the synthesis and EPR investigation of a novel synthetic crown-ether macrocycle containing a stable nitroxide moiety into the structure. Due to the EPR spectral features shown by the new macrocycle forming complexes with alkali, earth-alkali metal and organic cations, significant variations in the spectral parameters (multiplicity and hyperfine constant) were detected comparing the complexed and non-complexed forms. By using EPR spectroscopy and computer simulations, the complexation equilibrium constants (K_a) were calculated up to 160000, thus making possible future applications in metal sensing and in molecular machinery.

INDEX

CHAPTER 1: INTRODUCTION

1.1. FROM MECHANICALLY INTERLOCKED MOLECULES (MIMS) TO MOLECULAR MACHINES

1.1.1 Mechanically Interlocked Molecules (MIMs)

Intermolecular and non-covalent interactions are involved in the most part of biological processes, such as substrate-protein receptor binding, enzymatic reactions, immunological antigen-antibody association and so on. The research field studying such interactions is commonly named *supramolecular chemistry*, and extends over several scientific areas like organic chemistry and synthesis, coordination and recognition chemistry, physical chemical characterization, biochemistry, biology and materials science.[1][2] Donald Cram[3][4] and Jean-Marie Lehn[2] were the first introducing the new field of *chemistry beyond the molecule*, which defines the chemistry of supramolecular entities, referring to it respectively as *host-guest chemistry* and *supramolecular chemistry*. The importance of this research area increased definitely in 2016 with the Nobel Prizes to Sir. James Fraser Stoddart, Ben Feringa and Jeanne-Pierre Sauvage (**Figure 1.1**).

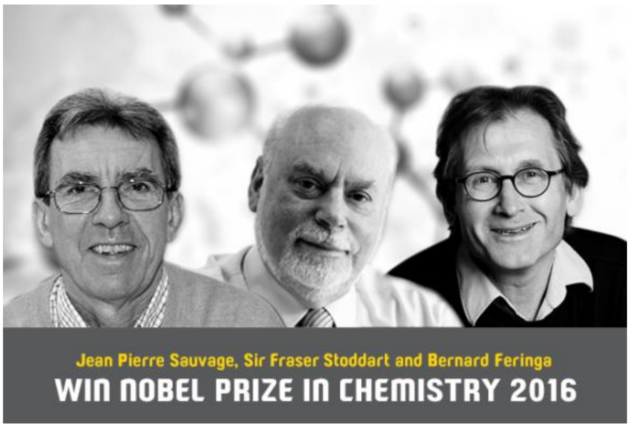

Figure 1.1. Chemistry Nobel prizes for the year 2016.

In the domain of supramolecular world, a new type of chemical interaction emerged, called *mechanical bond.* As well as the chemical bonds are shared between atoms, the *mechanical bond* is formed between a group of atoms or molecular entities, called *component parts*. This physical interaction arises only if the components have a determined topology enabling them to entangle with each other and create a supramolecular interlocked architecture. The stability of the *mechanical bond* derives from the repulsive forces that prevent the intersection of already existing bonds, so that the components cannot be separated without breaking or distorting the existing chemical bonds between the atoms. When two or more molecular entities possess a *mechanical bond*, they are defined as

Mechanically Interlocked Molecules (MIMs). *Mechanostereochemistry* is the scientific field interested in the study of MIMs, which enlarges over several fields of chemical research like supramolecular chemistry and chemical topology (**Figure 1.2**).[5][6][7][8][9]

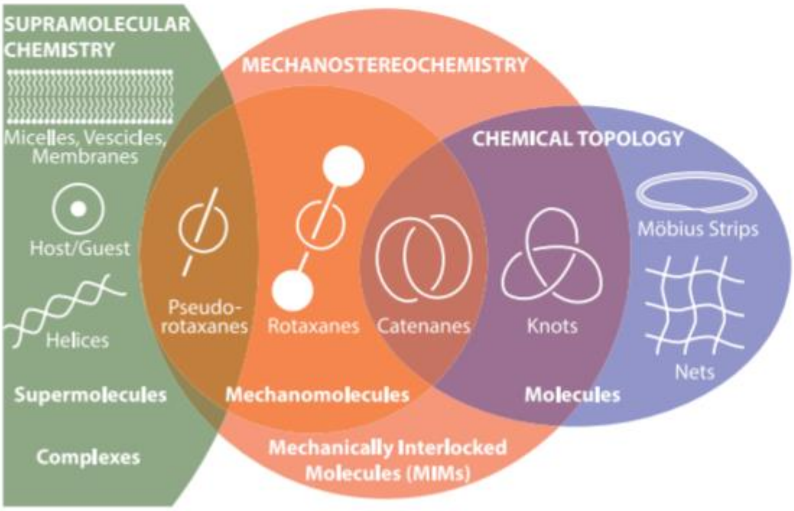

Figure 1.2. Intersecting scientific fields interested by *Mechanostereochemistry*.

The two most relevant examples of MIMs are rotaxanes and catenanes (**Figure 1.3**), which have been discovered in 1960 by Harrison and Wasserman.[10][11[12][13] The name catenane derives from the Latin word, *catena*, which means *chain*, and it is referred to an interlocked molecule involving two or more mechanically linked macrocyclic components (**Figure 1.3a**). Alternatively, a rotaxane consists of an axle component (thread) inserted inside a macrocyclic molecule that is topologically locked thanks to the presence of two bulky groups at the extremities of thread (**Figure 1.3b**).

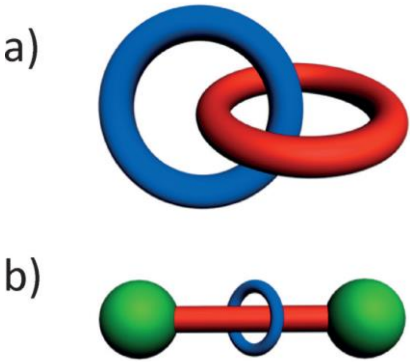

Figure 1.3. Representation of two Mechanically Interlocked Molecules (MIMs): a) Catenane; b) Rotaxane.

1.1.2 Synthesis of MIMs

The discovery of MIMs and of the *mechanical bond* has disclosed a *plethora* of new synthetic methodologies, devoted to the preparation of such highly complex architectures. The synthesis of these compounds requires the perfect intersection between supramolecular chemistry and traditional covalent synthesis, making mechanically interlocked molecules a combination between both supramolecular assemblies and covalently bonded molecules. In order to implement and optimize the synthetic protocols of such substrates, not only a deep knowledge of chemical topology and of the nature of chemical bond, but also the understanding of the fundamental concepts of molecular recognition, self-assembly and all that matters with non-covalent interactions is required.

Nowadays, a wide set of strategies (**Figure 1.4** and **1.5**) is available for the formation of rotaxanes and catenanes. The most part of these synthetic routes starts from a *pseudo-rotaxane* (**Figure 1.4**) precursor, consisting of a self-assembled complex between a pre-formed ring and a linear component.[14] Starting from the *pseudo-rotaxane* precursor, it is possible to achieve a [2]-catenane by *clipping* approach, which consists in a cyclization of the linear component of a *pseudo-rotaxane* over the cyclic molecule, forming two interlocked rings. A second approach, defined as *ring capture*, involves the trapping of a cyclic molecule by a coupling reaction occurring into the cavity of a second pre-formed ring. In this case, the process does not require the formation of a *pseudo-rotaxane*.

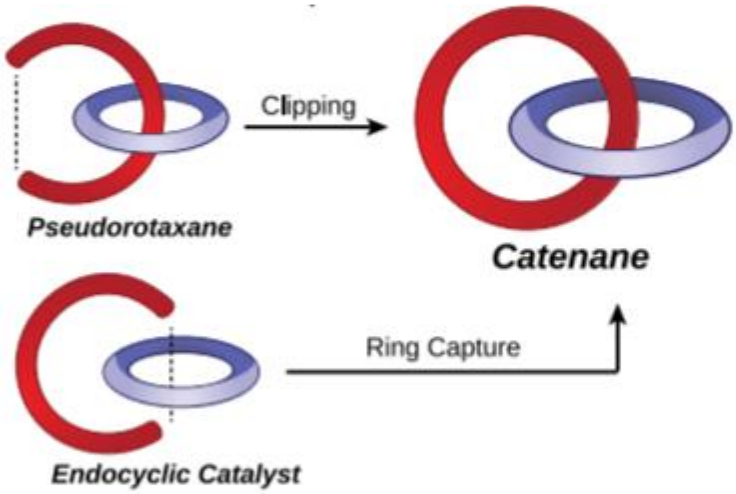

Figure 1.4. Synthetic approaches for the synthesis of catenanes.

On the other hand, the synthetic pathways toward rotaxanes are based on three different approaches: *stoppering, clipping* and *slipping* (**Figure 1.5**). Thanks to the *stoppering*, a *pseudo-rotaxane* is converted into the final rotaxane by linking two bulky groups (*stopper*) at the extremities of the half-thread, preventing the de-slipping of the ring. In general, it is possible to introduce two stopper on both extremities of the half-thread at the same time, or it is possible to insert a second stopper after the formation of a *pseudo-rotaxane* already bearing one stopper.[15][16] In a similar approach introduced by Chiu,[17][18] initially the linear component of a *pseudo-rotaxane* contains smaller stoppers, that cannot prevent the de-slipping of the ring, then, a *"swelling"* reaction is employed to increase their effective size. Alternatively, the inverse approach can be employed by reducing the ring size (*shrinking*).[19] Differently, the *clipping* and *slipping* approaches do not involve the formation of a *pseudo-rotaxane*. The *clipping* is obtained when a macrocycle is formed around a completely pre-formed thread, containing the two *stoppers* at both extremities. Finally, the *slipping* occurs when a cyclic molecule forms a complex with an already pre-formed dumbbell. The structures obtained by *slipping* are not formally considered as rotaxanes, but "kinetically-favoured *pseudo-rotaxanes*".[20]

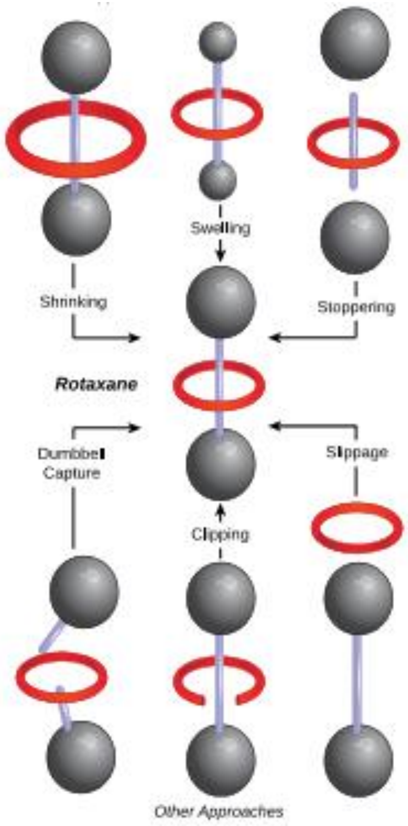

Figure 1.5. General strategies for the preparation of rotaxanes.

In most of the cases, the *pseudo-rotaxane* complex is formed by interaction between a macrocycle and a half-thread, and this process is generally called *threading*. However, how we can achieve the molecular recognition between these initial components for the following formation of the self-assembly? In the beginning, the preparation of MIMs was achieved by statistical methods (**Figure 1.6a**),[21] which relied on the probability of cyclic and acyclic molecules to entangle spontaneously in solution. This strategy involved very difficult isolation of the product from the starting materials, as well as very low yields. As second approach, directed synthesis (**Figure 1.6b**) was based on the construction of mechanically interlocked molecules by formation of covalent bonds between functional groups incorporated in the starting components.[22] Directed synthesis improved the efficiencies of the preparations but still presented some disadvantages, because it required numerous synthetic steps to achieve the final compounds. Today, the most widely used protocols employ template-directed synthesis, in which the starting component parts are assembled by non-covalent interactions between different recognition sites placed on the substrates themselves (**Figure 1.6c**). Finally, the use of active template synthesis[23] emerged recently as a powerful technique for the preparation of MIMs. Active template synthesis of MIMs (**Figure 1.6d**) relies on interactions between molecular components that are promoted by endocyclic species, such as a transition metal centre, which play the role of templates and catalysts at the same time.

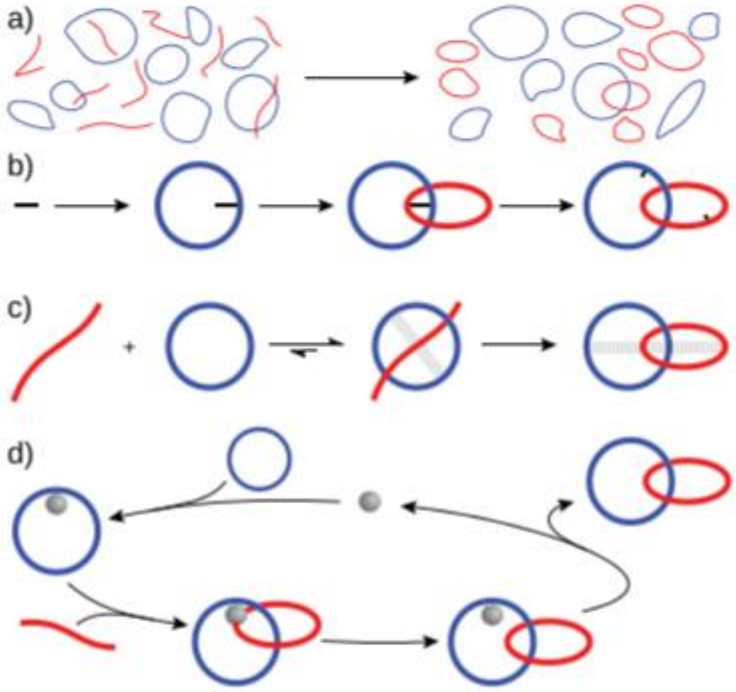

Figure 1.6. (a) Statistical Synthesis; (b) Directed Synthesis); (c) Template-Directed Synthesis; (d) Active Template Synthesis.

This PhD work dealt prevalently with the use of template-directed synthesis and the *threading stoppering* approach for the preparation of MIMs. The next paragraph contains a more accurate description of this synthetic strategy, as well as some practical examples reported in the literature.

Template-directed synthesis of MIMs

Even if active-template synthesis is certainly the most efficient synthetic pathway for the preparation of MIMs, not all the substrates are suitable for this kind of approach, thus, limiting its use in organic chemistry. For this reason, template-directed synthesis remains the most commonly employed route towards MIMs. Jean-Pierre Sauvage was the first introducing this synthetic approach in 1983, exploiting the idea of host-guest chemistry to achieve a [2]-catenane.[24] After that discovery, the template-directed synthesis of mechanically interlocked compounds has been explored many times in the literature.[25][26][27] This approach starts from the formation of non-covalently bonded host-guest complexes between cyclic and acyclic molecules, which represent the starting templates for the following mechanical bond formation and further conversion into MIMs. The non-covalent interactions involved in template-directed synthesis may include solvophobic forces, hydrogen bonding, donor-acceptor interactions, halogen bonding, anion binding, coordination to transition metals or other cations, ion pairing and so on.

There are a large number of possible macrocyclic hosts employable for the construction of MIMs by template-directed synthesis and able to provide efficient non-covalent bonds, such as crown-ethers, aza-crown ethers, cyclobis-(paraquat-*p*-phenylene) (**CBPQT^{4+}**) rings, Cucurbiturils, Cyclodextrines and Calixarenes (**Figure 1.7**).

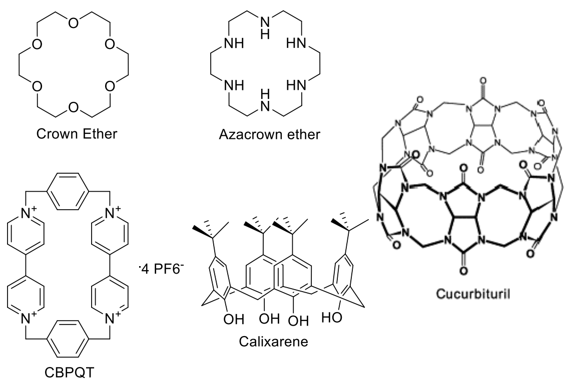

Figure 1.7. Crown ethers, aza-crown ethers, Cucurbiturils (CBs), Calixarenes and cyclobis-(paraquat-*p*-phenylene) (**CBPQT^{4+}**).

Among these substrates, crown-ether-based macrocycles are excellent candidates for the application of template-directed synthesis, because they are a very efficient class of ionophores, able to bind several types of cationic guests, both organic and inorganic, by hydrogen-bond interactions.[28][29] In fact, each unshared electron pair of the oxygen atoms contained in the crown-ether structure is able to provide a dipole-to-ion interaction with the included guest. Pedersen[30] was the first demonstrating the possibility of synthesizing cyclic poly-ethers of various size (**Figure 1.8**) able to complex alkali metal cations and also certain types of organic salts, such as thiourea, primary and secondary ammonium cations.

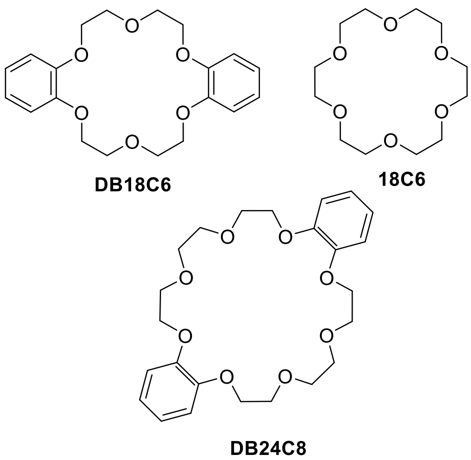

Figure 1.8. Crown ether-based macrocycles described by Pedersen.[30]

The self-assembly between crown ethers and secondary dialkylammonium ions is one of the most commonly used pseudo-rotaxane templates for the construction of MIMs,[31] [32] [33] thanks to the good binding affinity, the availability of the starting materials and their good solubility in organic solvents. In 1995, Stoddart and co-workers synthesized the first pseudo-rotaxane consisting of a dibenzo-crown ether **DB24C8** (**Figure 1.8**) and a dialkylammonium cation half-thread.[34] After that discovery, a large number of pseudo-rotaxanes based on these components have been introduced in the scientific scenario.

The efficiency of the host-guest complex formation (**Figure 1.9**), as well as the binding affinity between the components, strongly depends on the ring size and on the substituents presents in the dialkylammonium cation. The association constants and crystal structures of various pseudo-rotaxanes templates of this kind have been reported in literature.[35] [36] [37]

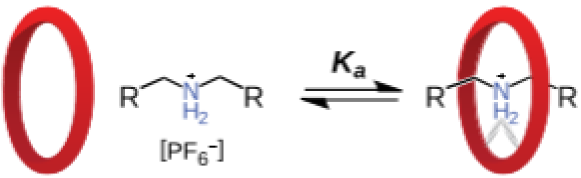

Figure 1.9. Complexation equilibrium between secondary ammonium salts and crown-ether rings.

Other parameters, such as the solvent polarity and counter-ion effect, can significantly affect the binding affinity of the host-guest complex. In particular, it is known that the association constants of these complexes have an inverse proportionality with the polarity of the solvent.[37] Thus, the higher is the polarity of the medium, the lower affinity there is between the components. On the other hand, Gibson[38][39] investigated the role of counter-ion pairing effect on the binding constants of dibenzylammonium salts $Bn_2NH_2^+X^-$ and **DB24C8** complexes bearing different counter-ions (X^- = PF_6^-, BF_4^-, OTs^-, and TFA^-). Even if the estimated K_a values can vary consistently with the concentration, they followed the trend $PF_6^- > BF_4^- > OTs^- > TFA^-$. Thus, dialkylammonium cations are employed most effectively as PF_6^- or BF_4^- salts for the following reasons: a) such counter-ions increase the solubility in apolar solvents; b) they have a weaker interaction with the dialkylammonium moiety, enhancing the latter affinity for the crown ether host.

DB24C8 and other crown ethers show binding affinity also toward other hydrogen-bonding guests, such as bipyridinium ions (BPY^{2+}) (**Figure 1.10**). The first rotaxanes of this type were prepared[40] by stoppering a pseudo-rotaxane based on a bis(α-bromoxylyl)-4,4′-bipyridinium included in a **DB24C8, BMP25C8** or **DP24C8** (**Figure 1.10**) ring. However, even if it is theoretically possible to isolate such host-guest complexes, pseudo-rotaxanes based on this recognition motif have always evidenced a low binding affinity, compared with the one showed in the presence of dialkylammonium salts, resulting also in very low yields. For this reason, the crown-ether/dialkylammonium template is generally one of the most efficiently employed for the preparation of MIMs.

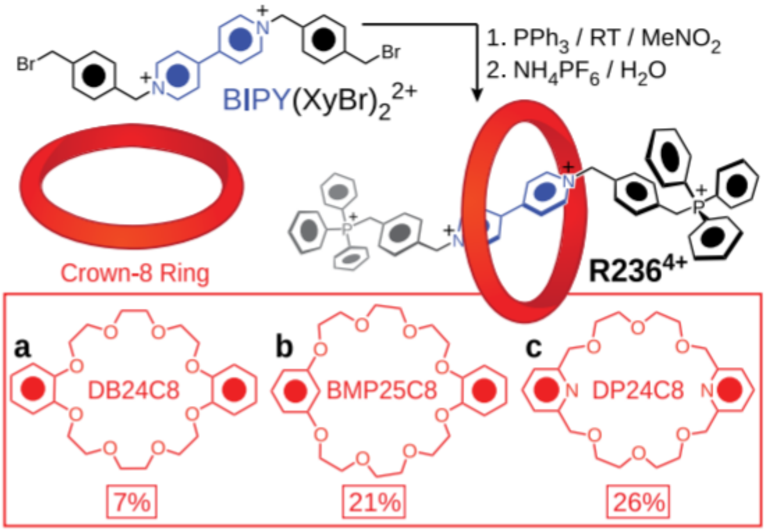

Figure 1.10. Scheme of the threading and stoppering approach employed for the preparation of rotaxanes containing a **DB24C8, BMP25C8** or **DP24C8** ring on a bis(α-bromoxylyl)-4,4′-bipyridinium thread.[40]

The resulting self-assembled complex between a crown ether and a dialkylammonium salt is further converted into MIM by one of the synthetic routes mentioned in the previous paragraph (*stoppering*, *clipping*, *swelling* or *shrinking* approaches). Among these, *stoppering* is the easiest and most commonly used approach for affording rotaxanes. These reactions generally require relatively mild conditions, since strong bases or nucleophiles can deprotonate the ammonium moiety, causing the dissociation of the assembly. In addition, as already described above, hard-binding anions can compete in the complexation between the component parts, interacting prevalently with the ammonium group. Based on these premises, many types of stoppering reactions have been explored for obtaining rotaxanes, such as amide and ester reactions, nucleophilic substitutions, metal-catalysed cross-couplings, reactions involving azides and so on (examples in **Figure 1.11**).[41] [42] [43] [44] [45]

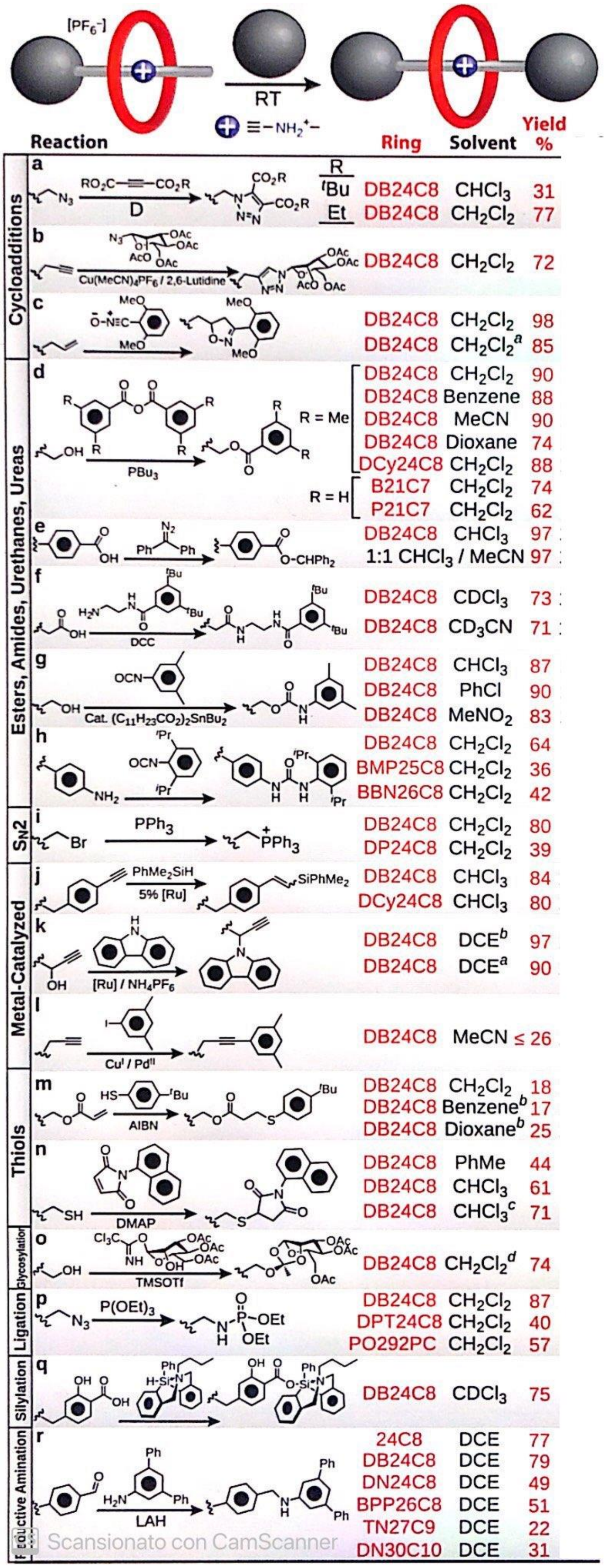

Figure 1.11. Examples of stoppering reactions starting from crown-ether and dialkylammonium pseudo-rotaxanes.

1.1.3 Molecular Machines and Switches

Inside the scenario of Mechanically Interlocked Architectures, the new scientific field of *Molecular Motors* has been gaining an increasing interest during the last decades. In biology, there are several examples of macromolecular machines, which usually perform tasks that are essential for life, such as DNA replication and ATP synthesis. For this reason, a large number of scientists have attempted, with various degrees of success, to artificially reproduce and control the features of machines found in the natural world into their laboratories, introducing the field of *Artificial Molecular Machines*. The preparation and design of artificial molecular motors disclosed a large number of possible applications in medicine, biology, biochemistry and Molecular Electronic Devices (MED). Artificial MIMs containing two or more recognition sites have represented the perfect starting point for the realization a large number of molecular dynamics and molecular engines.

In order to understand the basis of molecular motions in MIMs, it is important to clarify the important concept of *bistability*. A bistable compound is characterized by two *co-conformations* located at an energetic minimum. In a bistable mechanically interlocked molecule (MIM), the ground state co-conformation (GSCC) is referred to the global energetic minimum, and any other existing higher-energy minimum is called metastable state co-conformation (MSCC). The switching process of a molecular machine typically relies on the application of an external stimulus,[46] which serves to eliminate or destroy the interactions stabilizing the GSCC. The application of the external input results in the population of the secondary MSCC, which turns to be the most favoured of the two possible states. When a counter-stimulus is applied, the system relaxes back to the GSCC and re-stores the initial state (**Figure 1.12**). Based on this, it is, therefore, possible to create interlocked molecules, such as rotaxanes and catenanes, able to interconvert into other co-isomers as results of a dynamic process. In this case, the compound is defined as *Molecular Switch* or *Molecular Machine*.[47]

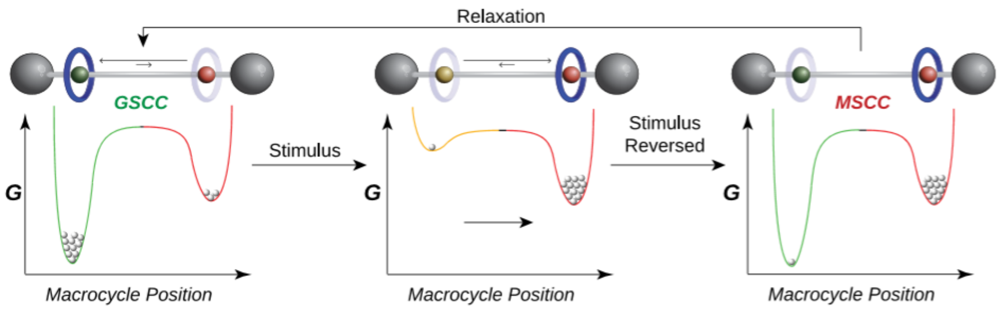

Figure 1.12. Energy diagrams of the different co-conformations assumed by a bistable rotaxane.

Generally, rotaxanes can undergo to a large number of different motions:

a) *Shuttling* or *translation*, referred to the displacement of the macrocycle between two or more recognition sites situated on the thread (**Figure 1.13a**);

b) *Pirouetting*, which is the rotation of the macrocycle around its axis (**Figure 1.13b**);

c) The change of the dihedral angles between the planes of the rings, also called *rocking* (**Figure 1.13c**).

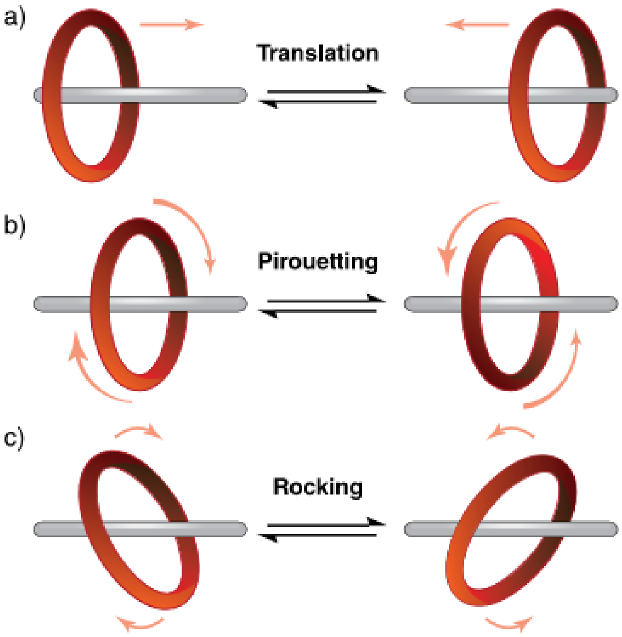

Figure 1.13. Dynamic processes available in rotaxanes.

Starting from this, there are some fundamental requirements for building an efficient molecular engine. First, the power source or stimulus must be directly available and easy convertible by the system, or even better, recyclable. Furthermore, it is important to consider sources that do not generate accumulation of side-products, which can affect the efficiency of the system. On the other hand, the accumulation of side-products may be employed to switch on or off the engine depending on the necessity. Nevertheless, the energetic variations leading to the different equilibrium states of the process must be taken into account, because only a little disproportion between the energy levels may inhibit the completion of a full cycle of motions. Finally, the mechanism of movement in a molecular machine must be irreversible and able to restore the initial state, allowing performing different cycles in continuity. The actual state of art reports a large number of artificial engines exploiting the above-mentioned features and able to mimic the efficiency of biological nano-machine systems. Molecular machines can be differentiated by the way the stimulus or power is supplied to the system: a) chemically; b) electrochemically; c) photo-chemically.[48][49][50]

The use of electrochemical stimuli for promoting the switching of molecular machines was among the first to be discovered. This approach presents different advantages related to: a) the generation of small amount of waste; b) its applicability to molecular electronic devices (MED);[51][52][53] c) the large number of recognition sites that can be adapted to this approach, including π-associated donor-acceptor MIMs, transition metal-complexed MIMs, hydrogen-bonded MIMs, and MIMs based on the hydrophobic effect.[54][55][56] Donor-acceptor rotaxanes based π interactions are very suitable for redox-driven switching, because the π-conjugated sites are, in most of the cases, also redox-actives. The oxidative or reductive switching leads to perturbation of the electronic structures, influencing the non-covalent interactions between the components and forcing, in turn, a dynamic process. One of the most famous examples of redox-switchable molecular machines is illustrated in **Scheme 1.1**. The rotaxane[57] consists in a cyclobis-(paraquat-*p*-phenylene) (**$CBPQT^{4+}$**; blue ring) encircling a dumbbell composed by a tetrathiafulvalene (TTF, green station) and a 1,5-dioxynaphthalene (DNP; pink station) recognition sites. The one electron oxidation of the TTF moiety to $TTF^{\cdot+}$[57] [58] [59] forces the shuttling of the ring on the secondary DNP site, forming the corresponding co-conformer (**state B**). Then, reversible reduction of $TTF^{\cdot+}$ re-stores the initial TTF group, thus, causing the shuttling back of the macrocycle on the original site. The shuttling mechanism of this molecular machine and the one of the similar [2]-catenane[60] was proved by cyclic voltammetry, in particular by comparing the electrochemical behaviours of the [2]-rotaxane and the corresponding free dumbbell upon oxidation of the TTF moiety. Also ^{1}H-NMR experiments provided the confirmation of the shuttling mechanism of the [2]-rotaxane.

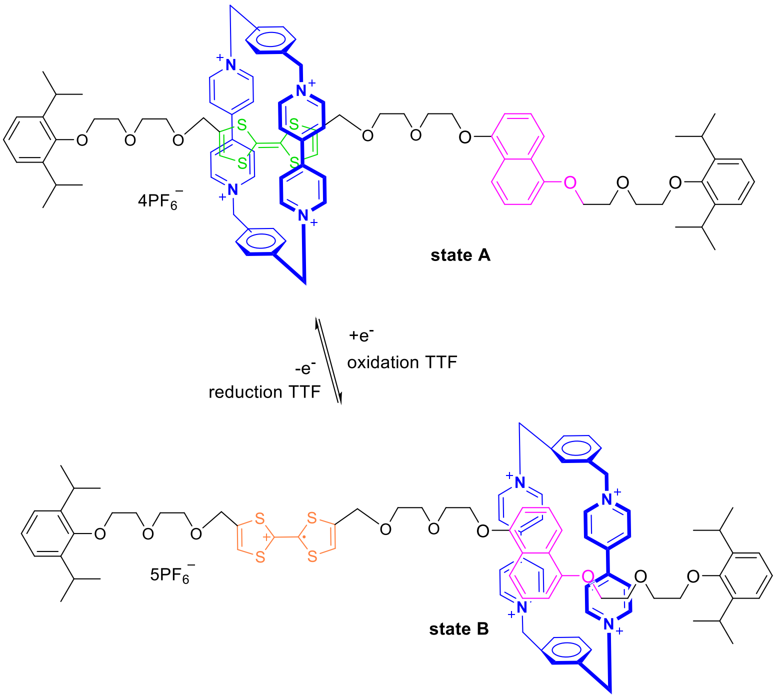

Scheme 1.1. Redox-switchable CBPQT-based bistable rotaxane by Stoddart *et al.* [57]

Some years later, the same research group employed a similar [2]-rotaxane for an application in the field of molecular muscles. The CBPQT-based rotaxane was incorporated between a gold AFM cantilever and a silica support (**Figure 1.14**).[61] This substrate allowed measuring the force of switching of the rotaxane by using the tip as a dynamometer. They found that the force variation between the two co-conformations corresponded to 79 pN, which is a significantly high value for a single molecule. This work was chosen to represent a crucial example of how molecular machines can find impressive applications in materials technologies and in other scientific areas.

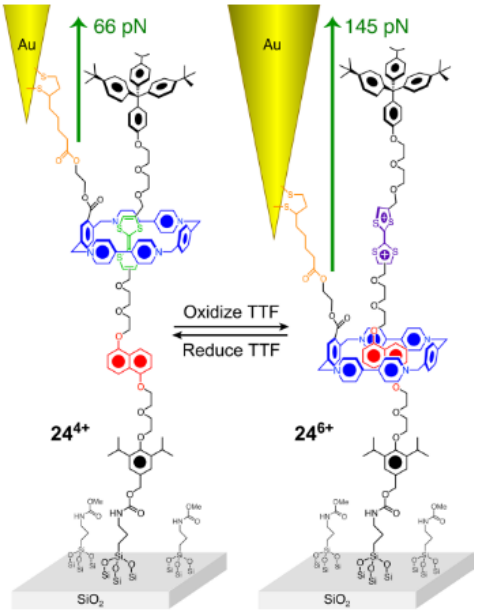

Figure 1.14. AFM-SiO_2 rotaxane system described by Stoddart *et al.*[61]

Although photo and redox-switchable molecular machines present several advantages in terms of recycling, efficiency and versatility, also acid-base switchable rotaxanes and catenanes have been largely studied and investigated in literature. In general, acid-base switching processes rely on the addition or removal of protons to one or more recognition sites of the substrate, leading to a variation of the affinity between the components and ultimately causing the displacement of one or more parts. Stoddart *et al.* developed one of the first and most famous examples of chemically fuelled molecular machines. They described a [2]-rotaxane containing a dibenzo-24-crown-8 macrocycle (**DB24C8**) around a dumbbell composed by a dialkylammonium (**NH_2^+**) and a 4,4'-bypiridinium stations (**BPY^{2+}**) (**Scheme 1.2**).[48] The **DB24C8** ring has well known ability to perform hydrogen bonds with dialkylammonium organic cations (**Paragraph 1.1.1**).

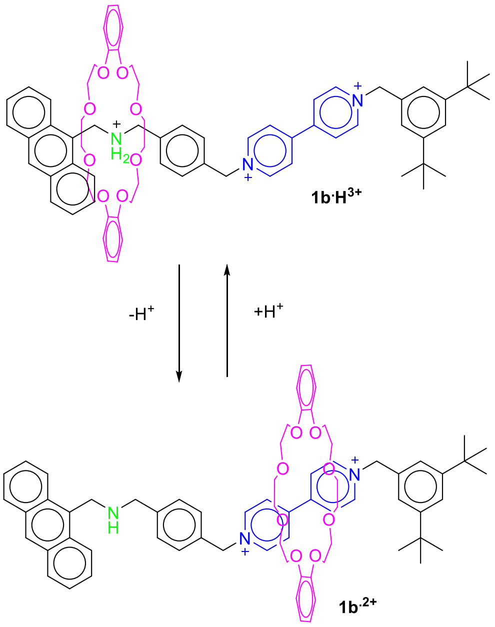

Scheme 1.2. Bistable acid-base switchable rotaxane reported by Stoddart *et al.* [48]

For this reason, the starting state of the bistable rotaxane has the macrocycle mainly located on the $\mathbf{NH_2}^+$ site. It was important to consider that the generation of hydrogen bonds in the starting state resulted in an enhanced basic character of the $\mathbf{NH_2}^+$, thus requiring the employment of an excess of base to deprotonate it. After deprotonation of the $\mathbf{NH_2}^+$ group, the electrostatic repulsion between the lone electron pairs of NH and the oxygen atoms forced the displacement of the ring on the $\mathbf{BPY}^{2+}$ site (**Scheme 1.2**). The reversibility of the process was guaranteed by re-protonation of the amine group using one equivalent of trifluoroacetic acid (TFA), which led to the shuttling back of the macrocycle on the starting recognition site. The full cycle of motions was verified by NMR experiments, UV-visible spectroscopy and cyclic voltammetry (**Figure 1.15**), which served for evidencing the displacement of the ring on the secondary recognition site. The back and forth motion of the target rotaxane was also reproducible for many cycles, but every addition of TFA led to the accumulation of side-products that decrease the cycling ability of the system.

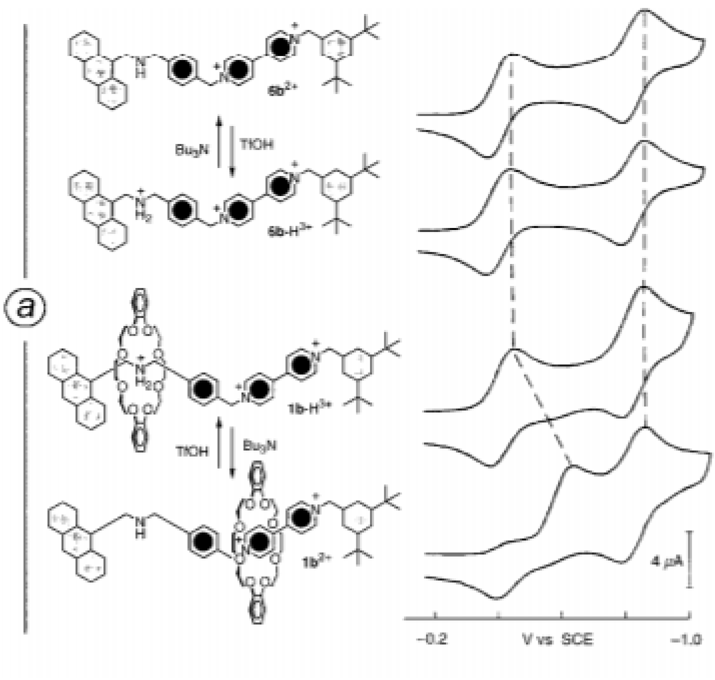

Figure 1.15. Cyclic voltammetric analysis performed on the dumbbell components **$6b^{2+}$/$6b$-H^{3+}** and [2]-rotaxanes **$1b$-H^{3+}/$1b^{2+}$**.

On this outline, in 2018 Ragazzon *et al.* reported a further investigation of the above-described rotaxane, showing that the secondary **BPY^{2+}** site can be used for the modulation of the basicity of the **NH_2^+** station. The variation of the oxidation state of the bipyridinium unit, that can be electrochemically reduced to radical cation (**$BPY^{+\bullet}$**) or diradical (**$BPY^{\bullet\bullet}$**), led to a decreased affinity of the latter for the binding with **DB24C8**, thus affecting the ability of the macrocycle to shuttle. The pK_a value of the ammonium site was enhanced of 7 units in the presence of **$BPY^{\bullet\bullet}$** compared with the pKa registered for **BPY^{2+}**. Thus, the ternary electrochemical switching at a remote site of the **BPY^{2+}** unit provided the possibility to modulate the pKa of an ammonium residue in the axle of a [2]-rotaxane, affecting the translation process (**Figure 1.16**).[62]

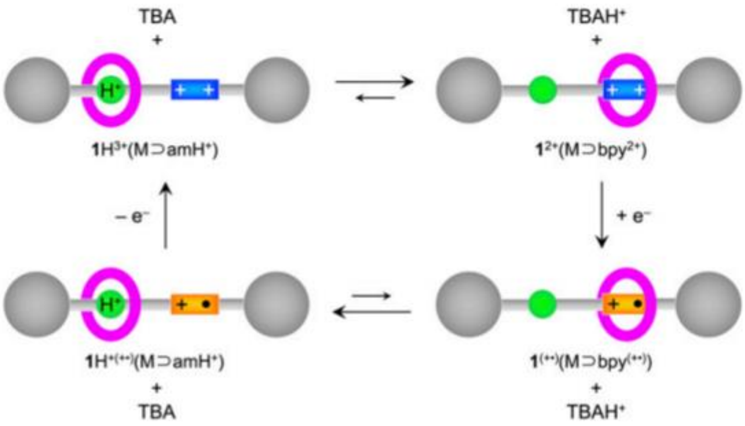

Figure 1.16. Comparison between the acid–base (horizontal) and electrochemical (vertical) switching processes observed for rotaxane **1H**$^{3+}$.[62]

These works take part into the effort and the big scientific challenge of obtaining autonomous and continuous-working molecular devices similar to the biological partners, exploiting the intrinsic properties of the components of MIMs. This topic is founding more and more importance among the scientific community and whereas biology has perfected its machines over billions of years of evolution, chemists keen to imitate these structures are just getting started. Leigh was convinced that what the field needs is a killer application. *‘As soon as you find one thing that molecular machines can do that can’t be done any other way, then they undeniably become a useful technology. Biology has found through evolution that molecular machines are the best way to get things done. I’m sure that’s going to be true for mankind as well.’*

1.2. EPR INVESTIGATIONS OF SUPRAMOLECULAR ASSEMBLIES AND MIMS

1.2.1. Principles of Electronic Paramagnetic Resonance

Electron Paramagnetic Resonance (EPR) is a spectroscopic technique, similar to Nuclear Magnetic Resonance (NMR), able to detect transitions relative to unpaired electrons. This kind of spectroscopy is employed for the study of paramagnetic inorganic and organic compounds, which are not detectable by NMR. EPR was discovered in 1921, when Stern and Garlach observed a peculiar spectroscopic response of a group of Silver atoms passing through a magnetic field.[63] Later, thanks to this result, electron spin (s) was defined as an intrinsic property of the electron.[64] Finally, Zavoisky performed the first EPR experiment in 1944.[65]

Similarly to the proton, every electron has a specific magnetic moment associated to its spin (s). There are two possible spin states, corresponding to the two orientation assumed by the electron in the space. In absence of external fields, these states are located at the same energy level and the electrons assume a random orientation. Then, when a magnetic field is applied, the Zeeman effect causes the splitting of the two spin states into different energy levels, causing a differentiation of population between the two (**Figure 1.17**). The difference of energy between the two spin states is calculated as follow:

$$\Delta E = g * \mu_B * B_0$$

Where B_0 is the value of the magnetic field, μ_B is the Bohr magneton, and g is an a-dimensional constant. Similarly to NMR, there is a proportional correlation between the difference of energy, ΔE, and the magnitude of the applied electromagnetic field. An unpaired electron can move between the two energy levels by absorbing or emitting a photon of energy, respecting the condition: $\Delta E = h\nu$. The possible transition between different energy levels are, then, detected as EPR signals.

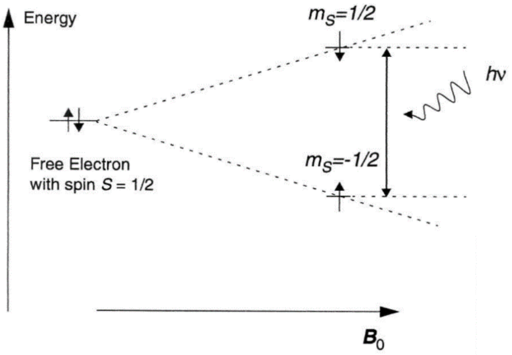

Figure 1.17. The electron Zeeman effect leading to the energy splitting of the two spin states.

Differently than in NMR spectroscopy, in the EPR spectra the first derivative of the absorption curve is reported in order to obtain a higher sensitivity. Furthermore, the excess of population between the two energy states of the electron spin is around the order of 10^{-3} in EPR spectroscopy, while for NMR is around 10^{-5}, thus leading to a higher sensitivity of EPR, which is able to record the presence of radicals at concentrations up to 10^{-7} M. EPR provides the possibility of performing kinetic studies at the sub-microsecond time range and of measuring distances between two or more radical moieties present in the substrate, in a range from 0 Å up to 100 Å.[66] Thanks to these features, EPR spectroscopy represents an efficient complementary technique for the investigation of systems containing persistent radicals, which cannot be monitored by classical NMR analysis.

EPR experiments are characterized by some important parameters:

- *g-factor*: When a magnetic field is present, the unpaired electron presents not only its spin angular momentum but also an extra orbital momentum, and the effective g value (*g-factor*) is slightly different from that of the free electron (g). This results in an alteration of the condition of resonance ($h\nu = g * \mu_B * B_0$), so that radicals with different *g-factors* resonate at different magnetic fields that are typical of the interested compound, similarly to the chemical shifts in NMR. For organic radicals, the *g-factor* is generally very similar to the one of the free electron (2.0026), even if it could be affected by the presence of heteroatoms, as well as the presence of a π-system near the radical centre.[67] For this reason, the *g-factor* can give information about a paramagnetic centre's electronic structure.
- *Hyperfine coupling*: In the presence of a single unpaired electron, the EPR spectrum results in a single spectral line (only one possible electronic transition, **Figure 1.17**). Greater complexity arises if the unpaired electron couples with nearby nuclear spins, generating a *hyperfine coupling*.[68] This parameter is correlated to the interaction between the unpaired electron and an adjacent magnetic nucleus placed on the α or β position (^{1}H, ^{13}C, ^{14}N etc…). For β-nuclei a is given by an equation similar to the Karplus equation for NMR:

  $$a = (A + Bcos^2\theta)\rho$$

  where ρ is the spin population, which is the probability to find the unpaired electron on a specific atomic nucleus, and A and B are empirical constants.
- *Multiplicity:* The number of lines of an EPR spectrum is correlated to the number and type of magnetic nuclei able to couple with the unpaired electron. Many nuclei have a net nuclear spin, *I*, leading to different orientations of the nucleus when placed in a magnetic field. For

example, those with nuclear spin $I = 1/2$ have two possible orientations (+1/2, -1/2) in the corresponding magnetic moment, while those with $I=1$ have three orientations (+1, 0, −1) and so on. Thus, if a coupling with a spin active nucleus with $I = ½$ is present, the resulting EPR spectrum is expected to show two resolved lines (two possible transitions), where the separation between the two is given by the hyperfine coupling constant (a) (**Figure 1.18**).

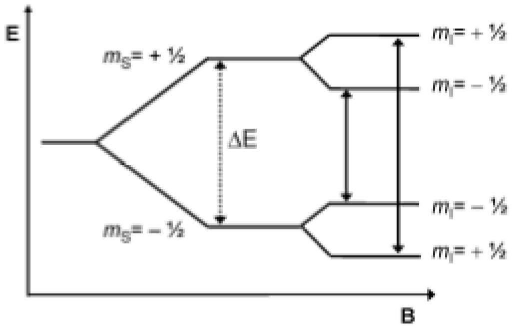

Figure 1.18. Splitting of the energy levels of an unpaired electron coupling with a nucleus having $I = ½$.

In general, the number of EPR spectral lines of a radical where an unpaired electron couples with n equivalent magnetic nuclei with nuclear spin I, is calculated as follow:

$$N = 2nI + 1$$

When the unpaired electron interacts with different groups of equivalent magnetic nuclei, the EPR spectrum becomes more complicated and the number of spectral lines N is given by:

$$N = (2n_1I_1 + 1)(2n_2I_2 + 1)(2n_3I_3 + 1)\ldots\ldots\ldots (2n_kI_k + 1)$$

For example, the EPR spectrum of a system where an unpaired electron couples with an adjacent nucleus having $I = 1$ (*i.e.* ^{14}N) and another having $I = ½$ (*i.e.* ^{1}H) results in six spectral lines. The relative intensities of the peaks follow the rule of Tartaglia’s triangle, as in NMR spectroscopy.

- *Line width:* This is a parameter influenced by the relaxation times of the electron. Alternatively, if not related to relaxation times, it can be influenced by many other factors leading to fluctuations of the field in the proximities of the unpaired electron, such as intermolecular or intramolecular dynamic phenomena, polarity of the medium and so on.

- *Spin-spin exchange coupling*: If a system contains two or more unpaired electrons that are sufficiently close to interact with each other, it leads to a spin-spin exchange interaction accompanied by the appearance of extra lines in the EPR spectrum, whose intensity is related to the magnitude of the exchange constant (J).[69] In order to obtain this condition, the spin-spin exchange constant J needs to be comparable or higher than the a constant. On the contrary, if the paramagnetic centres are too far away to give exchange interaction ($J = 0$), the EPR spectrum will be comparable to that of the single mono-radicals. It is also important to mention that the interaction between two radical centres can occur through-space, if the distance between them is low enough, or through-bond, if a conjugate system is present, enabling the "communication" between the radical units. For example, **Figure 1.19** compares the spectra of a single nitroxide radical with the one of a di-radical where the nitroxide moieties undergo a through-space interaction. The spectrum changes from a multiplicity of three lines (with intensity 1: 1: 1) to one of five lines (with intensity 1: 2: 3: 2: 1).[70] [71] It is evident that the relative intensity of the exchange spectral lines may vary from the expected one, depending on the number of molecules assuming the conformations that have an effective spin-spin exchange ($J \neq 0$). Conformational changes or supramolecular phenomena can affect the interaction between the radical moieties, resulting in a variation from the attended relative intensity of the exchange spectral lines.

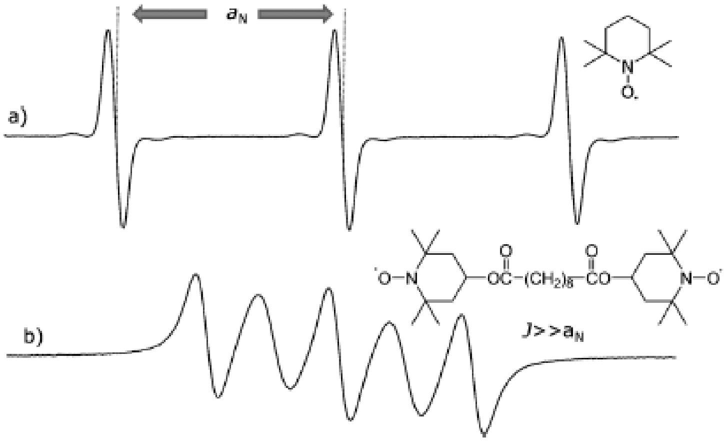

Figure 1.19. EPR spectra of: a) Single TEMPO radical; b) Bis-TEMPO radical having a through-space spin-spin exchange.

The analytic observation of all these EPR parameters can be employed for studying complex biological and non-biological architectures containing persistent radicals and for investigating the processes occurring in the target systems with the support of EPR techniques.

1.2.2 Nitroxide Radicals: Description and Properties

Organic radicals are commonly employed for EPR investigations of a large number of synthetic and natural substrates. However, most of them are transient species, with a short lifetime, and this can limit their investigation and detection through EPR techniques. Among all the organic radicals that are employable for EPR investigations, nitroxide radicals are optimal candidates, because they are suitable for chemical design and they are also characterized by chemical stability and long lifetimes (**Figure 1.20**).[72]

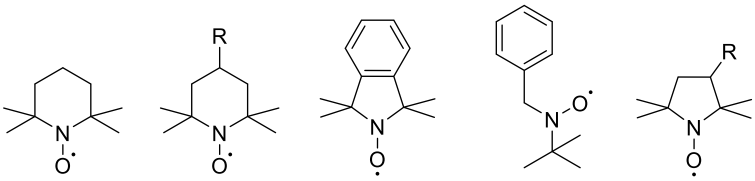

Figure 1.20. Some nitroxide derivatives.

The nitroxide radical consists of an aminoxyl moiety where the unpaired electron can occupy the π-orbitals of both the nitrogen and the oxygen atoms, leading to two possible resonance structures (**Scheme 1.3**).

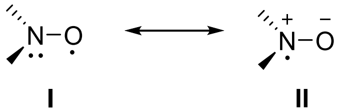

Scheme 1.3. Possible resonance structures of the aminoxyl radical.

Figure 1.21 reports the schematic representation of the molecular orbitals of the N-O· bond and evidences the notable gain in terms of energy, due to the delocalization of the three electrons on the π orbitals deriving from the overlapping of the 2*p* orbitals of the nitrogen and the oxygen.

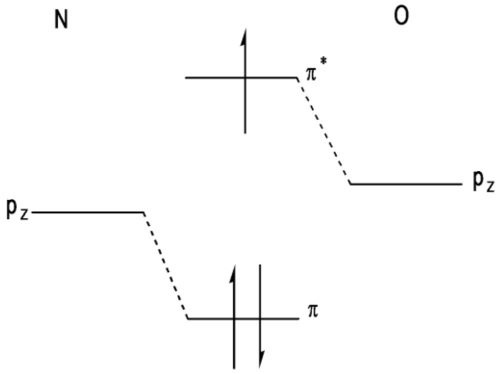

Figure 1.21. Molecular orbitals deriving from the overlapping of the two atomic 2*p* orbitals of the N-O$^{\cdot}$ group.

N-O$^{\cdot}$ radicals are more chemically stable compared to hypothetic radicals where a delocalization of the unpaired electron is not present.[73] Actually, the dimerization process that occur by formation of the O-O bond between two aminoxyl moieties is highly disfavoured in this case, because the gain of energy deriving from the formation of the new O-O bond only partially compensates the loss of delocalization of the unpaired electron (**Scheme 1.4a**). In addition, certain types of nitroxides are characterized by long lifetimes, depending on the molecular structure of the radical. This persistence is observed only in the presence of alkyl groups on the β carbons, because in absence of them, the nitroxide can irreversibly lead to the formation of the corresponding hydroxylamine and nitrone by-products by disproportion reaction (**Scheme 1.4b**).

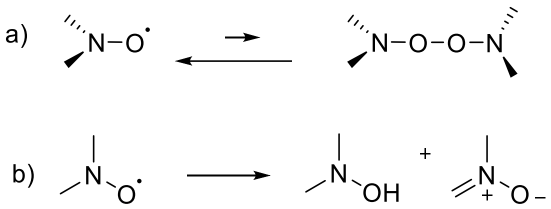

Scheme 1.4. Representations of: a) dimerization reaction; b) disproportion reaction leading to a molecule of hydroxylamine and a nitrone.

A stable nitroxide radical is generally characterized by a three lines EPR spectrum, deriving from the coupling between the unpaired electron and the ^{14}N atom, (I = 1) as described in **Paragraph 1.2.1** (**Figure 1.22**). The hyperfine coupling between the unpaired electron and the ^{14}N atom (a_N) is calculated as the distance between two consecutives spectral lines.

Figure 1.22. Typical EPR spectrum of a nitroxide radical.

The EPR spectrum of a nitroxide group can give important information about the surrounding chemical environment. For example, the presence of hydrogen bond donors, or a more polar environment results in an increase of the a_N value, because these phenomena affect the electronic structure of the radical, influencing the spin density on the nitrogen atom (**Figure 1.23**) (**Paragraph 1.2.1**).

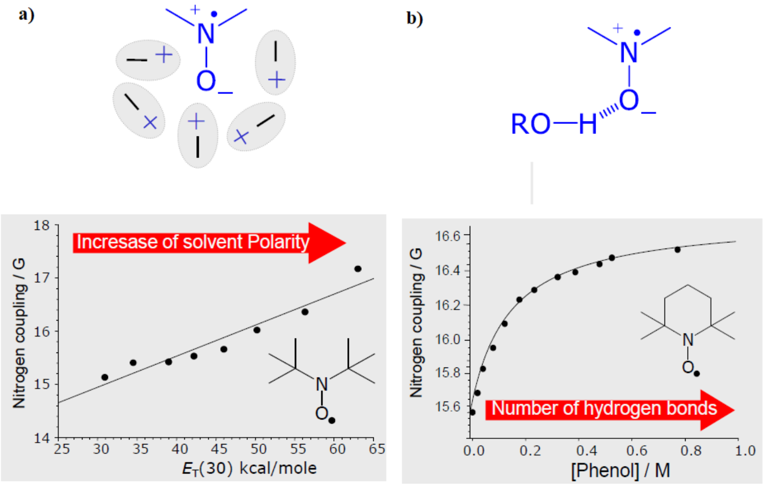

Figure 1.23. The effect of: a) dipolar interactions; b) hydrogen bonds, on the a_N value.

Also the other EPR parameters of a nitroxide group can be strongly influenced by conformational and dynamic events, intramolecular and intermolecular interactions, polarity of the medium and so on. The most commonly used persistent nitroxide radicals are 2,2,6,6-tetramethylpiperidin-N-oxyl (TEMPO) and its derivatives (**Figure 1.24**), where the persistence is guaranteed by the presence of methyl or ethyl groups, instead of hydrogens, in the β position at the aminoxyl unit.

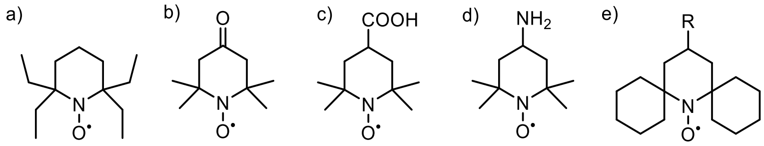

Figure 1.24. Derivative of TEMPO: a) 2,2,6,6-tetraethyl-piperidin-N-oxyl, b) 4-oxo-TEMPO, c) 4-carboxy-TEMPO, d) 4-amino-TEMPO, e) bis-spirocyclohexyl-piperidin-N-oxyl.

TEMPO derivatives can be employed for many biological and chemical applications thanks to their availability, easy manipulation, stability and lifetime. They are commonly used as spin labels[74] [75] for EPR bio-investigations and for oximetry[76] [77] studies, as contrast-enhancing agents for magnetic resonance imaging (MRI)[78][79] and for electron paramagnetic resonance imaging (EPRI).[80][81] However, one of their disadvantages is that most of them can be easily reduced to the corresponding diamagnetic adduct (hydroxylamine) *in vivo* conditions (**Scheme 1.5**). This problem can limit their use for biological investigations.

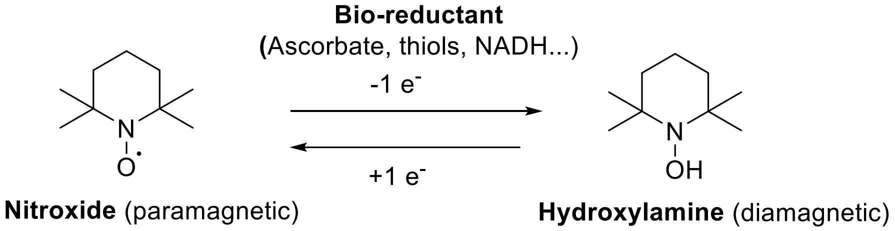

Scheme 1.5. Redox reaction between TEMPO and a bio-reductant in biological tissues.

The reduction rate of a nitroxide radical can be varied by modifying the ring size and the steric hindrance of β-substituents, and it is therefore controllable by a proper design of the radical. Five-membered nitroxides generally have a longer lifetime than six member rings; for example, 3-Carboxy-PROXYL (**Figure 1.25**) is one of the most commonly used nitroxides for *in vivo* applications, because of its resistance to bio-reduction.[82]

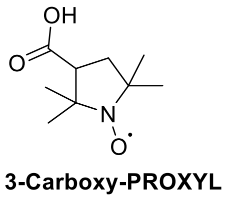

Figure 1.25. Molecular structure of 3-Carboxy-PROXYL.

It is also known that sterically shielded nitroxides, in particular tetraethyl-substituted nitroxides, are more resistant towards reduction compared with the tetra-methyl-substituted derivatives.[83] Thus, also the steric hindrance of the β-substituents plays a key role in the enhancement of the radical lifetime. For example, the tetraethyl pyrrolidine nitroxides shown in **Figure 1.26** have been recently used to spin label a chaperone protein for *in-cell* EPR investigations. These compounds showed only a minimal reduction of the paramagnetic centre when placed in biological environment, allowing the EPR structural studies of the target protein.[84]

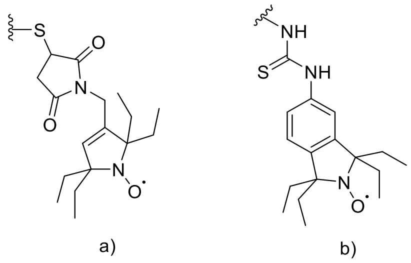

Figure 1.26. a) Tetraethyl-substituted pyrrolidine nitroxide; b) Tetraethyl-substituted iso-indoline nitroxide for *in vivo* EPR studies.

1.2.3 Spin labelling and spin probing of supramolecular assemblies using nitroxide radicals

Part of this paragraph is taken from the scientific review:

M. Lucarini, ***Improving Spin Probe Methodologies to Investigate Supramolecular Assemblies,*** *Eur. J. Org. Chem., 2020.*

EPR investigations using persistent organic radicals have expanded over biology, structural biochemistry and other scientific fields, being explored several times over the years.[85] [86] [87] [88] We can distinguish two main approaches for performing EPR investigations using organic radicals, called *spin labelling* and *spin probing*. *Spin labelling* is the incorporation of a paramagnetic centre in a particular substrate by a covalent bond. It was introduced more than 50 years ago from H. McConnel,[89] and nowadays is still a powerful tool for the determination of structural characteristics of biological membranes and proteins of various molecular weights.[90] [91] [92] [93]

Alternatively, *spin probing* is the non-covalent insertion of a radical probe in the target environment. Even if these techniques may employ any persistent free radical, the 99% of the studies reported in the literature utilize nitroxide labels or probes (i.e. TEMPO, BTBN etc…). As already mentioned above (**Paragraph 1.2.1**), the hyperfine constant (a_N) of dialkyl nitroxides and the other EPR parameters (line broadening, g-factor etc...) are highly sensitive to the environment surrounding the paramagnetic moiety. This effect is highly important for studying host-guest and self-assembly processes, as well as conformational variations and molecular dynamics that occur very often in biological systems. In the last years, our research group and many others have reported several examples concerning the application of *spin labelling* and *spin probing* using persistent nitroxide radicals for the investigation of supramolecular assemblies.

Tert-butylnitroxide (**BTBN, Figure 1.27**) was one of the first *spin probes* employed by our group for investigating host-guest assemblies with different hosts, such as Cyclodextrines (CDs), Cucurbiturils (CBs) and Calixarenes. **BTBN** presents a shorter lifetime compared with the above-mentioned TEMPO radical, because of the presence hydrogen atoms on one of the two β-carbons. However, the presence of a *tert*-butyl group enhances the radical lifetime enough to permit its investigation by EPR.[66]

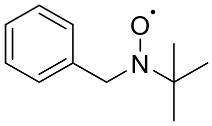

BTBN

Figure 1.27. Molecular structure of **BTBN**.

In 1999, our group has investigated the inclusion of **BTBN** in both β-CD and γ-CD, which resulted in a significant variation of both nitrogen (a_N) and β-proton (a_H) hyperfine constants, as well as an evident line broadening of the spectral lines (**Figure 1.28**). Since the association/dissociation processes were comparable to the EPR timescale, it was possible to extrapolate the rate constants for the processes thanks to the support of computer simulations.[94]

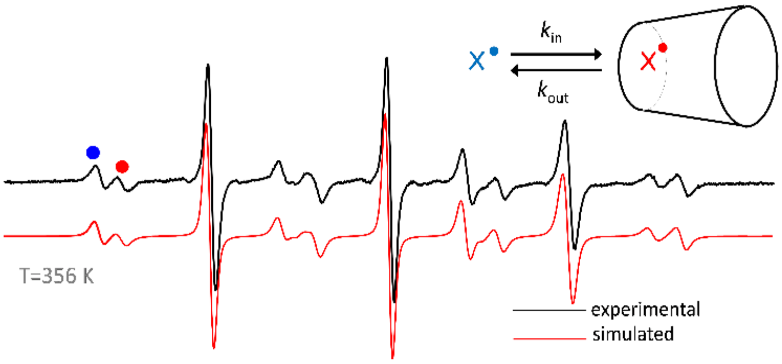

Figure 1.28. Experimental (up) and simulated (down) EPR spectra of **BTBN** recorded in water in the presence of β-CD.

In the following years, EPR studies were also performed comparing the inclusion of **BTBN** and TEMPO nitroxide radicals in other similar hosts, such as Cyclodextrines (CDs) and Calixarenes. In all the cases, EPR analysis allowed to measure for the first time the rate constants and the activation parameters for the inclusion of the probe into the target host, by observing the spectral variations associated to the a_N constants of the EPR spectra.[95] [96] [97] [98] [99] [100] [101] [102] All these works have encouraged the further investigations of other host-probe complexes, which have been performed by several research groups in the following years.[103]

As a more applicative example of this approach, **BTBN** derivatives (containing an aliphatic hydrocarbon or fluorinated chain at the *para* position of the aromatic ring) were used to study hosts of higher complexity (**Figure 1.29**), for example hydrogenated (**NP1**) or fluorinated (**NP2**, **NP3a**, **NP3b**) monolayer of protected gold nanoparticles (AuNPs) with different sizes.

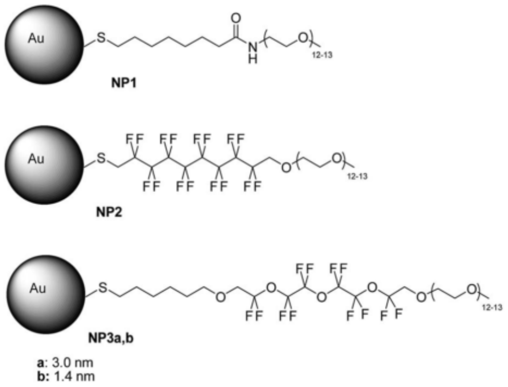

Figure 1.29. Structures of the investigated AuNPs.

The aim of the study was to evaluate their possible use in drug delivery applications. In these systems, the organic monolayer of the nanoparticle created 'hydrophobic pockets' where organic solutes, such as **BTBN** probes, could be partitioned. The a_N values in the EPR spectrum of the **BTBN** probes were significantly different when the radical was situated inside the cavities of the monolayer than that measured when it was placed in the surrounding aqueous environment (**Figure 1.30, Figure 1.31**).

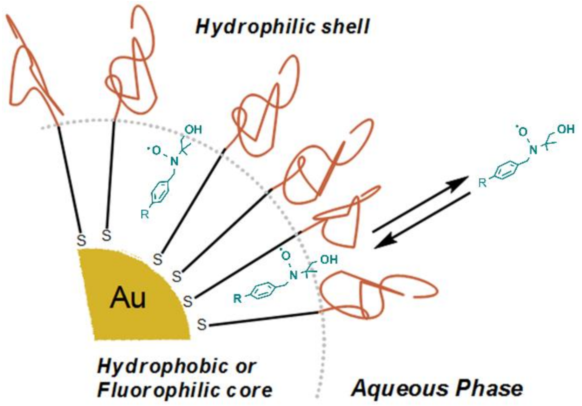

Figure 1.30. The investigated partition equilibria between the **BTBN** probes and the AuNPs.

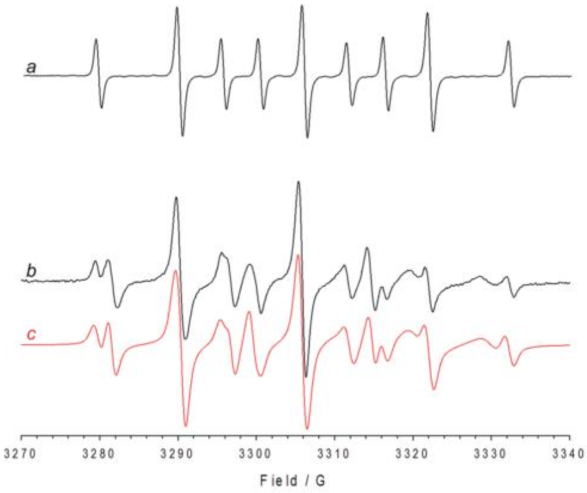

Figure 1.31. EPR spectra of **BTBN** probe recorded a) in water at 298 K; b) in presence of **NP3b;** c) computational simulation of the EPR spectrum (b).

It was, therefore, possible to distinguish two different signals related to the free radical and the nitroxide located inside the monolayer and this allowed measuring the affinity of the organic probe as a function of the monolayer composition or nanoparticle diameter. This feature was successfully exploited to study the topology of soluble gold NPs by means of EPR spectroscopy.[104]

In the field of spin probing, EPR spectroscopy allows also to identify nitroxide probes that are engaged in halogen-bonded complexes. The formation of a new halogen bond involving the N-O$^{\cdot}$ centre leads to an increase of the spin density on the nitrogen atom, which is reflected by the increment of the EPR hyperfine constant (**Paragraph 1.2.1**). Such property was employed for the first time by our group for investigating the formation of halogen bonded TEMPO probes by using EPR spectroscopy. The formation of a X–bonded TEMPO was manifested as an increase in the nitrogen hyperfine coupling a_N, accompanied by a marked broadening of the EPR lines (**Figure 1.32**).

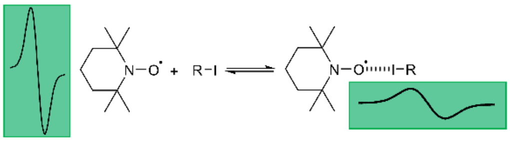

Figure 1.32. Comparison between the EPR responses of a free TEMPO radical and a halogen-bonded TEMPO radical.

More recently, other nitroxide probes have been used for this kind of studies, such as iso-indoline nitroxides (TMIO)[105] and other BTBN derivatives.[106]

In the course of the last decades a large number of data relatives to the interaction of different molecular hosts with nitroxide spin probes have been collected. On the other hand, the *spin labelling* approach provides the opportunity to study host-guest processes from the opposite point of view, by covalently incorporating a paramagnetic unit in a macrocyclic host and using EPR spectroscopy for detecting the inclusion of inorganic and organic guests into its cavity. In addition, a further opportunity is to incorporate such spin-labelled macrocycles in Mechanically Interlocked Molecules (MIMs) for studying the conformational or dynamic events affecting the system by EPR techniques. In fact, among the most recent research focus of our group, there is the preparation of spin-labelled MIMs for applications in the field of molecular machines.

As described in **Paragraph 1.1.3**, there are different methodologies that can be employed to probe the movement of molecular machines, such as NMR, UV-visible spectroscopy and cyclic voltammetry among the others. Electronic Paramagnetic Resonance (EPR) recently came out as an efficient supplementary technique for verifying the molecular dynamics in spin-labelled molecular machines. However, there are still only few examples of the use of EPR techniques for this purpose. A first evaluation of this *spin-labelling* approach was reported in 2012 and described the functionalization of α-CD with a TEMPO radical by *click* reaction (**Figure 1.33**).[107]

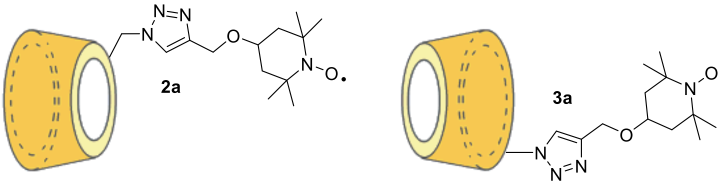

Figure 1.33. Structures of the TEMPO-functionalized α-CDs.[107]

The target CD-macrocycles were employed for preparing a α-CD-based rotaxane containing TEMPO labels on the wheel and on the thread (**7a**, **Scheme 1.6**). Starting from the CD-macrocycle **2a**, the bis-labelled rotaxane was prepared by reacting the corresponding pseudo-rotaxane **5** with an alkyne-**TEMPO** (**1**), using the threading-stoppering approach (**Scheme 1.6**). By EPR measurements of the through-space spin exchange between the two mechanically assembled nitroxide units, it was possible to assume that the rotaxanation provided only one of the two possible structures predicted on the basis of the orientation of the CD along the thread (the so-called "*close isomer*"). In this conformation, there was a spin-spin exchange interaction due to the closer distance between the two radical moieties (**Figure 1.34**).

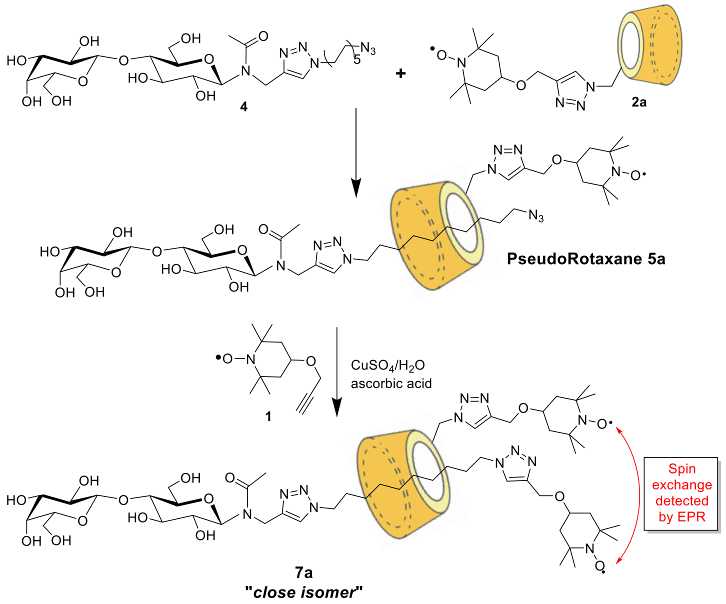

Scheme 1.6. Synthesis of the bis-labelled rotaxane **7a**.

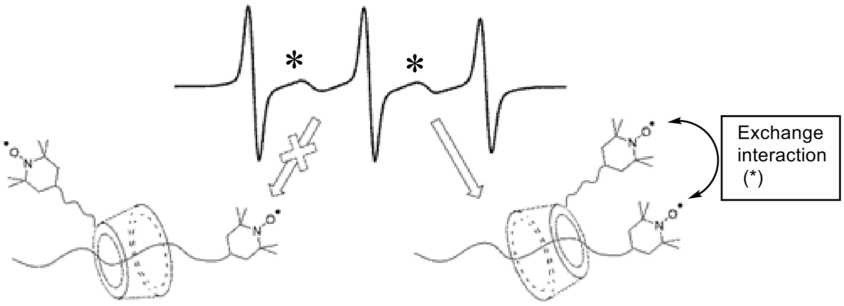

Figure 1.34. EPR spectrum of the CD-based rotaxane **7a** evidencing the exchange interaction between the TEMPO units on the ring and on the thread.

More recently, two paramagnetic spin labelled crown-ethers were synthesized and studied (**Figure 1.35**).

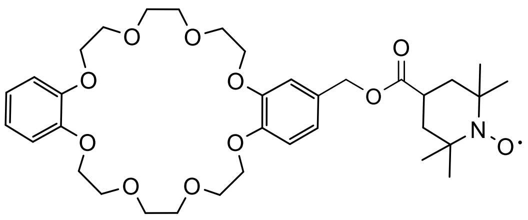
DB24C8_NO1

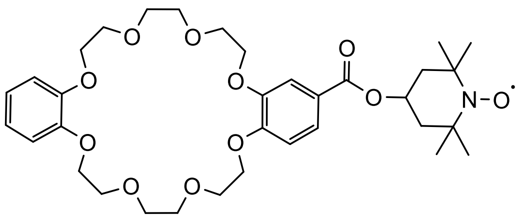
DB24C8_NO2

Figure 1.35. Spin labelled crown ethers **DB24C8_NO1** and **DB24C8_NO2.**

These structures were suitable for the preparation of two bis-TEMPO functionalized acid-base switchable rotaxanes. The first rotaxane consisted of the electron rich macrocycle **DB24C8_NO1**,[108] encircling a dumbbell containing a dibenzylammonium site (**NH_2^+**), a bipyridinium (**BPY^{2+}**) secondary site and a TEMPO stopper (**Scheme 1.7**). The shuttling of the macrocycle from the primary **NH_2^+** site to the **BPY^{2+}** station was induced by pH variations (**Scheme 1.7**). In this case, the interaction between the two radical centres was exploited for studying the shuttling process of the target acid-base switchable rotaxane using EPR spectroscopy.[108]

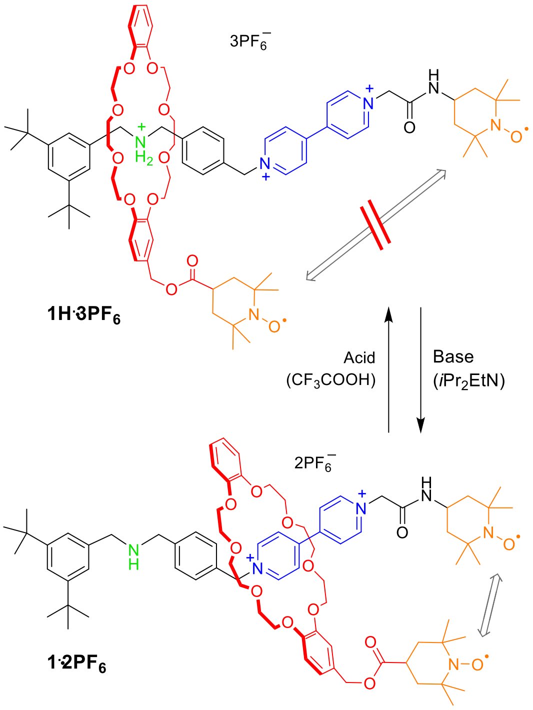

Scheme 1.7. Shuttling of the [2]-rotaxane **1H·3PF$_6$** described by Lucarini *et al.* in 2015.[108]

It was observed that the EPR spectrum of the starting rotaxane consisted of the typical three lines of an isolated TEMPO radical (g = 2.0060, a_N = 15.75 G), which indicated no interactions between the two radical moieties present in the rotaxane. As shown in **Scheme 1.7,** after deprotonation of the **NH_2^+** site by diisopropylethylamine (DIPEA), the macrocycle shuttled on the second **BPY^{2+}** site, leading to an evident change in the EPR spectrum, thus registering five lines (**Figure 1.36**). The additional lines observed were attributed to a spin-spin coupling exchange between the two radical groups in the secondary co-conformation of the rotaxane (**Scheme 1.7**). However, the relative intensity of the spectral lines was different from the characteristic 1:2:3:2:1 expected in case all the conformations of the [2]-rotaxane were characterized by strong spin exchange between the nitroxide units. Actually, owing to the relatively large flexibility of the dumbbell, the EPR spectrum of the [2]-rotaxane registered after deprotonation showed superposition of signals of non-interacting (three-line spectrum) and interacting spin labels (five-line spectrum). By measuring the relative EPR line intensities (trace b in the inset, **Figure 1.36**) it was possible to estimate that about 15% of the molecules assumed co-conformations in which the two TEMPO radicals showed a strong electron exchange ($J>a_N$).

If an acid (TFA) was added to the system, the starting state was restored and the macrocycle could shuttle back to the original site. In this case, the original EPR spectrum was observed, evidencing the reversibility of the cycle of motions.

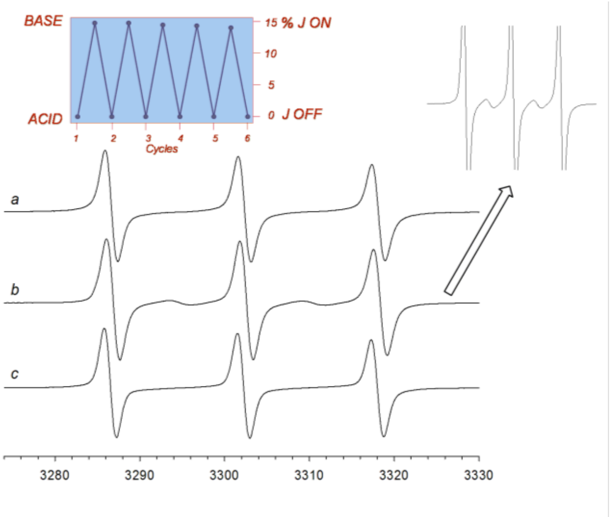

Figure 1.36. EPR spectra of **$1H{\cdot}3PF_6$** before (a) and after (b) the sequential addition of DIPEA. In-set right: zoom of spectrum (b) showing the extra exchange spectral lines. In-set left: percentage of exchange couplings versus the percentage of sequential additions of acid/base.

The case of the bis-labelled rotaxane **$1'H{\cdot}3PF_6$** containing macrocycle **DB24C8_NO2** (**Scheme 1.8**) was studied thanks to a pulsed EPR technique, called PELDOR. Lucarini *et al.* employed PELDOR spectroscopy supported by MD simulations for the measurement of the distances between the two radical groups of the rotaxane in the two co-conformations.[109] Differently from the rotaxane described above, in this case, the pH-induced movement of the macrocycle on the secondary site produced a very small variation in the distance between the two radical centres of the MIM (from 22.6 Å to 24.2 Å). Since the distance distribution between the nitroxide labels was not significantly affected by ring shuttling, a conformational variation of the crown ether was supposed occurring when the macrocycle shuttled from the **NH_2^+** site to the **BPY^{2+}** (**Scheme 1.8**). MD simulations of the EPR spectra confirmed this hypothesis.

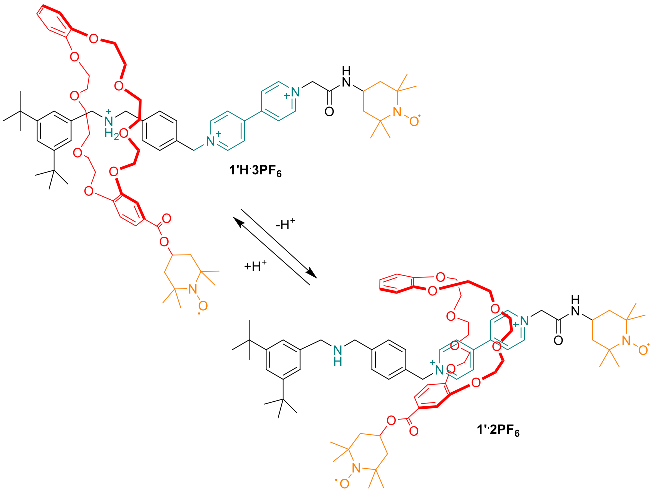

Scheme 1.8. Shuttling process causing the conformational changes of the crown ether ring of bistable acid-base switchable rotaxane **$1'H^{\cdot}3PF_6$**.

Some years ago a spin-labelled cyclobis-(paraquat-*p*-phenylene) ring (**1a**$^{\cdot}$) was synthesized and studied.[110] This molecule is among the most famous hosts employed in host-guest chemistry, because of its ability to include electron rich molecules like 1,5-dimethoxynaphthalene (**Figure 1.37**).

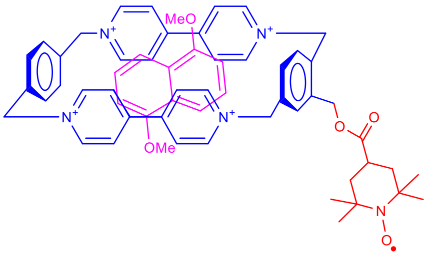

Figure 1.37. Host-guest complex between 1,5-dimethoxynaphthalene and a spin-labelled CBPQT^{4+} (**1a**$^{\cdot}$).

The spin-labelled host, **1a**$^{\cdot}$, and its diamagnetic partner **CBPQT**$^{4+}$ were employed as rings of a series of Stoddart-type [2]-rotaxanes, from **Rot1**$^{2\cdot4+}$ to **Rot6**$^{2\cdot4+}$ (**Figure 1.38**),[111] [112] [113] which were then investigated by EPR, observing the through-space spin–spin interactions between the two TEMPO moieties incorporated in the systems.

Among these, **Rot6**$^{2\cdot4+}$ was employed as redox-induced molecular switch, thanks to the possibility of reversibly displacing the ring component between the tetrathiafulvalene (**TTF**) and dioxynaphtalene (**DNP**) sites presents on the thread (**Paragraph 1.1.3**).[113] By EPR spectroscopy it was possible to observe the spin–spin exchange interactions between the TEMPO moieties and the TTF radical cation (**Figure 1.39**), deriving from the redox-induced movement of the wheel over the dumbbell. Such example confirmed EPR as an efficient technique for monitoring the movement in spin-labelled molecular machines.

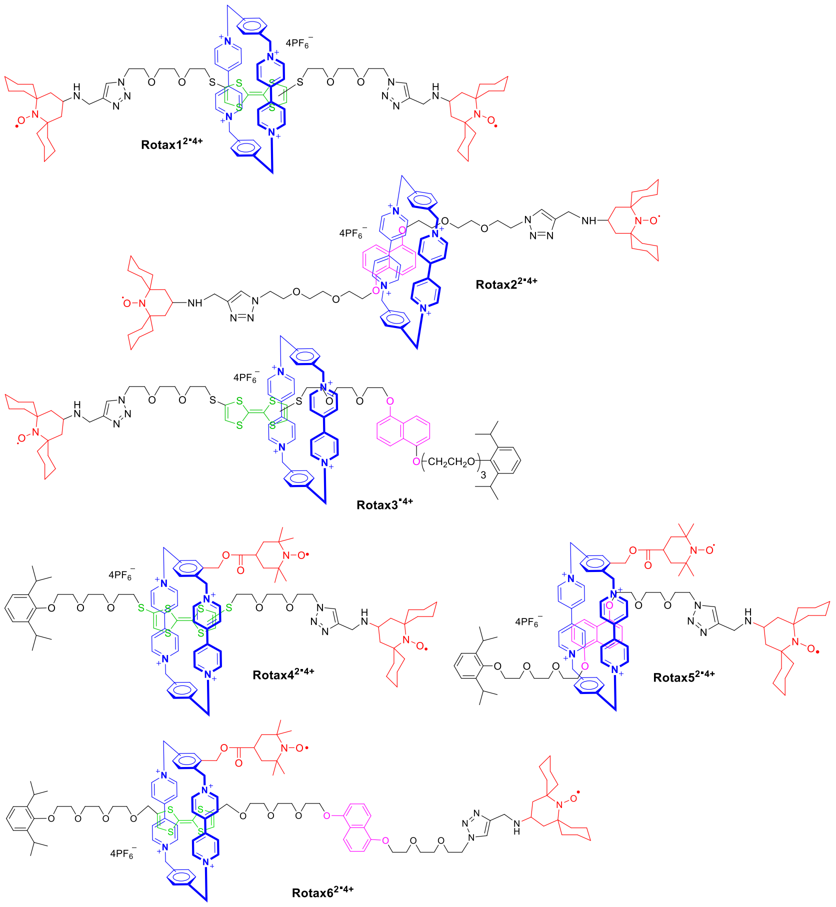

Figure 1.38. The series of Stoddart-type spin-labelled [2]-rotaxanes.

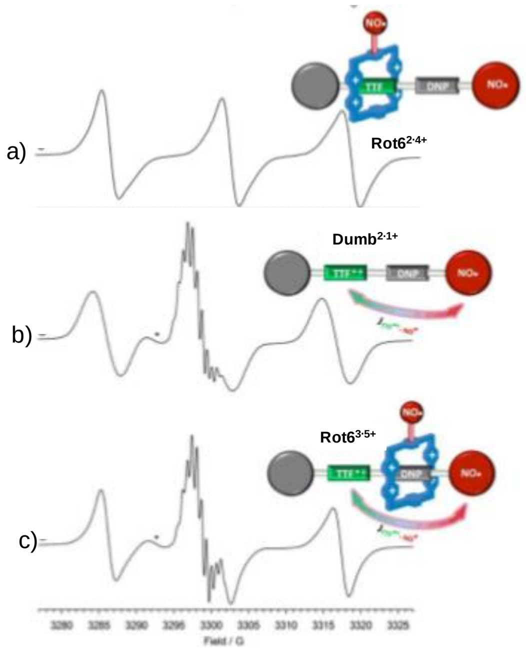

Figure 1.39. EPR spectra recorded in ACN at 328 K of: a) **Rot6**$^{2\cdot4+}$; b) Free dumbbell **Dumb**$^{2\cdot1+}$; and c) **Rot6**$^{3\cdot5+}$ after the addition of 1 equiv. of $Fe(ClO_4)_3$. Stars symbols specify exchange lines in the EPR spectrum.

1.2.4 Synthesis and EPR study of a novel paramagnetic rotaxane based on a crown-ether like macrocycle incorporating a nitroxide motif

Part of this paragraph is based on the scientific article:

V. Bleve, P. Franchi, E. Konstanteli, L. Gualandi, S. M. Goldup, E. Mezzina, M. Lucarini, ***Synthesis and EPR study of novel paramagnetic rotaxane based on a crown-ether like macrocycle incorporating a nitroxide motif****, Chem Eur. J., 2018.*

All the research described in the previous Paragraph reported the use of nitroxide radicals as external labels for probing the shuttling process in molecular switches. In those examples, the paramagnetic unit does not participate nor in non-covalent interactions or in the molecular recognition processes between the component parts of the MIM. Indeed, the preparation of rotaxanes where the nitroxide group acts as a real recognition site, directly involved in the molecular recognition process, remains unexplored. This is actually surprising considering the promising properties of nitroxides, compared with the most commonly employed recognition groups, such as amides, imines, ureas etc…[114] The dipole moment of a nitroxide is one of the highest known in chemistry and this make this class of molecules good bond acceptors,[115] able to perform hydrogen and halogen bonds,[106][116] which are very useful for molecular recognition and host-guest chemistry. In fact, the oxygen atom of a N-O·

group incorporated in a macrocyclic structure may have a key role in the interaction and complexation of ions guests situated inside the cavity.

Based on these premises, in 2018 a novel paramagnetic crown ether (**Figure 1.40**) was designed and synthesized, where the radical group was not an external "pendant" of the ring but it was part of the macrocycle itself. The dimensions of the cavity were comparable to those of common macrocycles contained in bistable rotaxanes (7 oxygen atoms).[108]

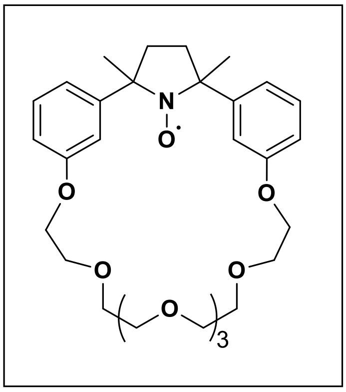

Figure 1.40. Structure of the paramagnetic macrocycle described by Bleve *et al.*

The synthesis of this compound was not easy to optimize, even if it was inspired by the work of Keana *et al.* in 1983,[117] related to the synthesis of *ortho*-substituted paramagnetic crown ethers. The complete synthetic pathway towards the target macrocycle is illustrated in **Scheme 1.9**. In this case, the final major isomer *cis*-**8** was employed for further investigations.

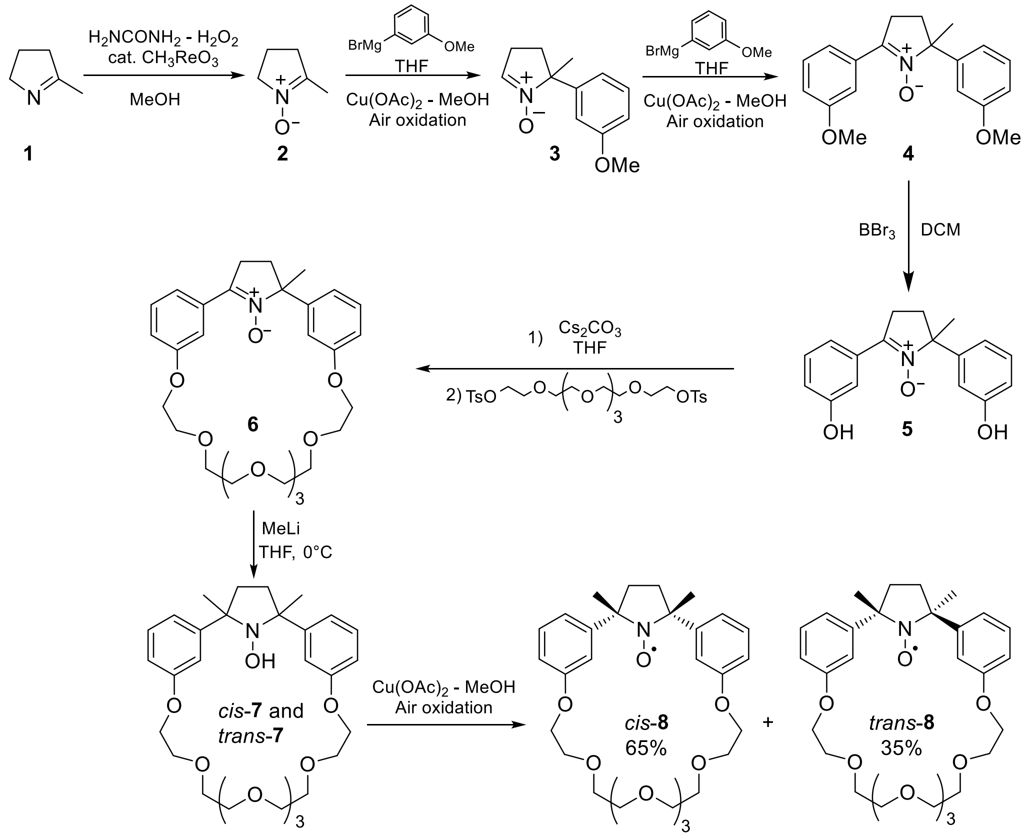

Scheme 1.9. Synthetic pathway toward macrocycle *cis*-**8.**

The macrocycle was characterized and studied by EPR spectroscopy, in order to evaluate its complexation properties towards metal and organic cationic guests. Promising EPR response towards inclusion of organic cations was observed using dibenzyl viologen salt (**DBV**). In particular, the complexation of **DBV** produced an enhancement of the nitrogen hyperfine constant (a_N) value from 14.32 G to 14.85 G. Conversely, small variations of a_N were detected in the spectrum of the paramagnetic ring in the presence of inorganic cations or dibenzylammonium (**DBA**) salt.

Even if the nature of the interaction in the case of **DBV** guest is not already clear, the a_N variation was attributed to a charge-dipole interaction between the N-O$^{\bullet}$ group and the pyridinium ion, as shown in **Scheme 1.10**.

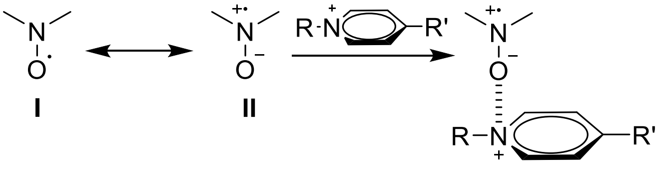

Scheme 1.10. Representation of the charge-dipole interaction between a nitroxide radical and a pyridinium unit.

Such non-covalent interaction favours the resonance structure **II** that presents a higher spin density on the nitrogen atom, thus resulting in an enhancement of the hyperfine constant value in the EPR spectrum (**Paragraph 1.2.1**). This effect was verified by performing molecular dynamic simulations, which revealed absence of interaction between the $N\text{-}O^{\bullet}$ unit and **DBA** guest, and a possible charge-dipole effect involving **DBV** guest. In addition, the complexation equilibrium constant, K_{eq}, was also determined by EPR titration, registering the variation of a_N as a function of increasing concentrations of **DBV** in a solution containing the target macrocycle (**Figure 1.41).** The resulting value of K_{eq} was comparable to that obtained for the diamagnetic crown ether **DB24C8** in the presence of **DBV** guest.[118]

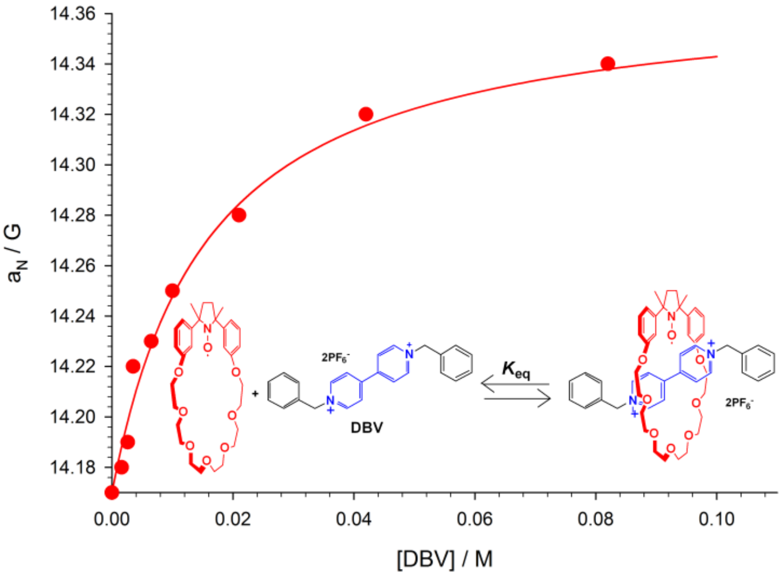

Figure 1.41. Hyperfine coupling values a_N of target macrocycle *cis*-**8** registered for increasing concentrations of **DBV**.

Thanks to these results, it was evaluated the possibility of introducing the radical macrocycle as ring in a bistable rotaxane having the classical recognition sites $\mathbf{NH_2^+}$ and $\mathbf{BPY^{2+}}$ and employable as acid-base switchable molecular machine. The rotaxane was prepared following the threading and stoppering approach illustrated in the **Paragraph 1.1.2**, achieving rotaxane **11H•3PF$_6$** (**Scheme 1.11).**

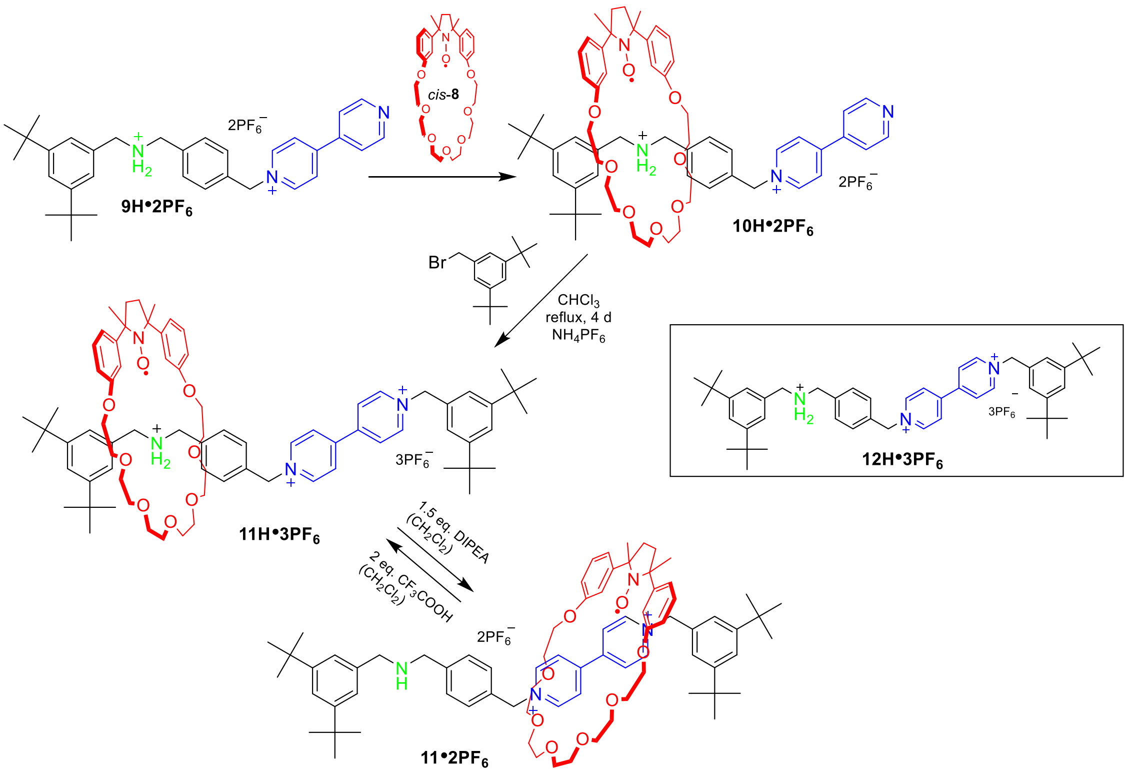

Scheme 1.11. Synthesis of the target rotaxane **$11H•3PF_6$**.

The formation of the rotaxane was verified and confirmed by ESI-MS, UV-visible, NMR and EPR spectroscopies.

As already described in **Paragraph 1.1.2,** crown ethers displayed a higher affinity for the **NH_2^+** site compared with the **BPY^{2+}** group in other similar rotaxanes. In addition, the a_N value in the EPR spectrum of the starting rotaxane was comparable to that observed during the complexation studies with **DBA** guest. For these reasons, in the starting state of rotaxane **$11H•3PF_6$**, the ring was prevalently located on the **NH_2^+** group. The pH-induced shuttling process of the ring towards the **BPY^{2+}** secondary unit was verified by EPR and UV-visible experiments. Observing UV spectra (**Figure 1.42**) after treatment of the target rotaxane with a non-nucleophile base (DIPEA),[119] a perturbation of the band at 259 nm, related to the viologen group, was observed. The deprotonation was accompanied by a *blue shift* and an enhancement of the band relative to the viologen. This result was attributed to the occurrence of a charge-dipole interaction between the $N\text{-}O^{\cdot}$ moiety and the **BPY^{2+}** unit stabilizing the ground state of the viologen group, and so affecting the UV band of the latter. On the contrary, no relevant UV spectral variations were observed after deprotonation of the free thread, confirming the hypothesis of the shuttling mechanism in the rotaxane.[48]

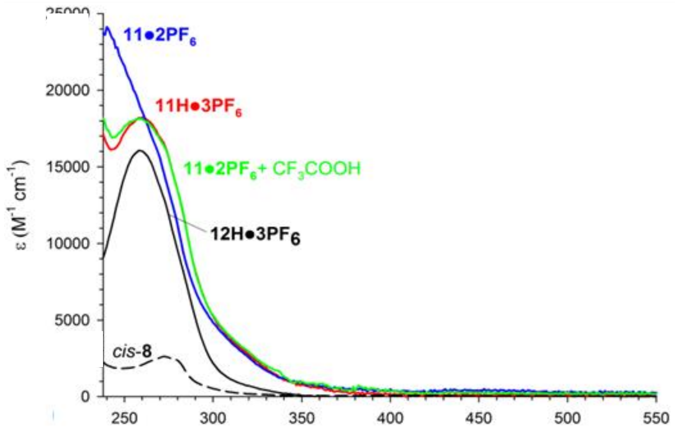

Figure 1.42. UV spectra of rotaxanes **11H•3PF$_6$** (red line) and **11•2PF$_6$** (blue line), free thread **12H•3PF$_6$** (black line), free ring (dashed line), and a mixture 1:1 of rotaxane **11•2PF$_6$** and TFA (green line)**.**

However, the most interesting evidence of the displacement was observed in the EPR experiments. In this case, after addition of one equivalent of base, we could observe a relevant increase (Δa_N = +0.43 G) of the a_N constant (**Table 1.1** and **Figure 1.43**). This increment was comparable to that obtained by the free macrocycle in the presence of **DBV** guest. The switching process led also to a slight increment of the correlation time τ from 2,0×10^{-10} to 2,6 ×10^{-10} s (**Table 1.1**)**,** which may be associated to a reduced capacity of the ring to rotate around the thread when it is located on the **BPY^{2+}** site. These spectral variations were, then, compared with the ones registered for a 1:1 mixture of free macrocycle and free thread, which showed no evident spectral perturbations. Such results, confirmed again that the registered EPR spectral changes derived from a shuttling process of the bistable rotaxane, which led to an interaction between the nitroxide radical and the secondary **BPY^{2+}** site**.** Finally, the addition of one equivalent of TFA caused the shuttling back of the ring on the **NH$_2^+$** site, restoring the initial EPR spectrum without significant variations. The cycle of motions was repeated several times without appreciable variations of the EPR parameters, evidencing the reversibility of the process.

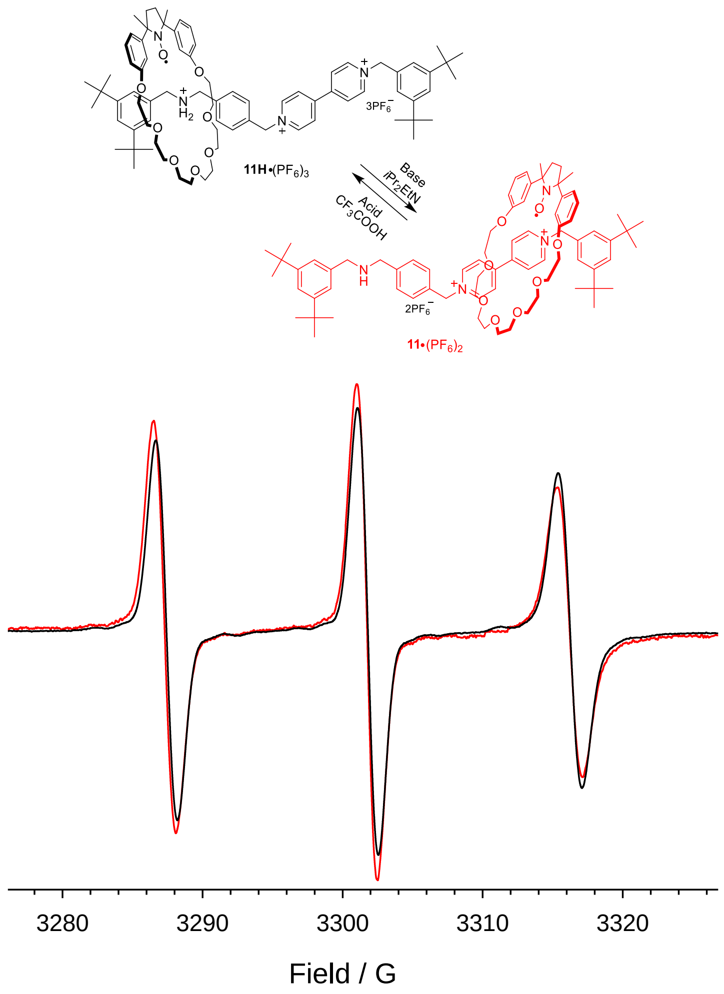

Figure 1.43. Up: pH-induced switching process of rotaxane **11H•3PF$_6$**. Down: Superimposition between the EPR spectra of rotaxanes **11H•3PF$_6$** (black line) and **11•2PF$_6$** (red line).

In conclusion, this work represented the first example of a bistable rotaxane in which the paramagnetic unit on the wheel acts as recognition site during the shuttling process of the molecular machine.[120]

Compound	a_N/G	Line width of the central line/*G*	h_0/h_{-1}	Correlation time τ / *s*
cis-**8**	14.35	1.38	1.10	4.6×10^{-11}
11H•3PF$_6$	14.39	1.42	1.47	2.0×10^{-10}
11•2PF$_6$	14.82	1.41	1.65	2.6×10^{-10}

Table 1.1. EPR parameters of the target species registered in CH_2Cl_2 at 298K.

All the previously described works have represented the starting point of this PhD thesis, which has been devoted to the synthesis and EPR investigation of novel spin-labelled architectures for applications in the field of MIMs and radical molecular machines.

REFERENCES

[1] P. O'Niel and M. A. J., What is Life? The Next Fifty Years: "Speculations on The Future of Biology", Cambridge: Cambridge University Press, 1997.

[2] J. M. Lehn, “Supramolecular Chemistry: Concepts and Perspectives,” *Wiley Connection,* 1995.

[3] D. Cram, *Angew. Chem. Int. Ed. Engl.,* vol. 27, pp. 1009-1020, 1988.

[4] D. Cram and J. Cram, “Container Molecules and Their Guests,” *The Royal Society of Chemistry*, 1994.

[5] P. L. Anelli, P. R. Ashton, R. Ballardini, V. Balzani, M. Delgado, M. T. Gandolfi, T. T. Goodnow, A. E. Kaifer, D. Philp, M. Pietraszkiewicz, L. Prodi, M. V. Reddington, A. M. Z. Slawin, N. Spencer, J. F. Stoddart, C. Vicent and D. Williams, *J. Am. Chem. Soc.* , vol. 114, p. 193–218, 1992.

[6] D. B. Amabilino and J. F. Stoddart, *Chem. Rev.*, vol. 95, p. 2725–2828, 1995.

[7] J. F. Stoddart, *Chem. Soc. Rev.* , vol. 38, p. 1802–1820, 2009.

[8] H. L. Frisch and E. Wasserman, *J. Am. Chem. Soc.* , vol. 83, p. 3789–3795, 1961.

[9] V. I. Sokolov, *Russian Chem. Rev.*, vol. 42, p. 452–463, 1973.

[10] G. Schill, Catenanes, Rotaxanes and Knots, New York: Academic Press, 1972.

[11] E. Wasserman, *J. Am. Chem. Soc.,* vol. 82, pp. 4433-4434, 1960.

[12] T. Harrison and S. J. Harrison, *J. Am. Chem. Soc.,* vol. 89, pp. 5723-5724, 1967.

[13] G. Schill and H. Zollenkopf, *Ann. Chem.,* vol. 721, p. 53–74, 1969.

[14] P. R. Ashton, D. Philip, N. Spencer and J. F. Stoddart, *J. Chem. Soc., Chem. Commun.,* p. 1677–1679. , 1991.

[15] A. Liittrighaus, F. Cramer, H. Prinzbach and F. Henglein, *Ann. Chem.,* vol. 613, pp. 185-198, 1958.

[16] P. R. Ashton, E. J. T. Chrystal, P. T. Glink, P. Menzer, C. Schiavo, N. Spencer, J. F. Stoddart, P. Tasker, A. J. P. White and D. .. Williams, *Chem. Eur. J.,* vol. 2, pp. 709-728, 1996.

[17] C. W. Chiu, C. C. Lai and S. H. Chiu, *J. Am. Chem. Soc.,* vol. 129, p. 3500–3501, 2007.

[18] J. L. Ko, S. H. Ueng, C. W. Chiu, C. C. Lai, Y. H. Liu, S. M. Peng and S. H. Chiu, *Chem. Eur. J.,* vol. 16, p. 6950–6960, 2010.

[19] I. Yoon, M. Narita, T. Shimizu and M. Asakawa, *J. Am. Chem. Soc.,* vol. 126, p. 16740–16741, 2004.

[20] W. L. Mock, T. A. Irra, J. P. Wepsiec and M. Adhya, *J. Org. Chem.* , vol. 54, p. 5302–5308, 1989 .

[21] E. Wasserman, *J. Am. Chem. Soc,* vol. 82, p. 4433–4434, 1960.

[22] J. F. Stoddart, *Angew. Chem., Int. Ed.* , vol. 53, p. 11102–11104, 2014.

[23] J. D. Crowley, S. M. Goldup, A.-L. Lee, D. A. Leigh and R. T. McBurney, *Chem. Soc. Rev.,* vol. 38, p. 1530–1541, 2009.

[24] C. Dietrich-Buchercker and J. P. Sauvage, *Tetrahedron Letters*, vol. 24, pp. 5095-5098, 1983.

[25] R. Hoss and F. Vögtle, *Angew. Chem., Int. Ed. Engl.* , vol. 33, p. 375–384, 1994.

[26] T. J. Hubin and D. H. Busch, *Coord. Chem. Rev.* , vol. 200, p. 5–52, 2000.

[27] B. H. Northrop, F. Aricó, N. Tangchiavang, J. D. Badjić, and J. F. Stoddart, *Org. Lett.,* vol. 8, p. 3899-3902, 2006.

[28] I. Goldberg, Complexes of Crown Ethers with Molecular Guests, London: Academic Press, 1984.

[29] J. S. Bradshaw, R. M. Izatt, A. V. Bordunov, C. Y. Zhu and J. K. Hathaway, Crown Ethers, Oxford: Pergamon, 1997.

[30] C. J. Pedersen, *J. Am. Chem. Soc.* , vol. 89, p. 2495, 1967.

[31] P. T. Glink, C. Schiavo, J. F. Stoddart and D. J. Williams, *Chem. Commun.* , vol. 19, p. 1483–1490, 1996.

[32] D. Thibeault and J. F. Morin, *Molecules*, vol. 15, p. 3709–3730, 2010.

[33] A. Späth and B. König, *J. Org. Chem.* , vol. 6, p. 32, 2010.

[34] P. R. Ashtona, R. A. Bartschb, S. J. Cantrillc, R. E. Hanes, J. S. K. Hickingbottom, J. N. Lowec, J. A. Preece, J. F. Stoddart, V. S. Talanov and Z. H. Wang, *Tetrahedron Letters,* vol. 40, no. 19, pp. 3661-3664, 1999.

[35] P. R. Ashton, P. J. Campbell, E. J. T. Chrystal, P. T. Glink, S. Menzer, D. Philp, N. Spencer, J. F. Stoddart, P. A. Tasker and D. J. Williams, *Angew. Chem., Int. Ed. Engl.*, vol. 34, p. 1865–1869, 1995.

[36] S. Dasgupta and J. Wu, *Chem. Sci.* , vol. 3, p. 425–432, 2012.

[37] C. Zhang, S. Li, J. Zhang, K. Zhu, N. Li and F. Huang, *Org. Lett.,* vol. 9, p. 5553–5556, 2007.

[38] J. W. Jones and H. W. Gibson, *J. Am. Chem. Soc.,* vol. 125, p. 7001–7004, 2003.

[39] H. W. Gibson, J. W. Jones, L. N. Zakharov, A. L. Rheingold and C. Slebodnick, *Chem. Eur. J.* , vol. 17, p. 3192–3206, 2011.

[40] A. B. Braunschweig, C. M. Ronconi, J. Y. Han, F. Aricó, S. J. Cantrill, J. F. Stoddart, S. I. Khan, A. J. P. White and D. J. Williams, *J. Org. Chem.*, p. 1857–1866., 2006.

[41] K. Nakazono, T. Oku and T. Takata, *Tetrahedron Lett.* , vol. 48, p. 3409–3411, 2007.

[42] P. N. Cheng, P. Y. Huang, W. S. Li, S. H. Ueng, W. C. Hung, Y. H. Liu, C. C. Lai, Y. Wang, S. M. Peng, I. Chao and S. H. Chiu, *J. Org. Chem.*, vol. 71, p. 2373–2383, 2006.

[43] F. Coutrot, E. Busseron and J. L. Montero, *Org. Lett.*, vol. 10, pp. 753-756, 2008.

[44] H. Kawasaki, N. Kihara and T. Takata, *Chem. Lett.*, pp. 1015-1016, 1999.

[45] S. Rowan, S. J. Cantrill and J. F. Stoddart, *Org. Lett.*, vol. 1, pp. 129-132, 1999.

[46] V. Balzani, A. Credi and M. Venturi, Molecular Devices and Machines: Concepts and Perspectives for the NanoWorld, Weinheim: Wiley-VCH, 2008.

[47] C. J. Burns and J. F. Stoddart, The Nature of the Mechanical Bond, Wiley Publications, 2017.

[48] P. R. Ashton, R. Ballardini, V. Balzani, I. Baxter, A. Credi, M. C. T. Fyfe, M. T. Gandolfi, M. Gomez-Lopez, M. V. Martinez-Diaz, A. Piersanti, N. Spencer, J. F. Stoddart, M. Venturi, A. J. P. White and D. J. Williams, *J. Am. Chem. Soc.*, vol. 120, pp. 11932-11942, 1998.

[49] V. Bermudez, N. Capron, T. Gase, F. G. Gatti, F. Kajzar, D. A. Leigh, F. Zerbetto and S. W. Zhang, *Nature*, vol. 406, pp. 608-611, 2000.

[50] R. Ballardini, V. Balzani, M. T. Gandolfi, L. Prodi, M. Venturi, D. Philp, H. G. Ricketts and J. F. Stoddart, *Angew. Chem. Int. Ed.*, vol. 32, pp. 1301-1303, 1993.

[51] J. R. Heath and M. A. Ratner, *Phys. Today* , vol. 56, pp. 43-49, 2003.

[52] M. A. Reed and J. M. Tour, *Sci. Am.* , vol. 282, pp. 86-93, 2000.

[53] Y. Luo, C. P. Collier, J. O. Jeppesen, K. A. Nielsen, E. Delonno, G. Ho, J. Perkins, H.-R. Tseng, T. Yamamoto, J. F. Stoddart, T. Heathamoto, J. F. Stoddart, a. T. Heath, J. F. Stoddart and J. R. Heath, *ChemPhysChem* , vol. 3, pp. 519-525, 2002.

[54] D. G. Truhlar, B. C. Garret and S. J. Klippestain, *J. Phys. Chem.*, vol. 100, pp. 12771-12800, 1996.

[55] N. N. P. Moonen, A. H. Flood, J. M. Fernandez and S. J. F., *Top Curr. Chem.*, vol. 262, pp. 99-132, 2005.

[56] A. C. Benninston, *Chem. Soc. Rev.*, vol. 25, pp. 427-435, 1996.

[57] V. Balzani, A. Credi, G. Mattersteig, O. A. Matthews, F. M. Raymo, J. F. Stoddart, M. Venturi, A. J. P. White and D. J. Williams, *J. Org. Chem.* , vol. 65, pp. 1924-1936, 2000.

[58] H. R. Tseng, S. A. Vignon and J. F. Stoddart, *Angew. Chem., Int Ed.,* vol. 42, pp. 1491-1495, 2003.

[59] K. Nikitin and D. Fitzmaurice, *J. Am. Chem. Soc.* , vol. 127, pp. 8067-8076, 2005.

[60] C. P. Collier, G. Mattersteig, E. W. Wong, Y. Luo, K. Beverly, J. Sampaio, F. M. Raymo, J. F. Stoddart and J. R. Heath, *Science* , vol. 289, pp. 1172-1175, 2000.

[61] B. Brough, B. H. Northrop, J. J. Schmidt, H.-R. Tseng, K. N. Houk, J. F. Stoddart and C.-M. Ho, *PNAS,* vol. 103, pp. 8583 - 8588, 2006.

[62] G. Ragazzon, C. Schäfer, P. Franchi, S. Silvi, B. Colasson, M. Lucarini and A. Credi, *PNAS,* vol. 115, p. 9385–9390, 2018.

[63] W. Gerlach and O. Stern, *Zeitschrift für Physik,* vol. 9, pp. 349-352, 1922.

[64] S. Uhlenbeck and G. E. Goudsmit, *Physica,* vol. 6, pp. 273-290, 1926.

[65] E. Zavoisky, *Fizicheskiĭ Zhurnal,* vol. 211, pp. 211-245, 1945.

[66] Electron Paramagnetic Resonance: a practitioner's toolkit, Hoboken: John Wiley & Sons Inc., 2009.

[67] M. Lucarini, "Electron Spin Resonance (ESR) of Organic Free Radicals: selected examples from the literature".

[68] R. S. Shankland, *Physics Today.,* vol. 27, p. 37–43., 1974.

[69] M. Abe, *Chem. Rev.* , vol. 113, p. 7011–7088, 2013.

[70] J. A. Weil, J. R. Bolton and J. E. Wertz, Electron Paramagnetic Resonance: Elementary Theory and Practical Applications, New York: Wiley, 1994.

[71] N. M. Atherton, Principles of Electron Spin Resonance, Chichester: Ellis Horwood and Prentice Hall, 1993.

[72] R. G. Hicks, "Stable Radicals Fundamentals and Applied Aspects of Odd-Electron Compounds", John Wiley & Sons Ltd., 2010.

[73] D. Griller and K. U. Ingold, *Acc. Chem. Res.,* vol. 9, p. 13, 1976.

[74] R. I. Zhdanov, Bioactive Spin Labels I and II, Heidelberg: Springer-Verlag, 1992.

[75] L. J. Berliner, Spin-labelling. Theory and Applications. I and II, New-York: Academic Press;, 1976, 1979.

[76] P. Kuppusamy, P. Wang and J. L. Zweier, *Magn. Reson. Chem.* , vol. 33, pp. 123-128, 1995.

[77] A. Iannone, A. Tomasi, V. Quaresima and M. Ferrari, *Res. Chem. Intermed.* , vol. 19, pp. 715-731, 1993.

[78] J. F. W. Keana, L. Lex, J. S. Mann, J. M. May, J. H. Park, S. Pou, V. S. Prabhu, G. M. Rosen, B. J. Sweetman and Y. Wu, *Pure Appl. Chem.*, vol. 62, p. 201–205, 1990.

[79] G. Sosnovsky, N. U. M. Rao, S. W. Li and H. M. Swartz, *J. Org. Chem.* , vol. 54, p. 3667–3674, 1989.

[80] P. Kuppusamy, M. Chzan and J. L. Zweier, *J. Magn. Resonance Ser. B* , vol. 106, pp. 122-130, 1995.

[81] A. Sotgiu, G. Placidi, G. Gualtieri, C. Tatone and C. Campanella, *Magn. Reson. Chem.* , vol. 33, pp. 160-165, 1995.

[82] F. Hyodo, K. Matsumoto, A. Matsumoto, J. B. Mitchell and M. C. Krishna, *Cancer Res.*, vol. 66, p. 9921–9928, 2006.

[83] A. P. Jagtap, I. Krstic, N. C. Kunjir, R. Hansel, T. F. Prisner and S. T. Sigurdsson, *Free Radical Res.* , vol. 49, p. 78−85, 2015.

[84] G. Karthikeyan, A. Bonucci, G. Casano, G. Gerbaud, S. Abel, V. Thome, L. Kodjabachian, A. Magalon, B. Guigliarelli, V. Belle, O. Ouari and E. Mileo, *Angew. Chem.* , vol. 130, p. 1380−1384., 2018.

[85] E. G. Bagryanskaya and S. R. A. Marque, *Electron Paramag. Reson.,* vol. 25, pp. 180-235, 2017.

[86] E. Mezzina, R. Manoni, F. Romano and M. Lucarini, *Asian J. Org. Chem.,* vol. 4, pp. 296-310, 2015.

[87] M. Lucarini, Encyclopedia of Radicals in Chemistry, Biology and Materials, Vol. 1, Chichester: Wiley, 2012.

[88] D. Bardelang, M. Hardy, O. Ouari and P. Tordo, Encyclopedia of Radicals in Chemistry, Biology and Materials, Vol. 4, Chichester: Wiley, 2012.

[89] T. J. Stone, T. Buckam, T. L. Nordio and H. M. McConnel, *Proc. Nat. Acad. Sci. U. S. A.*, vol. 54, pp. 1010-1017, 1965.

[90] M. Bennati and T. F. Prisner, *Rep. Prog. Phys,* vol. 68, pp. 411-448, 2005.

[91] O. H. Griffith and P. C. Jost, Lipid spin labels in biological membranes, in Spin Labeling: Theory and Applications, New York: L. J. Berliner, Academic Press, 1976.

[92] H. M. McConnel, Molecular motion in biological membranes, in Spin Labeling: Theory and Applications, New York: L. J.Berliner, Acedemic Press, 1976.

[93] M. A. Hemminga and L. J. Berliner, ERS spectroscopy in membrane biophysics, in Biological and Magnetic Resonance, New York: Springer, 2007.

[94] M. Lucarini, B. Luppi, G. F. Pedulli and B. P. Roberts, *Chem. Eur. J.*, vol. 5, pp. 2048-2054, 1999.

[95] P. Franchi, C. Casati, E. Mezzina and M. Lucarini, *Org. Biomol. Chem.*, vol. 9, pp. 6396-6401, 2011.

[96] T. Oshikiri, Y. Takashima, H. Yamaguchi and A. Harada, *J. Am. Chem. Soc.*, vol. 127, pp. 12186-12187, 2005.

[97] P. Franchi, M. Lucarini and G. F. Pedulli, *Angew. Chem. Int. Ed.*, vol. 42, pp. 1842-1845, 2003.

[98] Cucurbiturils. Chemistry, Supramolecular Chemistry and Applications, London: World Scientific Publishing Europe Ltd, 2018.

[99] E. Mezzina, F. Cruciani, G. F. Pedulli and M. Lucarini, *Chem. Eur. J.*, vol. 13, pp. 7223-7233, 2007.

[100] E. Mezzina, F. Cruciani, G. F. Pedulli and M. Lucarini, *Chem. Eur. J.*, vol. 13, pp. 7223-7233, 2007.

[101] M. Okazaki and K. Kuwata, *J. Phys. Chem.*, vol. 88, pp. 3163-3165, 1984.

[102] P. Franchi, M. Lucarini, G. F. Pedulli and D. Sciotto, *Angew. Chem. Int. Ed.*, vol. 39, pp. 263-266, 2000.

[103] D. Bardelang, K. Banaszak, H. Karoui, A. Rockenbauer, M. Waite, K. Udachin, J. A. Ripmeester, C. I. Ratcliffe, O. Ouari and P. Tordo, *J. Am. Chem. Soc.*, vol. 131, pp. 5402-5404., 2009.

[104] M. Boccalon, S. Bidoggia, F. Romano, L. Gualandi, P. Franchi, M. Lucarini, P. Pengo and L. Pasquato, *J. Mater. Chem. B*, vol. 3, pp. 432 - 439, 2015.

[105] G. R. Hanson, P. Jensen, J. McMurtrie, L. Rintoul and A. S. Micallef, *Chem. Eur. J.*, vol. 15, pp. 4156-4164, 2009.

[106] L. Gualandi, E. Mezzina, P. Franchi and M. Lucarini, *Chem. Eur. J.*, vol. 22, pp. 16017-16021, 2016.

[107] C. Casati, P. Franchi, R. Pievo, E. Mezzina and M. Lucarini, *J. Am. Chem. Soc.*, vol. 134, pp. 19108-19117, 2012.

[108] V. Bleve, C. Schäfer, P. Franchi, S. Silvi, E. Mezzina, A. Credi and M. Lucarini, *ChemistryOpen*, vol. 4, p. 18–21, 2015.

[109] P. Franchi, V. Bleve, E. Mezzina, C. Schaefer, G. Ragazzon, M. Albertini, D. Carbonera, A. Credi, M. DiValentin and M. Lucarini, *Chem. Eur.J.,* vol. 22, pp. 8745 - 8750, 2016.

[110] A. Margotti, C. Casati, M. Lucarini and E. Mezzina, *Tetrahedron Lett.*, vol. 49, pp. 4784-4787, 2008.

[111] R. Manoni, F. Romano, C. Casati, P. Franchi, E. Mezzina and M. Lucarini, *Org. Chem. Front.*, vol. 1, pp. 477-483, 2014.

[112] F. Romano, R. Manoni, P. Franchi, E. Mezzina and M. Lucarini, *Chem. Eur. J.,* vol. 21, pp. 2775-2779, 2015.

[113] V. Bleve, P. Franchi, L. Gualandi, F. Romano, E. Mezzina and M. Lucarini, *Org. Chem. Front.,* vol. 5, pp. 1579-1585, 2018.

[114] Comprehensive Supramolecular Chemistry, Oxford: J. M. Lehn Pergamon, 1996.

[115] N. Kocherginsky and H. M. Swartz, Nitroxide Spin Labels: Reactions in Biology and Chemistry, Boca Raton: CRC press, 1995.

[116] P. L. M. Franchi, P. Pedrielli and G. F. Pedulli, *ChemPhysChem,* vol. 3, pp. 789-793, 2002.

[117] J. F. W. Keana, J. Cuomo, L. Lex and S. S. E., *J. Org. Chem.*, vol. 48, pp. 2647-2654, 1983.

[118] A. B. Braunschweig, C. M. Ronconi, J. Y. Han, F. Aricó, S. J. Cantrill, J. F. Stoddart, S. I. Khan, A. J. P. White and D. J. Williams, *Eur. J. Org. Chem.*, p. 1857–1866, 2006.

[119] M. V. Martínez-Díaz, N. Spencer and J. F. Stoddart, *Angew. Chem. Int. Ed. Engl.,* vol. 36, p. 1904–1907, 1997.

[120] V. Bleve, P. Franchi, E. Konstanteli, L. Gualandi, S. M. Goldup, E. Mezzina and M. Lucarini, *Chem. Eur. J.,* vol. 24, p. 1198, 2018.

CHAPTER 2: AIM OF THE THESIS

In the course of the last decades, supramolecular chemists have designed several examples of artificial molecular machines based on MIMs (*i.e.* rotaxanes and catenanes) able to perform a large number of molecular dynamics under the influence of external stimuli (**Paragraph 1.1.3**).[1][2][3] However, the target of design autonomous, continuous, efficient and ecological molecular machines, able to mimic the features of the biological partners, is still challenging a large number of scientists.[4][5]

Dialkyl nitroxide radicals are an important class of organic compounds largely employed in many fields of chemistry and related sciences.[6] However, the use of nitroxides in supramolecular chemistry, host-guest chemistry processes and, in particular, in the field molecular machines, has not been largely explored until now. This is somewhat surprising given the intrinsic properties of nitroxides: the dipole moment of the nitroxide group is one of the highest between the functional groups known in chemistry and this make this class of molecules potentially useful for molecular recognition, host-guest chemistry and synthesis of MIMs. During the last years, some relevant examples of paramagnetic supramolecular architectures have been reported, where the nitroxide unit plays a key role both in the investigation of the dynamics of the target systems and in the recognition processes (**Paragraph 1.2.3**).[7][8][9][10]

Proceeding on this line, the aim of this thesis has been focused on the design, synthesis and EPR investigation of new supramolecular architectures and MIMs containing paramagnetic groups (*i.e.* nitroxides), in view of interesting applications in the fields of radical chemistry and molecular machinery.

The first research project (**Chapter 3**) concerned the EPR reduction kinetics studies of two synthetic paramagnetic macrocycles incorporating a nitroxide group inside their cavity (**Figure 2.1**).[10] Compared with other organic radicals (such as TEMPO) employed for *in vivo* EPR investigations, these compounds displayed interesting persistence and bio-resistance properties, which, together with their water solubility, make them suitable for many biological applications.

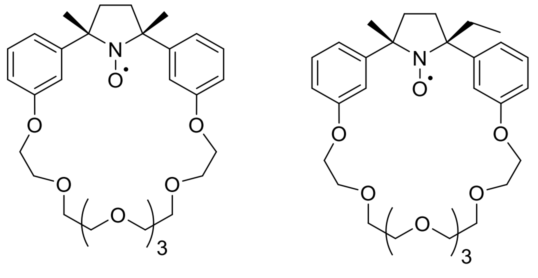

cis-**1** *cis*-**2**

Figure 2.1. Paramagnetic macrocycles reported by our research group.

Chapter 4 will describe the use of 2-phenyl-2-cyanopropanoic acid[4] as single fuel for triggering the full back and forth motions of a recently proposed bistable acid-base switchable paramagnetic rotaxane (**R1•(PF$_6$)$_2$**, **Scheme 2.1**). For the first time, EPR spectroscopy was employed to demonstrate and monitor the full cycle of movement of the paramagnetic rotaxane.[11] In addition, the studies confirmed that decarboxylative acids, such as 2-phenyl-2-cyanopropanoic acid, can be employed efficiently as chemical fuels for affording only-one-fuel switchable diamagnetic and paramagnetic molecular machines based on acid-base stimuli.

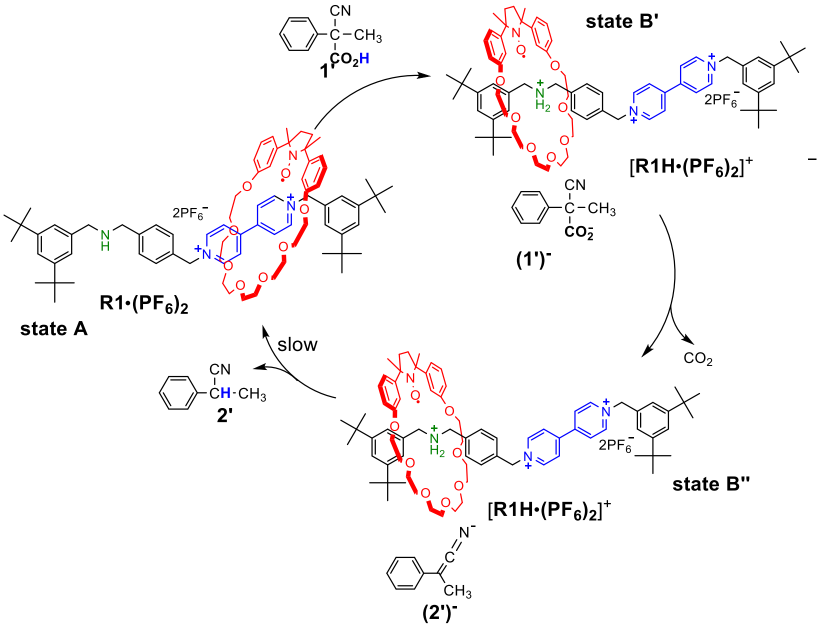

Scheme 2.1. Switching motions of rotaxane **R1•(PF$_6$)$_2$** fuelled by decarboxylative acid **1′**.

Successively, a further step towards the obtainment of autonomous and continuous molecular machines was made, which is illustrated in **Chapter 5.** Herein, the cycle of oxidation of alcohols catalysed by nitroxides was exploited for the achievement of an autonomous and continuous molecular switch based on an aerobic catalytic cycle (**Scheme 2.2**). The reduction of the oxoammonium group incorporated in the ring of a bistable rotaxane (**R1ox·(PF$_6$)$_2$NO$_3$**), powers the ring motion over the dumbbell leading to **R1·(PF$_6$)$_2$**, and in the presence of oxygen and cerium ammonium nitrate (CAN) as co-catalysts the continuous recycle of reactants was guaranteed. GC-MS studies and EPR spectroscopy were employed for monitoring and verifying the whole process under different reaction conditions.

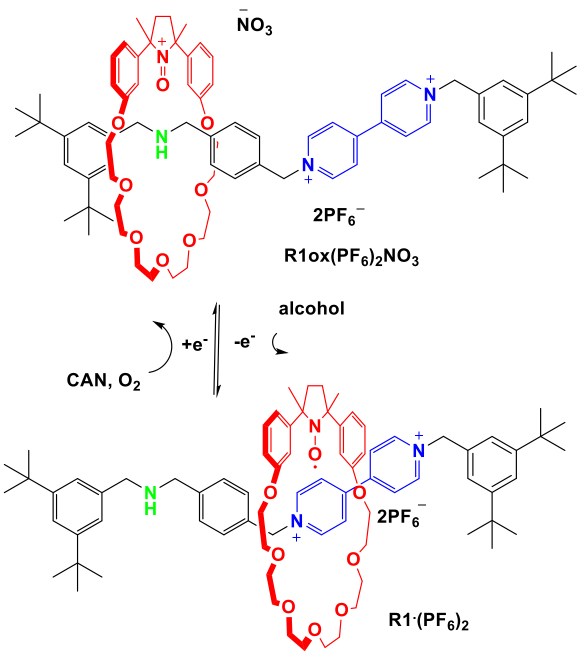

Scheme 2.2. Redox-driven switching motions of the bistable rotaxane **R1$^{\cdot}$(PF$_6$)$_2$** containing a nitroxide moiety.

Chapter 6 focuses on describing the synthesis and EPR characterization of a new paramagnetic macrocycle with enhanced complexation properties and sensitivity for several cationic guests. The novel paramagnetic macrocycle contains a nitroxide moiety incorporated in a crown ether-like wheel (**AC7O$^{\cdot}$**, **Figure 2.2**). In this case, the better exposure of the paramagnetic unit into the cavity provided a higher participation of the latter in the complexation processes, enhancing the EPR sensitivity of the substrate toward inclusion of several cationic guests. The inclusion of different organic and inorganic guests into the target host was investigated by means of EPR spectroscopy. In addition, the affinity of the macrocycle towards the target guests was estimated calculating the complexation equilibrium constants K_a.

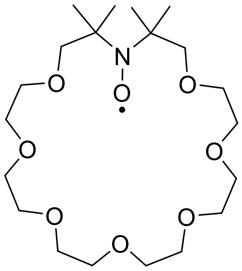

Figure 2.2 Structure of macrocycle **AC7O$^{\cdot}$.**

REFERENCES

[1] S. Kassem, T. van Leeuwen, A. S. Lubbe, M. R. Wilson, B. L. Feringa and D. A. Leigh, *Chem. Soc. Rev.*, vol. 46, pp. 2592-2621, 2017.

[2] *ChemistryOpen* , vol. 7, p. 169–179, 2018.

[3] *Nature,* vol. 369, pp. 133-137, 1994.

[4] J. A. Berrocal, C. Biagini, L. Mandolini and S. Di Stefano, *Angew. Chem. Int. Ed.*, vol. 55, pp. 6997-7001, 2016.

[5] M. R. Wilson, J. Solà, A. Carlone, S. M. Goldup, N. Lebrasseur and D. A. Leigh, *Nature* , vol. 534, pp. 235-240, 2016.

[6] G. I. Likhtenshtein, J. Yamauchi, S. Nakatsuji, S. Smirnov and R. Tamura, Nitroxides: Applications in Chemistry, Biomedicine and Materials Science, Winnehim: Wiley-VCH, 2008.

[7] V. Bleve, C. Schfer, P. Franchi, S. Silvi, E. Mezzina, A. Credi and M. Lucarini, *ChemistryOpen*, vol. 4, pp. 18 - 21, 2015.

[8] P. Franchi, V. Bleve, E. Mezzina, C. Schaefer, G. Ragazzon, M. Albertini, D. Carbonera, A. Credi, M. DiValentin and M. Lucarini, *Chem. Eur.J.*, vol. 22, pp. 8745 - 8750, 2016.

[9] V. Bleve, P. Franchi, L. Gualandi, F. Romano, E. Mezzina and M. Lucarini, *Org. Chem. Front.*, vol. 5, pp. 1579 -1585, 2018.

[10] V. Bleve, P. Franchi, E. Konstanteli, L. Gualandi, S. M. Goldup, E. Mezzina and M. Lucarini, *Chem. Eur. J.*, vol. 24, pp. 1198-1203, 2018.

[11] P. Franchi, C. Poderi, E. Mezzina, C. Biagini, S. Di Stefano and M. Lucarini, *J. Org. Chem.*, vol. 84, no. 14, pp. 9364-9368, 2019.

CHAPTER 3: REDUCTION KINETICS OF PARAMAGNETIC MACROCYCLES BASED ON NITROXIDE RADICALS

3.1 INTRODUCTION

Stable nitroxides are commonly employed in many biological applications, such as spin labelling and probing,[1][2][3] magnetic resonance imaging (MRI) and electron paramagnetic resonance imaging (EPRI) (**Paragraph 1.2.2**).[4][5][6][7][8] However, the rapid *in vivo* reduction of nitroxide probes to hydroxylamines, which are silent to EPR, represents a significant limitation for their EPR detection, thus, restricting their use in bio-investigations.[9] For this reason, the design of bio-resistant nitroxides became crucial for their application in novel research technologies. In the last years, several studies have been devoted to the design of novel persistent nitroxides and to the EPR investigation of their reduction in biological media. It is well known that the increment of the steric hindrance of the β alkyl substituents in nitroxide radicals represents an efficient method to increase their lifetime.[10][11][12] In addition, also the ring size can influence the persistence of the nitroxide group. In fact, five membered nitroxides,[13][14][15] in particular tetraethyl-substituted pyrrolidine nitroxides, are generally the most effectively employed for *in vivo* NMR and EPR imaging, because of their resistance against reduction.

Our research group has recently described the synthesis and characterization of a novel paramagnetic macrocycle (**Paragraph 1.2.4**) based on a crown-ether like structure incorporating a pyrrolidine nitroxide motif (**Figure 3.1, left**).[16] In order to assess the usefulness of these new spin probe in biological application, it was of prime importance to investigate its resistance to bio-reduction. To this aim, EPR kinetic studies were performed on the paramagnetic macrocycle *cis*-**1,** and on its mono-ethylated derivative, *cis*-**2** (**Figure 3.1 right**).

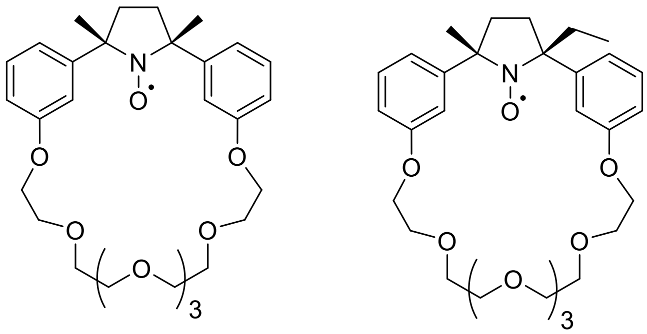

cis-**1** *cis*-**2**

Figure 3.1. Paramagnetic macrocycles investigated.

3.2 REDUCTION KINETICS OF TWO PARAMAGNETIC MACROCYCLES BASED ON NITROXIDE RADICALS

3.2.1. Synthesis and characterization

The synthesis of compound *cis*-**2** was afforded by adapting the synthetic procedure described for precursor *cis*-**1**,[16] achieving the final compound with a 20% overall yield (**Scheme 3.1**).

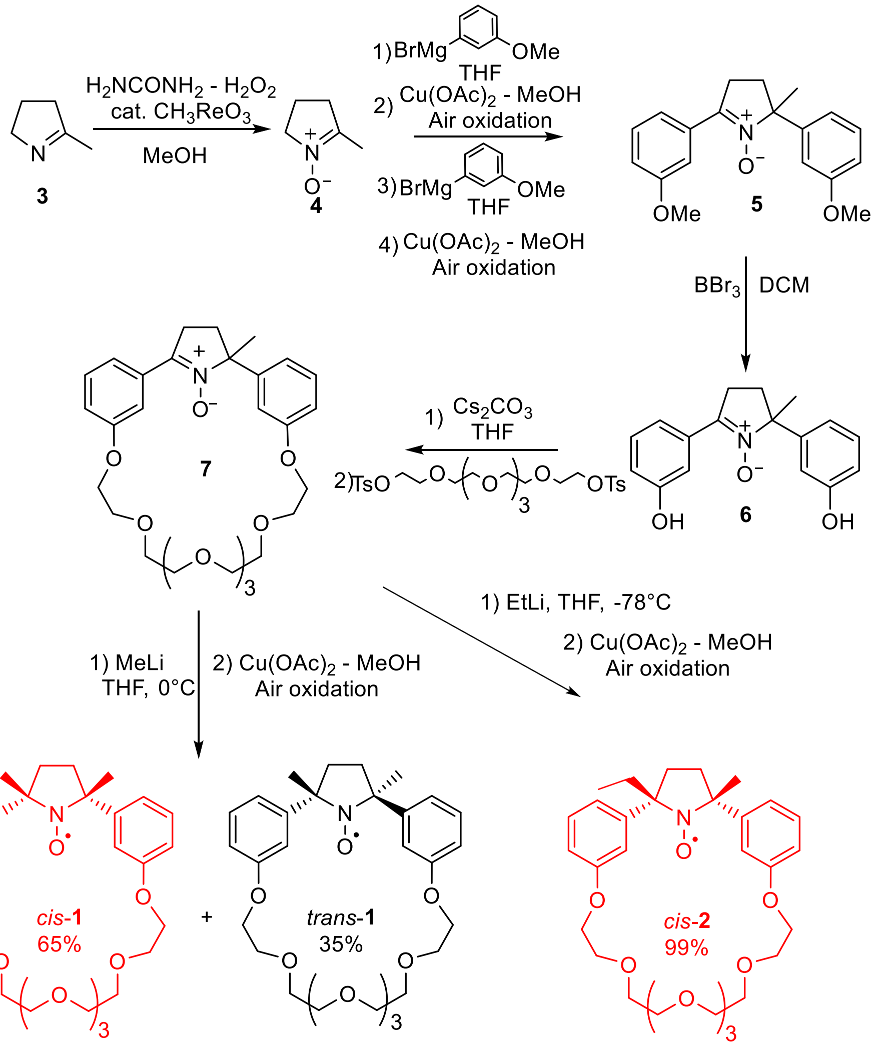

Scheme 3.1. Reaction scheme for the synthesis of macrocycles *cis*-**1** and *cis*-**2**.

A crucial step of this synthesis, already experienced during the preparation of *cis*-**1,** was the alkylation of the β carbon of compound **7**, which could theoretically lead to two possible isomers (*cis* and *trans*). Since it was not possible to obtain a crystal structure of the compound for X-ray analysis, we relied on *Shibata et al.* model [17] for the assignment of the stereochemistry of the major compound. This model affirms that the β attack of the organo-lithium prevalently occurred at the less hindered face of the five-member ring and in particular, on the opposite side of the bulky phenyl substituent present on the other β carbon of **7**, providing favourably the *cis* major isomer. However, differently from the 65:35 *cis:trans* ratio registered for macrocycle *cis*-**1**,[16] the ethyl attack at compound **7** (**Scheme 3.1**) provided only one single isomer (*cis*), which was directly oxidized to afford compound *cis*-**2**. This effect was attributed to the higher steric hindrance of the ethyl compared the methyl group of **1**, which significantly favoured the *cis* attack. ^{1}H-NMR experiments were performed by *in situ* oxidation of compound *cis*-**2** to oxoammonium salt using 5 equivalents of cerium ammonium nitrate (CAN) and confirmed the presence of the peaks relatives to a single isomer (**Figure 3.2**).

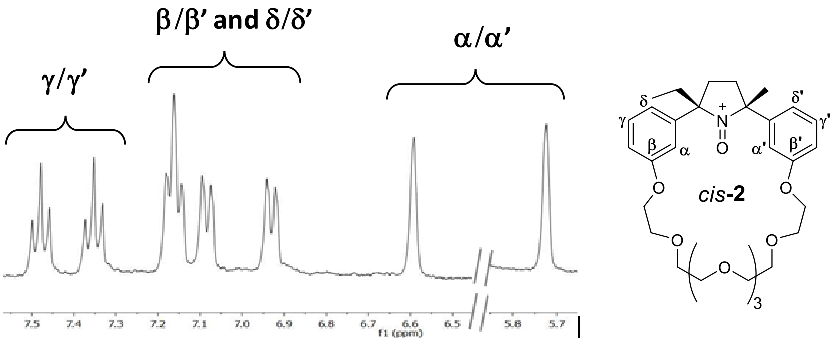

Figure 3.2. Partial ^{1}H NMR spectrum (400 MHz, CD_3CN, 298 K) of *cis*-**2** oxidized *in situ* with 5 eq. of CAN.

The *cis* major isomers of both macrocycles **1** and **2** were employed for the further investigations and kinetic studies.

3.2.2 Kinetic studies

The reduction kinetics of the target macrocycles *cis*-**1** and *cis*-**2** were evaluated by means of EPR spectroscopy. Ascorbate is the most popular reductant employed for the reduction kinetic studies of nitroxides.[10][11][12][13] It is a micronutrient largely present in biological systems and involved in multiple biological processes, such as post-translational hydroxylation of collagen, biosynthesis of carnitine, conversion of the neurotransmitter dopamine to norepinephrine, peptide amidation and tyrosine metabolism. The reaction of ascorbate with nitroxides in biological systems leads to ascorbate radical and the corresponding diamagnetic hydroxylamines, which are silent at EPR, resulting in a progressive decay of the EPR signal related to the nitroxide radical (**Scheme 3.2**).

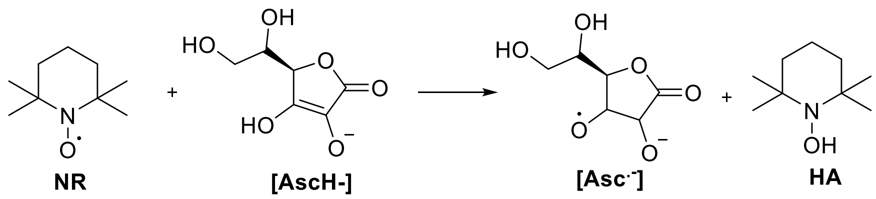

Scheme 3.2. Representation of the general mechanism of nitroxide reduction mediated by ascorbate.

Mechanistic studies[18] of the reduction of nitroxide radicals in the presence of ascorbate have evidenced that the reaction proceeds through several stages, as indicated in **Scheme 3.3**.

$$\mathrm{NR + AscH^-} \underset{k_{-1}}{\overset{k_1}{\rightleftharpoons}} \mathrm{HA + Asc^{\bullet -}} \qquad \textbf{(1)}$$

$$\mathrm{Asc^{\bullet -} + Asc^{\bullet -} + H^+} \underset{k_{-2}}{\overset{k_2}{\rightleftharpoons}} \mathrm{AscH^- + DHA} \qquad \textbf{(2)}$$

$$\mathrm{HA + DHA} \underset{k_{-3}}{\overset{k_3}{\rightleftharpoons}} \mathrm{NR + Asc^{\bullet -} + H^+} \qquad \textbf{(3)}$$

Scheme 3.3. Stages of the reduction of nitroxides mediated by ascorbate.

Where NR and HA denote nitroxide radical and its hydroxylamine, respectively, while AscH−, Asc•−, and DHA refer to ascorbate anion, ascorbate radical, dehydroascorbic acid.

In the presence of DHA and ascorbate radical Asc•−, the efficiency of the reduction process is affected by the retro-oxidation of HA back to NR (**eq. 3**) at high concentrations of the reagents. However, it has been demonstrated that the presence of glutathione (GSH) as co-reactant indirectly increased the rate of reduction of nitroxides in biological environment, acting as a secondary source of reducing agents.[18] This might be explained by the scavenging of the ascorbate radical by GSH, resulting in the inhibition of the retro-oxidation of HA. In according to that, reduction kinetic studies were performed by following the decay of the EPR signals of *cis*-**1** and *cis*-**2** as a function of time, using ascorbate as reductant and GSH as co-reductant.[19] In a typical experiment, stock solutions containing glutathione (50 mM) and nitroxides (*cis*-**1** or *cis*-**2**, 0.3 mM) in sodium phosphate buffer (pH 7.4), were prepared. All the stock solutions were initially purged with nitrogen, then, the necessary aliquots (from 30 mM to 111 mM) of ascorbate where added to the solutions, immediately registering the evolution of the EPR spectra. The I/I_0 ratios were recorded at regular time intervals (**Figure 3.3**), in which I_0 is the initial intensity of the nitroxide EPR signal (proportional to its concentration), while I is the peak intensity at each progressive time after the addition of ascorbate.

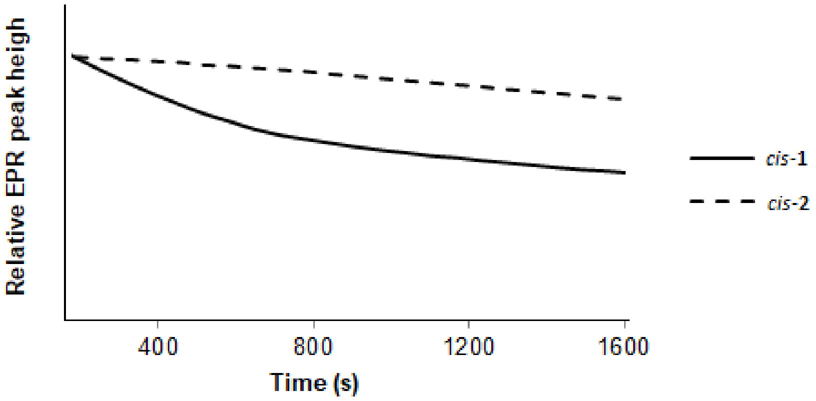

Figure 3.3. Plot of the EPR peak height as a function of time for *cis*-**1** and *cis*-**2** (0.3 mM) after addition of ascorbate (30 mM) in a phosphate buffer containing glutathione (50 mM), at pH 7.4, at 298 K.

In order to obtain a real comparison with the reduction rates of other reported nitroxides, it was necessary to extrapolate the reduction rate constants (*k*) for both macrocycles, which represent a measure of the persistence properties of the substrate. Considering the reduction of nitroxides as the bimolecular reaction shown in **Scheme 3.2,** the reaction rate in the presence of ascorbate is represented by the following equation:

$$\frac{dC}{dt} = k * [nitroxide][AscH^{-}]$$

If the concentration of ascorbate is maintained sufficiently larger than the concentration of nitroxide, the contribute [$AscH^-$] can be approximated as a constant. Thus, the above-described equation becomes:

$$\frac{dC}{dt} = k' * [nitroxide] = \ k_{EPR} * [nitroxide]$$

By integration of the two members of the equation, and considering the EPR peak intensity of the compound (*I*) as a function of the concentration of nitroxide, the following correlation is obtained:

$$ln\frac{[nitroxide]_0}{[nitroxide]_t} = ln\frac{[I]_0}{[I]_t} = k_{EPR} * t$$

Indeed, by plotting the $ln\frac{[I]_0}{[I]_t}$ as a function of time, a linear correlation was obtained, where the angular coefficients represented the first order rate constants k_{EPR} (**Figure 3.4**). The reduction studies were performed at different concentration of ascorbate, ranging from 30 mM, to 111 mM, respectively.

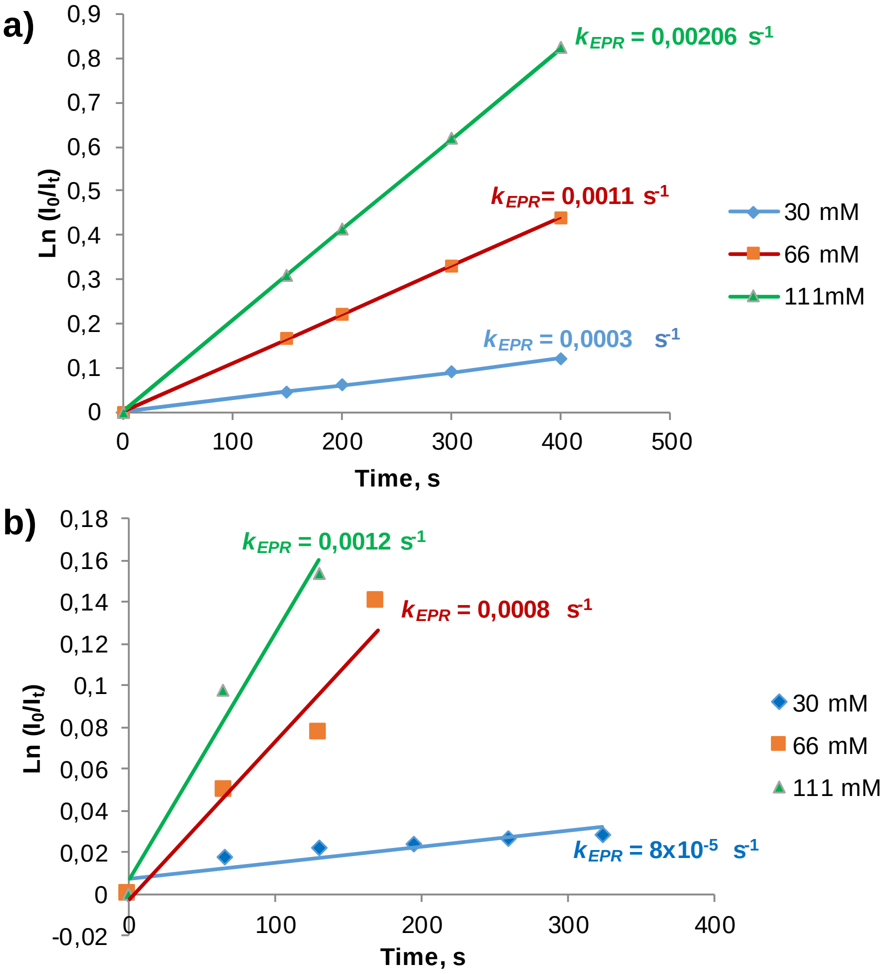

Figure 3.4. Plot of $ln\frac{[I]_0}{[I]_t}$ as function of time registered for nitroxide *cis*-**1** (a) and *cis*-**2** (b) (0.3 mM) after reduction with ascorbate at different concentrations (30 mM, 66 mM and 111 mM) in phosphate buffer and in the presence of glutathione (50 mM), pH 7.4, 293 K.

Successively, the reduction rate constants (k) were extrapolated by plotting the resulting k_{EPR} as a function of the different ascorbate concentrations (**Figure 3.5, Table 3.1**).

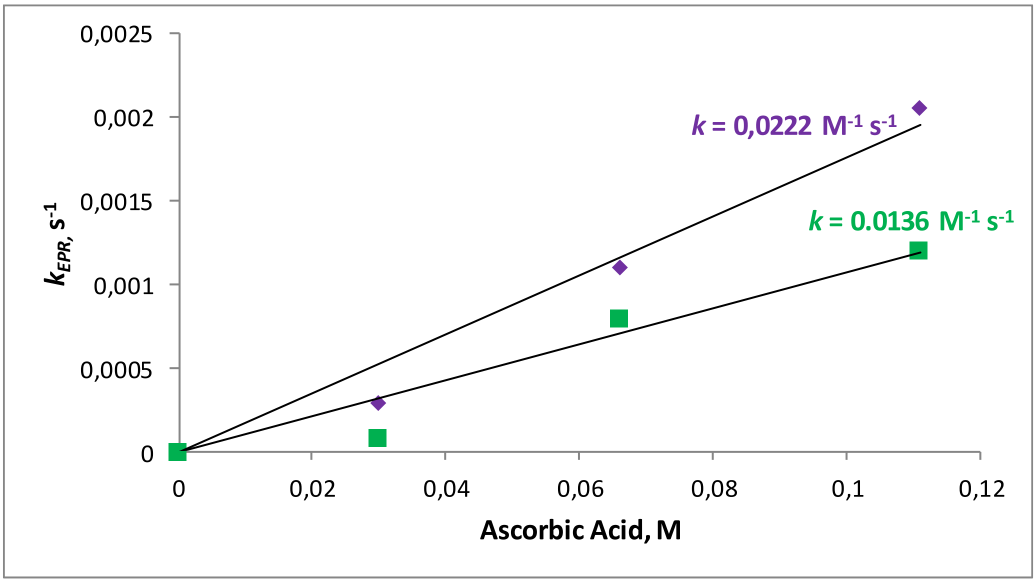

Figure 3.5. Plot of k_{EPR} constants versus concentration of ascorbate for nitroxides *cis*-**1** (violet) and *cis*-**2** (green).

Table 3.1. Second order kinetic constants calculated for the reduction of nitroxides *cis*-**1** and *cis*-**2** by ascorbate**.**

Entry	***k* (M^{-1}s^{-1})**
cis-**1**	0.0222
cis-**2**	0.0136

As expected, the ethyl derivative *cis*-**2** showed a lower *reduction rate* (k = 0.0136 M^{-1}s^{-1}) than derivative *cis*-**1** (k = 0.0222 M^{-1}s^{-1}), corresponding to a slightly higher resistance to reduction. This was attributed to the presence of a bulkier substituent on the β carbon, which served for enhancing the radical lifetime.[11][12] The difference could not be significant, because only one of the β-substituents was replaced for synthetic reasons. However, the interesting discovery was mainly determined by the fact that these compounds were found to be ten or even twenty times more resistant against reduction than TEMPO radical (k = 0.1000 M^{-1}s^{-1}).[20] This property, summed with the water solubility and ion-inclusion properties of these molecules,[21][22] could be interestingly exploited in future biological applications.

3.3 CONCLUSIONS

In this chapter, the synthesis and the EPR reduction kinetics studies of two novel paramagnetic macrocycles, *cis*-**1** and *cis*-**2**, based on a crown-ether structure incorporating a nitroxide group was described. The new compounds presented very high resistance against reduction with ascorbate in biocompatible medium, and for this reason, they can be suitably employed for biological applications.

REFERENCES

[1] R. I. Zhdanov, Bioactive Spin Labels I and II, Heidelberg: Springer-Verlag, 1992.

[2] L. J. Berliner, Spin-labelling. Theory and Applications. I and II, New-York: Academic Press;, 1976, 1979.

[3] P. Kuppusamy, P. Wang and J. L. Zweier, *Magn. Reson. Chem.* , vol. 33, pp. 123-128, 1995.

[4] A. Iannone, A. Tomasi, V. Quaresima and M. Ferrari, *Res. Chem. Intermed.* , vol. 19, pp. 715-731, 1993.

[5] J. F. W. Keana, L. Lex, J. S. Mann, J. M. May, J. H. Park, S. Pou, V. S. Prabhu, G. M. Rosen, B. J. Sweetman and Y. Wu, *Pure Appl. Chem.* , vol. 62, p. 201–205, 1990.

[6] G. Sosnovsky, N. U. M. Rao, S. W. Li and H. M. Swartz, *J. Org. Chem.* , vol. 54, p. 3667–3674, 1989.

[7] P. Kuppusamy, M. Chzan and J. L. Zweier, *J. Magn. Resonance Ser. B* , vol. 106, pp. 122-130, 1995.

[8] A. Sotgiu, G. Placidi, G. Gualtieri, C. Tatone and C. Campanella, *Magn. Reson. Chem.* , vol. 33, pp. 160-165, 1995.

[9] N. Kocherginsky and H. Swartz, Nitroxide Spin Labels: Reactions in Biology and Chemistry, Boca Raton, FL: CRC Press, 1995.

[10] J. T. Paletta, M. Pink, B. Foley, S. Rajca and A. Rajca, *Org Lett.* , vol. 14, p. 5322–5325, 2012.

[11] I. A. Kirilyuk, A. A. Bobko, S. V. Semenov, D. A. Komarov, I. G. Irtegova, I. A. Grigor’ev and E. Bagryanskaya, *J. Org. Chem.* , vol. 80, p. 9118−9125, 2015.

[12] T. Yamasaki, F. Mito, Y. Ito, S. Pandian, Y. Kinoshita, K. Nakano, R. Murugesan, K. Sakai, H. Utsumi and K. Yamada, *.J. Org. Chem.*, vol. 76, p. 435−440, 2011.

[13] A. P. Jagtap, I. Krstic, N. C. Kunjir, R. Hänsel, T. F. Prisner and S. T. Sigurdsson, *Free Radical Res.* , vol. 49, p. 78−85, 2015.

[14] Y. Wang, J. T. Paletta, K. Berg, E. Reinhart, S. Rajca and A. Rajca, *Org. Lett.* , vol. 16, p. 5298−5300, 2014.

[15] K. Sasaki, T. Ito, H. G. Fujii and S. Sato, *Chem. Pharm. Bull.*, vol. 64, p. 1509−1513, 2016.

[16] V. Bleve, P. Franchi, E. Konstanteli, G. L., S. M. Goldup, E. Mezzina and M. Lucarini, *Chem. Eur. J.*, vol. 24, pp. 1198-1201, 2018.

[17] T. Shibata, K. Uemae and Y. Yamamoto, *Tetrahedron: Asymmetry* , vol. 11, pp. 2339-2346, 2000.

[18] A. A. Bobko, I. A. Kirilyuk, I. A. Grigor’ev, J. L. Zweier and V. V. Khramtsov, *Free Radical Biol. Med.* , vol. 42, p. 404−412, 2007.

[19] S. A. Dobrynin, Y. I. Glazachev, Y. V. Gatilov, E. I. Chernyak and G. E. Salnikov, *J. Org. Chem.,* vol. 83, p. 5392−5397, 2018.

[20] J. J. Warren and J. M. Mayer, *J. Am. Chem. Soc.,* vol. 132, no. 22, p. 7784–7793, 2010 .

[21] I. Goldberg, Complexes of Crown Ethers with Molecular Guests, London: Academic Press, 1984.

[22] J. S. Bradshaw, R. M. Izatt, A. V. Bordunov, C. Y. Zhu and J. K. Hathaway, Crown Ethers, Oxford: Pergamon, 1997.

CHAPTER 4: AN AUTONOMOUS PARAMAGNETIC MOLECULAR SWITCH

4.1 INTRODUCTION

In the last years, many scientists focused their research on trying to reproduce and mimic chemical activities and efficiency of biological systems.[1][2] The most part of biological entities works as molecular engines, able to consume chemical, electrochemical or photochemical energy for performing specific motions that are essential for life. As already described in **Paragraph 1.1.3,** artificial molecular machines based on MIMs, such as rotaxanes and catenanes, can reproduce some of these biological features by performing a specific cycle of motions in response to an external supplied input.[3][4] In most of the cases, these artificial systems need an external stimulus, or *fuel* (chemical, electrochemical or photochemical), to move from the starting co-conformation (GSCC) to a non-equilibrium co-conformation (MSCC), and then a counter-stimulus (*anti-fuel*) for restoring the starting state.[5] Only few cases describe molecular machines that can perform a full cycle of motions exploiting only one external input and without the necessity of using a counter-stimulus.[6][7][8]

An impressive example of a molecular switch able to accomplish a full cycle of motions promoted by a single chemical input was reported by Di Stefano and co-workers, who coupled the decarboxylation of 2-cyano-2-phenylpropanoic acid with the movement of an acid-base switchable Sauvage-type [2]-catenane. The investigated [2]-catenane consisted of two interlocked macrocycles, each containing one 1,10-phenantroline moiety and its motion can be promoted by addition of one equivalent of trifluoroacetic acid (TFA) to a solution containing the [2]-catenane in CD_2Cl_2 (**Scheme 4.1**).[6] Successively, the initial state is re-stored by basic treatment, confirming the reversibility of the switching process.

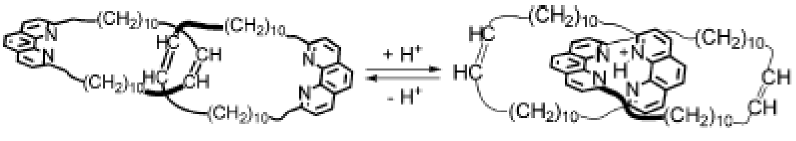

C1 **C1+**

Scheme 4.1. Switching of [2]-catenane **C1** promoted by acid-base equilibrium.

It is known that 2-cyano-2-phenylpropanoic acid is able to spontaneously decarboxylate in the presence of tertiary bases, such as Et_3N, by a three steps mechanism (**Scheme 4.2**):[9]

I) Proton transfer from **1’** to Et$_3$N (**B**), forming a carboxylate anion (**1’**)$^-$ and its counter-ion HB$^+$;

II) Decarboxylation of **(1’)$^-$**, forming adduct **(2’)$^-$**, which is always stabilized by the HB$^+$ counter-ion;

III) Fast back proton transfer from HB$^+$ to **(2’)**$^-$ affording the final product **2’** and base **B.**

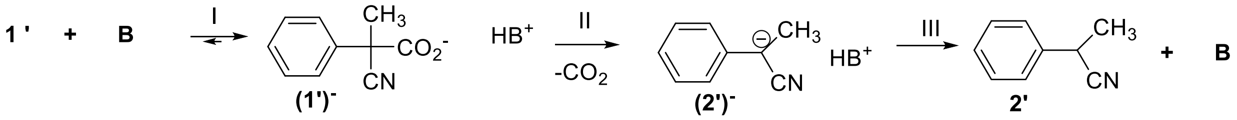

Scheme 4.2. Mechanism of decarboxylation of 2-cyano-2-phenylpropanoic acid, promoted by a tertiary base.

Since the phenantroline group of catenane **C1** can be identified as a tertiary base able to trap an acid proton, it was possible to compare the decarboxylation of compound **1’** promoted by Et$_3$N with the one promoted by catenane **C1.** Thus, Di Stefano and co-workers deduced that 2-cyano-2-phenylpropanoic acid could induce the acid-base switching motion of catenane **C1** by the mechanism reported in **Scheme 4.3.** Similarly to that described for Et$_3$N, the mechanism consisted in a fast proton transfer from acid **1’** to catenane **C1** (**state A → state B’**) followed by a fast decarboxylation step (**state B’ → state B’’**) leading to compounds **C1**$^+$ and **(2’)**$^-$ (fast steps**).** Successively, a final back proton transfer (slow step) from **C1**$^+$ to **(2’)**$^-$ (**state B’’ → state A**) led back to **C1** and **2’**, accomplishing a one-only stimulus supplied cycle of motions. The mechanism reported in **Scheme 4.3** was verified thanks to UV-visible and NMR spectroscopy experiments evidencing the progressive formation of adduct **2’**.

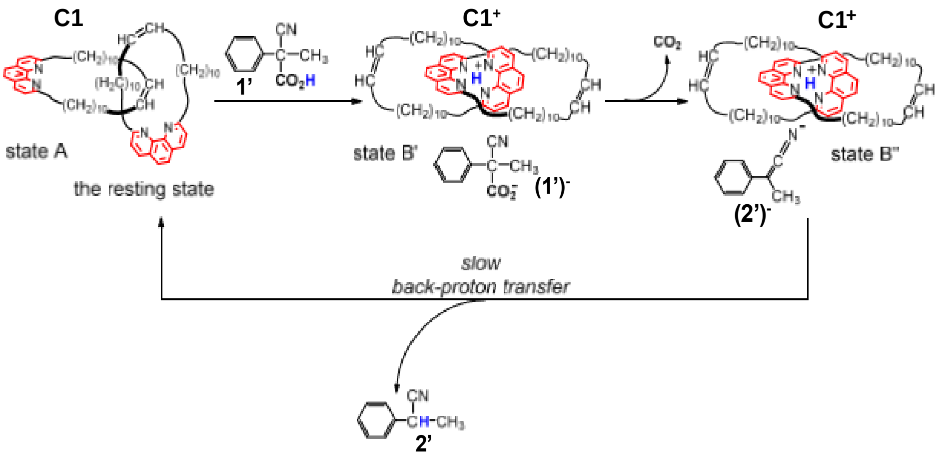

Scheme 4.3. Switching of catenane **C1** promoted by acid **1’**.

Since the insertion of different electron withdrawing (EWG) and electron donating (EDG) substituents in the *para* position of the aromatic ring of acid **1’** can strongly influence the basicity of the intermediates involved in the process, the effect of using different *para*-substituted derivatives of acid **1’** (**Figure 4.1**) on the *switching* rate constants of catenane **C1** was also investigated.[8]

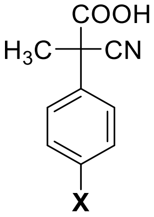

X= Cl, OCH_3, CH_3

Figure 4.1. Molecular structure of acid **1’** derivatives.

The total time required to accomplish a full cycle of motions of **C1** was determined by NMR experiments (**Figure 4.2**) on solutions containing **C1** and equimolar quantities of acids (X=Cl, CH_3 and OCH_3), by observing the peaks corresponding to the quantitative formation of adduct **2’** (**red stars**) as a proof of the conclusion of the cycle of motions.

The results evidenced that electron withdrawing groups complete the whole process faster than electron donating ones, giving the following order: $OCH_3 < CH_3 < H < Cl$.

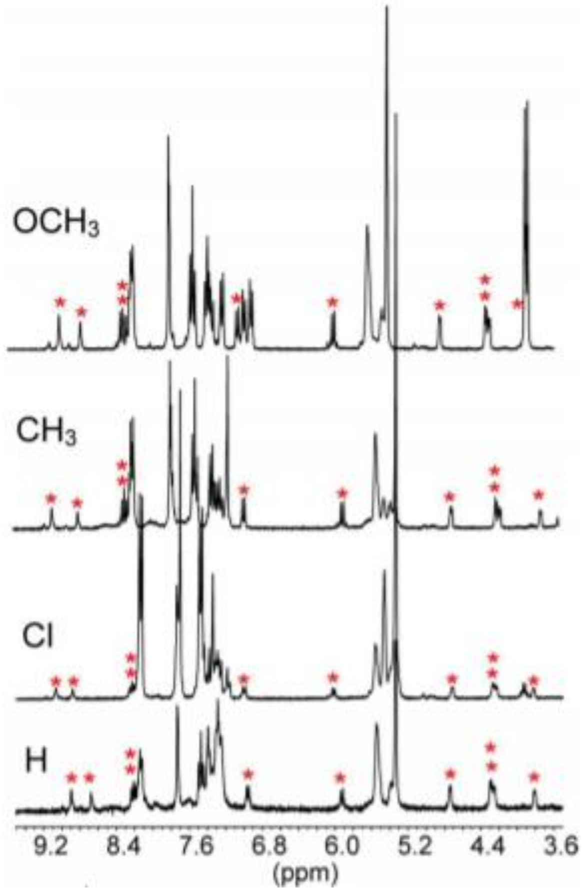

Figure 4.2. Portions of NMR spectra recorded in the course of the reaction of catenane **C1** with equimolar amounts of acid (X = H, Cl, CH_3 and OCH_3), after 3.5, 2.5, 7.5 and 44.5 min from start, respectively. Red stars indicate the peaks corresponding to the formation of compound **2'**.

The results were confirmed by performing UV-visible spectroscopy experiments (**Figure 4.3**). The UV spectra initially showed the appearance of an absorption band at λ=375 nm after first addition of acid to **C1**, relative to the formation of the intermediate carbanions of the **states B'** and **B''**. The maximum absorption value was achieved very fast in the presence of all the acid derivatives (fast step), in particular after 20 minutes for X= OCH_3, 3 minutes for X= CH_3 and 1.5 minutes for X = H. The rapid increase of the absorbance was successively followed by a slow decrease, deriving from the re-storage of the starting **state A** (slow step). While acids with X=H, CH_3 and OCH_3 required up to 2 days for re-storing the starting state, the derivative containing an EWG group (X = Cl) was able to complete the full cycle of motions in only 4 min.

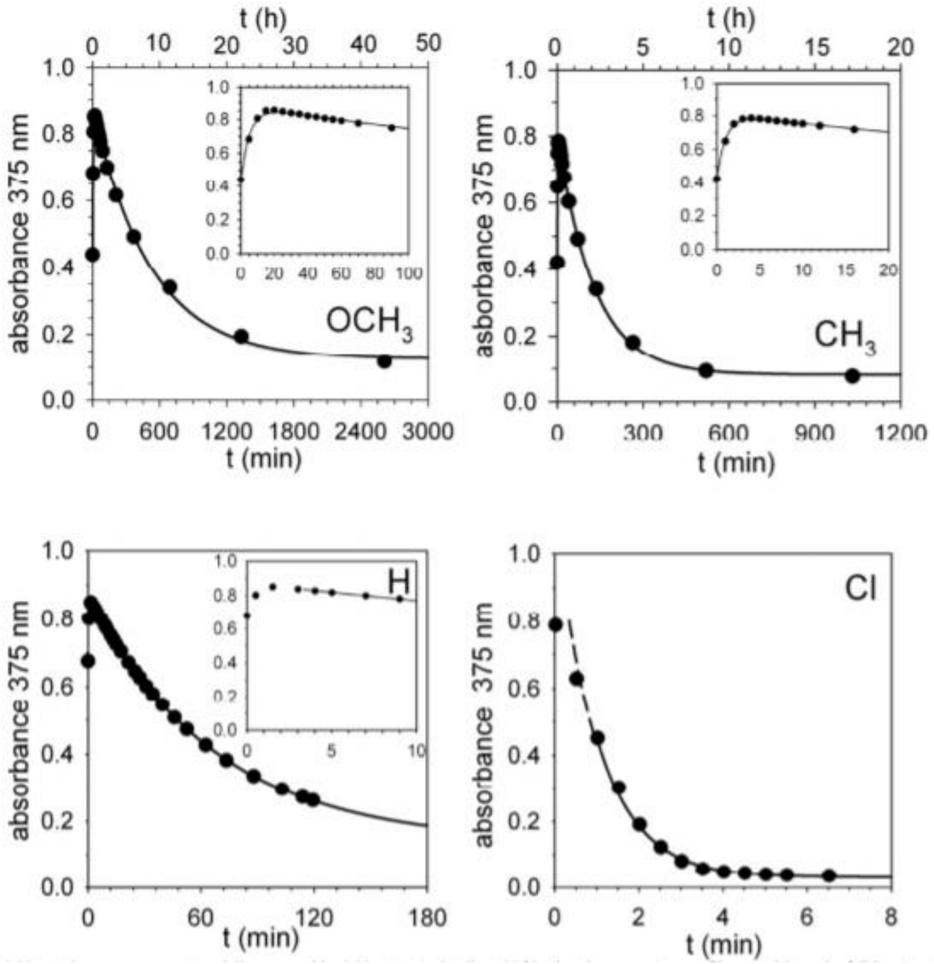

Figure 4.3. Absorbance *vs* time profiles showing the comparison between the slow decrease of the absorbance band (λ=375 nm) registered in the presence of acids X=H, CH_3 and OCH_3 and the one registered for X=Cl.

Kinetic treatment of UV-Vis data provided a quantitative estimation of the effect of the substituents on the rate of the back proton transfer, by considering the increase (**step A → B''**) and decrease (**step B'' → A**) of the absorption band at λ=375 nm as first order reactions having rate constants *k'* and *k''*, respectively. The results obtained indicated that the kinetic basicity of the intermediate anionic component formed in **state B''** was enhanced by the presence of EWG and depressed by EDG, thus resulting in a faster or slower back proton transfer restoring **state A**, respectively. In conclusion, Di Stefano and co-workers demonstrated that, not only 2-cyano-2-phenylpropanoic acid can be used as fuel for the back and forth motions of an acid-base switchable catenane without the necessity of an additional counter-stimulus, but also that the rate of the process is strongly influenced by the nature of the *para*-substituents of the aromatic ring of acid **1'**.

In particular, the use of EWG increased the rate of the process, while the insertion of EDG depressed the total rate. In their work, Di Stefano and co-workers affirmed that: *"any molecular switch or motor* *that moves between two states under the influence of protonation/deprotonation could utilize acid* **1**’*, or any other acid that undergoes base-promoted decarboxylation at a convenient rate, as a fuel”*. Starting from this, in this work the use 2-cyano-2-phenylpropanoic acid **1’** and its derivatives, as proper fuels for promoting the back and forth motion of a paramagnetic [2]-rotaxane, which is able to change co-conformation under acid-base stimulus, was explored.[10]

4.2 2-CYANO-2-PHENYLPROPANOIC ACID ACTS AS A PROPER FUEL FOR AN ACID–BASE-OPERATED PARAMAGNETIC MOLECULAR SWITCH

In this work, the use of 2-cyano-2-phenylpropanoic acid **1’** and derivatives **3’, 4’** and **5’** (**Figure 4.4**) as fuels for the back and forth motions of a recently proposed bistable nitroxide-containing rotaxane (**Paragraph 1.2.4**) able to change co-conformation under an acid-base stimulus was investigated.

The target [2]-rotaxane **R1H•(PF$_6$)$_3$** (**Scheme 4.4**) contains a crown-ether based macrocycle, which is mechanically interlocked on a thread having a dialkylammonium (**NH$_2$**$^+$) and a bipyridinium (**BPY**$^{2+}$) site. In the starting state, the macrocycle is prevalently located on the ammonium station, because of the formation of hydrogen bonds between the ammonium moiety and the unpaired electrons of the oxygen atoms of the ring. The displacement of the ring on the secondary site (**BPY**$^{2+}$) can be promoted by treatment with diisopropylethylamine (*i*Pr$_2$EtN),[11] leading to compound **R1•(PF$_6$)$_2$.**

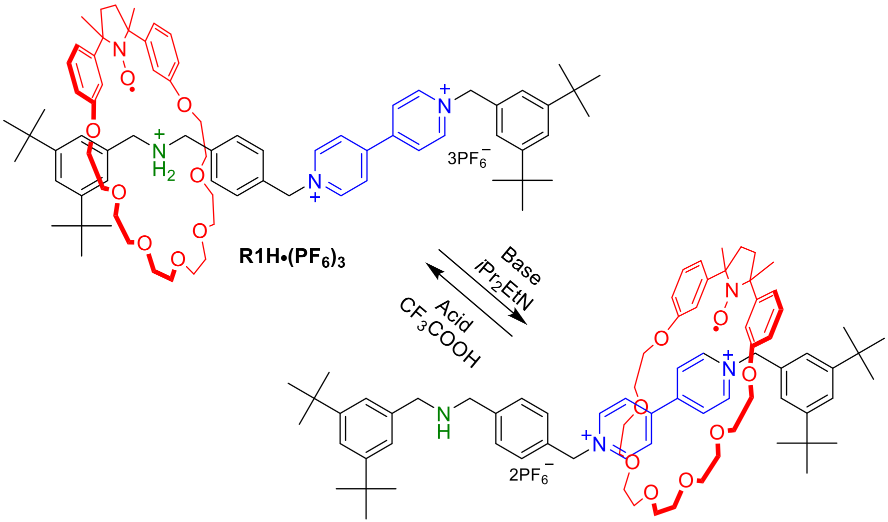

Scheme 4.4. Acid-base switching of paramagnetic rotaxane **R1H•(PF$_6$)$_3$.**

Successively, the addition of trifluoroacetic acid to rotaxane **R1•(PF$_6$)$_2$** restores the initial state, causing the shuttling back of the macrocycle on the original site. **Paragraph 1.2.4** illustrates how EPR could be employed for monitoring the shuttling process of the rotaxane, in particular by observing the significant variation of the a_N value in the rotaxane’s EPR spectrum (from 14.39 G to 14.82 G), before and after addition of *i*Pr$_2$EtN.

With the aim of obtaining a one-only stimulus supplied acid-base switchable rotaxane, acid **1’** was used to perform the full cycle of back and forth motions of **R1•(PF$_6$)$_2$**, by a mechanism similar to that described by Di Stefano and co-workers (**Scheme 4.5**).

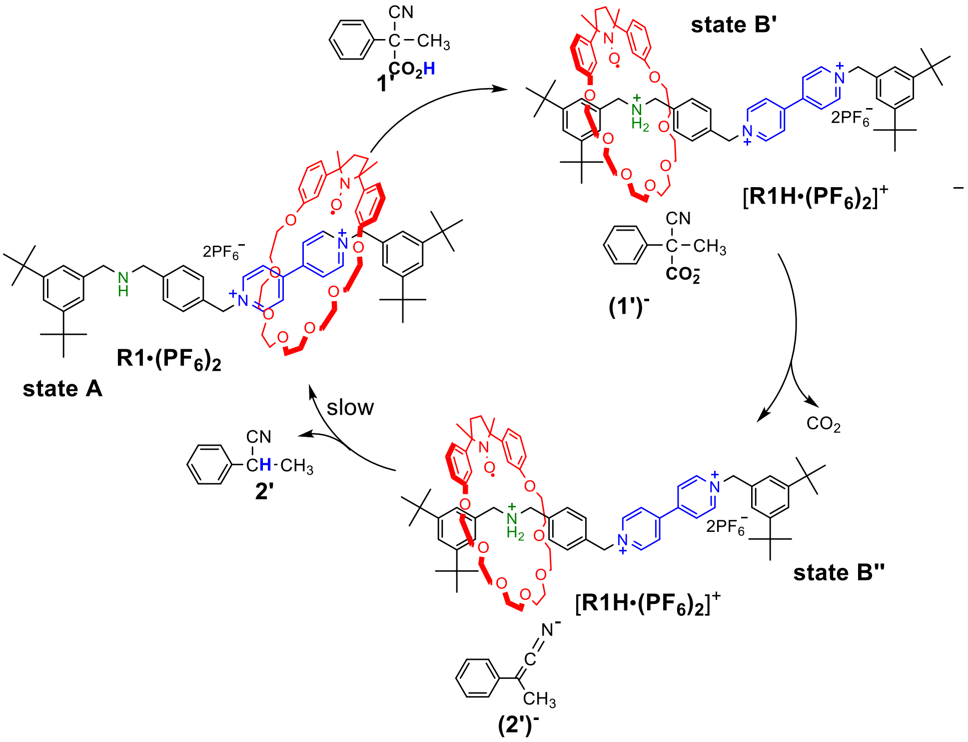

Scheme 4.5. Schematic representation of the full cycle of motions of deprotonated rotaxane **R1•(PF$_6$)$_2$** promoted by acid **1’.** The first quantitative proton transfer from **1’** to **R1•(PF$_6$)$_2$** (**state A→B’**) causes the ring displacement on the ammonium site, forming protonated rotaxane **[R1H•(PF$_6$)$_2$]$^+$** and **(1’)$^-$.** Decarboxylation (**state B’→B’’**) followed by the back proton transfer from **[R1H•(PF$_6$)$_2$]$^+$** to **(2’)$^-$** restores the original position of the macrocycle on the bipyridinium moiety (**state B’’→A**).

In order to perform this process, it was necessary to start from deprotonated rotaxane **R1•(PF$_6$)$_2$,** where the ring is prevalently located on the **BPY^{2+}** site. This rotaxane was obtained by treatment of the protonated form **R1H•(PF$_6$)$_3$** with 1 equivalent of *i*Pr$_2$EtN. Then, the addition of 1 equivalent of acid **1’** in a CH$_2$Cl$_2$ solution of the rotaxane led to the quantitative formation of **[R1H•(PF$_6$)$_2$]$^+$**. As reported by Di Stefano and co-workers, after fast decarboxylation of **(1’)$^-$** to **(2’)$^-$**, the system undergoes to a back proton transfer from **R1H•(PF$_6$)$_2$** to **(2’)$^-$** (slow step), restoring the starting rotaxane **R1•(PF$_6$)$_2$** and compound **2’**. In this case, EPR spectroscopy was fundamental for studying the shuttling process, because it allowed distinguishing the two possible co-conformations assumed by the rotaxane. In fact, the first addition of acid **1’** caused the fast decrease of the hyperfine constant

a_N in the EPR spectrum of the rotaxane (from 14.82 G to 14.39 G), related to the formation of **[R1H•(PF$_6$)$_2$]$^+$**. Then, a spontaneous slow increment of a_N was registered, returning to the original value during the next 60 minutes (re-positioning of the macrocycle on the **BPY^{2+}** site). The addition of a second equivalent of acid **1’** reproduced the same behaviour at EPR, showing a rapid decrease of a_N followed by the slow increment without significant variations.

For obtaining reproducible and comparable analysis, the EPR spectra were recorded at regular time intervals after the first addition of acid **1’** plotting the progressive registered values of a_N as a function of time (**Figure 4.5, inset**).

The rate of the final back proton transfer, in absence of alternative processes, determines the rate of the whole process and it can be influenced by the nature of the *para* substituents of the aromatic ring in **1’**.[8] Thus, the behaviour of the target rotaxane was monitored also in the presence of some *para*-substituted derivatives of acid **1’**, containing EWG (Cl) and EDG (CH_3 and OCH_3) (**Figure 4.4**).

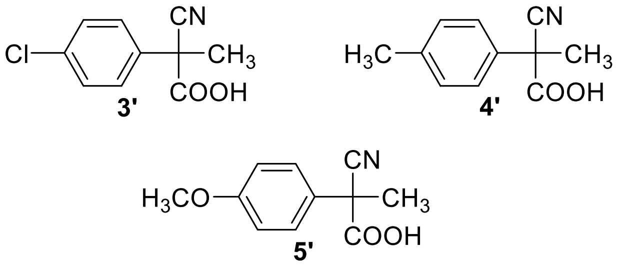

Figure 4.4. *Para*-substituted derivatives of acid **1’.**

Compound **5’** displayed the same behaviour reported by Di Stefano and co-workers, requiring a shorter time than acid **1’** to complete the full cycle of motions and restoring the original value of a_N. On the other hand, for derivatives **4’** and **5’**, the restore of the original a_N value (14.82 G) was not observed, even after many hours after addition of the acid, indicating an uncompleted cycle of motions of the rotaxane (**Figure 4.5**). This last result suggested the occurrence of an alternative process that competed with the final back proton transfer.

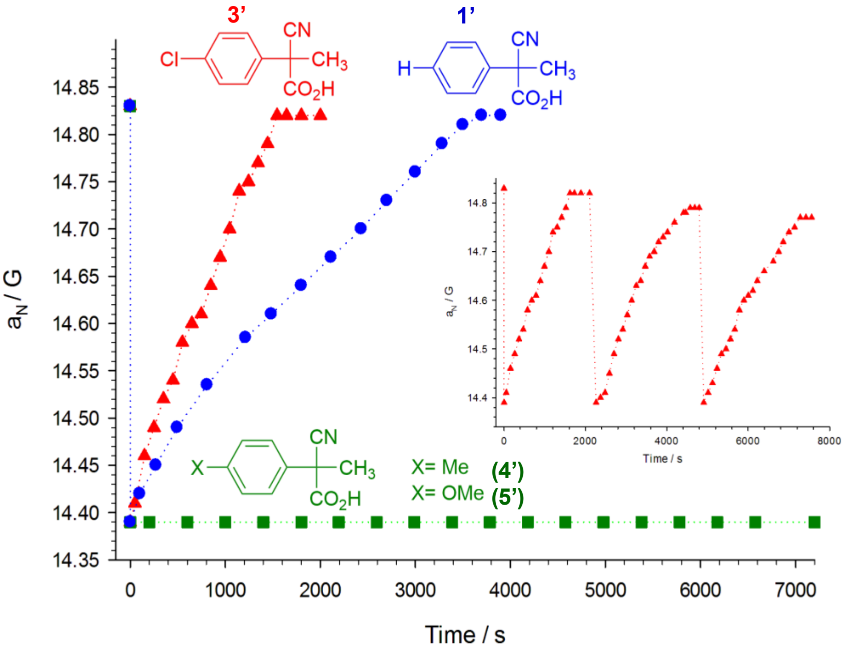

Figure 4.5. Time variation of a_N after the addition of equimolar quantities of different fuels (**1', 3', 4'** and **5'**) to rotaxane **R1•(PF$_6$)$_2$** in CH_2Cl_2. Inset: a_N variation in the EPR spectrum of rotaxane as function of sequential additions of fuel **1'**.

It is known that benzylic anions can undergo to formation of benzylic radicals by loss of one electron, and this effect is favoured if a EDG is present in the *para* position of the aromatic ring.[12][13] In addition, dialkyl-bipyridinium units can undergo to mono-electronic oxidation at low potentials (-0.42 vs SCE in ACN). Thus, a single electron transfer (SET) occurring from the benzylic anion of **state B''** to the **BPY^{2+}** cation of the rotaxane was assumed, which can compete with the final back proton transfer**.** The assumed SET process should lead to a **BPY** radical cation and a benzylic radical that, successively, can react with oxygen to afford a peroxyl radical (**Scheme 4.6**).

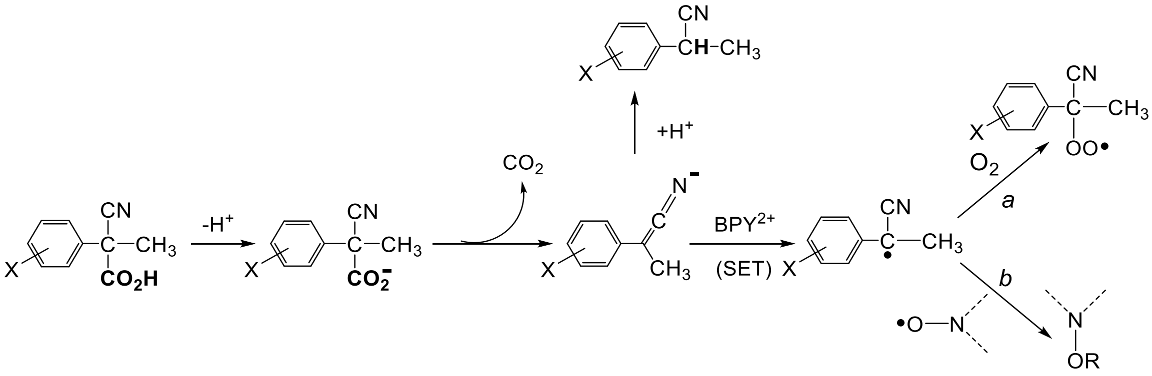

Scheme 4.6. SET process occurring in the presence of derivatives **4'** and **5'**.

EPR line width is sensitive to the concentration of oxygen in the solution, producing a strong line broadening on increasing concentration of oxygen (**Paragraph 1.2.1**).[14] Since the SET process led to the consumption of oxygen, the feasibility of this path was checked by following the evolution of EPR line width in a close tube containing the rotaxane after addition of acids **4'** and **5'**. As an efficient EPR parameter, the peak intensity, *I*, was chosen, which is reciprocal of the line width and proportional to radical concentration in solution. Thus, the progressive values of the peak to peak height (*I*) in the EPR spectra of rotaxane **R1•(PF$_6$)$_2$** were registered as function of time, after addition of fuel **4'** (**Figure 4.6**).

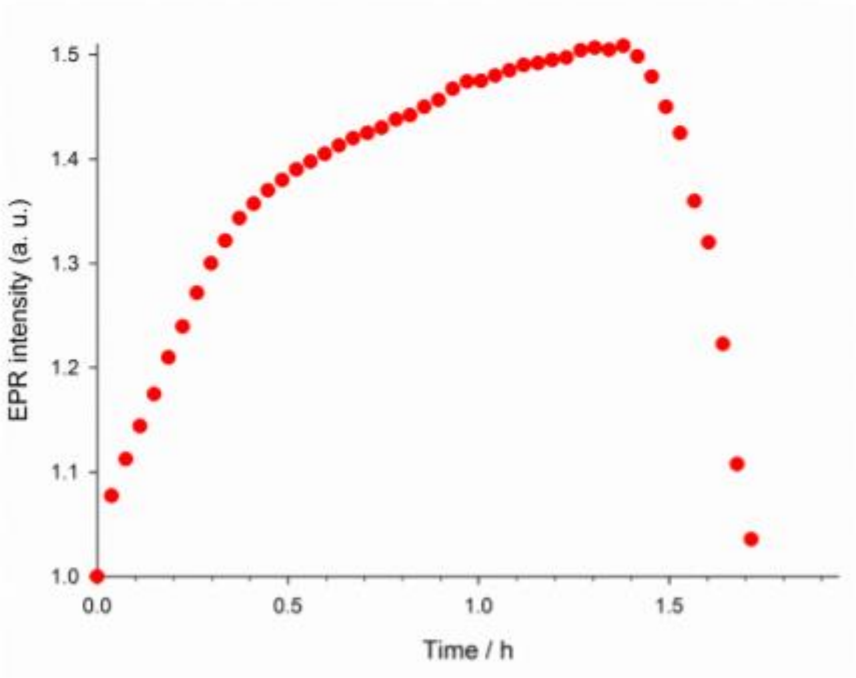

Figure 4.6. Experimental time dependence of the peak height (*I*) of the EPR spectrum of rotaxane **R1•(PF$_6$)$_2$** after addition of 1 equivalent of **4'**, at room temperature.

As evident from the plot, the EPR lines intensity initially increased (line width decreased), because the benzylic radical trapped the oxygen present in the solution (**Scheme 4.6**, path *a*).[15] Once completed the oxygen consumption the same radical reacted with the nitroxide moiety of protonated rotaxane **[R1H•(PF$_6$)$_2$]$^+$** (**Scheme 4.6**, path *b*) and the EPR line intensity decreased. These results confirmed the possibility of a SET alternative process competing with the final back proton transfer and affecting the completion of the cycle of motions. The same experiment was performed using fuels **1'** and **3',** which did not show any experimental evidence of the consumption of oxygen, confirming that the SET process is favored only in the presence of EDG in the *para* position of the aromatic ring of the fuel.

4.3 CONCLUSIONS

The paramagnetic rotaxane **R1•(PF$_6$)$_2$** described was able to undergo a full cycle of motions in the presence of 2-cyano-2-phenylpropanoic acid. Differently from all the cases previously reported, for which the movement of molecular switches was monitored by more common spectroscopic techniques (NMR, UV-visible etc..), in this case EPR spectroscopy was employed to demonstrate the movement. In addition, this work confirmed that 2-cyano-2-phenylpropanoic acid and its derivatives, with exclusion of those containing *para*-EDG in the aromatic ring, are able to act as proper fuels for the back and forth motion of acid-base switchable diamagnetic and paramagnetic molecular switches.[16]

REFERENCES

[1] A. Sorrenti, J. Leira-Iglesias, A. J. Markvoort, T. F. A. de Greef and T. M. Hermans, *Chem. Soc. Rev.*, vol. 46, pp. 5476-5490, 2017.

[2] J. H. van Esch and R. Klajn, *Chem. Soc. Rev*, vol. 46, pp. 5474-5475, 2017.

[3] J. P. Sauvage, *Angew. Chem. Int. Ed.*, vol. 56, pp. 11080-11093, 2017.

[4] J. Stoddart, *Angew. Chem. Int. Ed.*, vol. 56 , pp. 11094-11125, 2017.

[5] S. Erbaş-Çakmak, D. A. Leigh, C. T. McTernan and A. L. Nussbaumer, *Chem. Rev.*, vol. 115, pp. 10081-10206, 2015.

[6] J. A. Berrocal, C. Biagini, M. L. and S. Di Stefano, *Angew. Chem. Int.*, vol. 55, pp. 6997-7001, 2016.

[7] S. Erbas-Cakmak, S. D. Fielden, U. Karaca, D. A. Leigh, C. T. McTernan, D. J. Tetlow and M. R. Wilson, *Science*, vol. 358, p. 340–343, 2017.

[8] C. Biagini, S. Albano, R. Caruso, L. Mandolini, J. Berrocal and S. Di Stefano, *Chem Sci*, vol. 9, pp. 181-188, 2018.

[9] H. Schmidt and P. Brunner, *Eur. J. Org. Chem.*, pp. 2119-2133, 2000.

[10] V. Bleve, P. Franchi, E. Konstanteli, L. Gualandi, S. Goldup, E. Mezzina and M. Lucarini, *Chem. Eur. J.*, vol. 24, pp. 1198-1203, 2018.

[11] M. Martínez-Díaz, N. Spencer and J. F. Stoddart, *Angew. Chem. Int. Ed. Engl.*, vol. 36, pp. 1904-1907, 1997.

[12] B. A. Sim, P. H. Milne, D. Griller and D. D. M. Wayner, *J. Am. Chem. Soc.*, vol. 112, p. 6635−6638, 1990.

[13] D. D. M. Wayner, B. A. Sim and J. J. Dannenberg, *J. Org. Chem.*, vol. 56, p. 4853−4858, 1991.

[14] G. Pedulli, M. Lucarini, P. Pedrielli, M. Sagrini and M. Cipollone, *Res. Chem. Intermed.*, vol. 22, pp. 1-14, 1996.

[15] G. Ebbesen and T. W. Levey, *J. Phys. Chem.*, vol. 87, p. 829–832, 1983.

[16] P. Franchi, C. Poderi, E. Mezzina, C. Biagini, S. Di Stefano and M. Lucarini, *J. Org. Chem.*, vol. 84, no. 14, pp. 9364-9368, 2019.

CHAPTER 5:

INVESTIGATIONS ON THE AEROBIC OXIDATION OF ALCOHOLS PROMOTED BY A SYNTHETIC RADICAL CROWN-ETHER MACROCYCLE AND ITS INTERLOCKED DERIVATIVE

5.1 INTRODUCTION

One of the most relevant properties of nitroxide radicals is their ability to perform reversible oxidation and reduction, forming oxoammonium salts and hydroxylamines, respectively (**Scheme 5.1**).

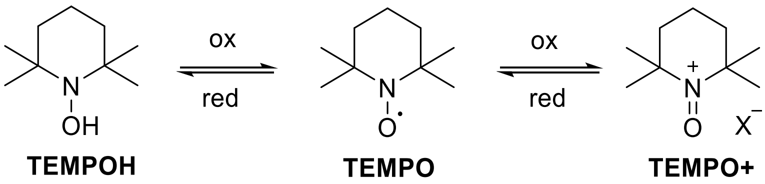

Scheme 5.1. Reversible redox reactions of **TEMPO** radical leading to hydroxylamine (**TEMPOH**) and oxoammonium salt (**TEMPO$^+$**).

This behaviour makes oxoammonium cations, such as **TEMPO$^+$**, highly oxidative species employed for the oxidation of different class of synthetic compounds, such as acetales, alcohols, silanes, amides, sulfates, heterocycles, esters and so on.[1][2]

During the past years, the oxoammonium-catalysed oxidation of primary and secondary alcohols to aldehydes or ketones has been widely explored.[3][4] In stoichiometric conditions, one molecule of oxoammonium salt is able to selectively convert alcohols to aldehydes or ketones, forming the corresponding hydroxylamine by-product, as shown in **Scheme 5.2**.

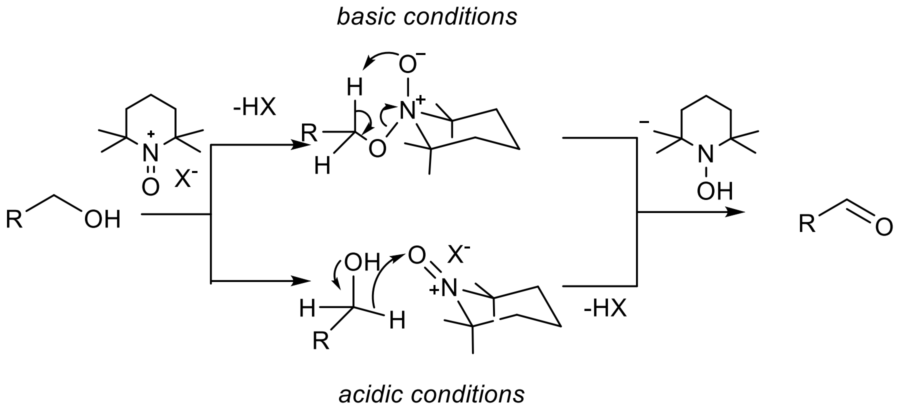

Scheme 5.2. Selective oxidation of alcohols promoted by **TEMPO**$^+$ in acidic and basic conditions.

If a co-oxidant is added to the reaction, it is possible to recover the oxoammonium salt (**TEMPO**$^+$) by re-oxidation of the hydroxylamine (**TEMPOH**). In this case, a catalytic cycle arises, which allows to use the oxoammonium in low amounts (**Scheme 5.3**).

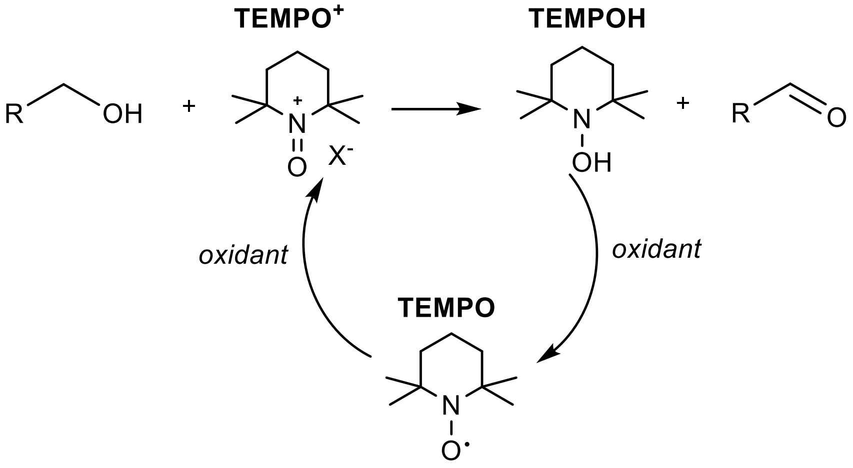

Scheme 5.3. Selective oxidation of alcohols promoted by **TEMPO**$^+$ in the presence of a co-oxidant.

A first equivalent of co-catalyst serves for the mono-electron oxidation of the hydroxylamine to nitroxide and a second equivalent for the further oxidation of the latter to oxoammonium salt. At present, there is a wide set of co-oxidants that have been employed in oxoammonium-catalysed oxidations, such as cerium ammonium nitrate,[5] sodium nitrite,[6] cobaltum and manganese nitrates,[7] polyoxometalates[8] or copper (I) and copper (II) free ions or complexed ions.[9] Among these, Cerium (IV) salts, in particular cerium ammonium nitrate (CAN), are the most efficient ones, being characterized by a high reduction potential (1.61 V). Moreover, CAN presents some advantages if compared to other oxidants, such as low toxicity, low price, solubility in organic solvents, air stability and easy handling. However, CAN needs to be used in very large amounts in order to obtain quantitative and efficient oxidations, especially in reactions carried out in organic solvents. In order to overcome this problem, some studies explored its use in the presence of a secondary oxidant able to re-store the Cerium (IV) starting from Ce (III) form. To this aim, the use of air, an ecological, inexhaustible and low cost secondary oxidant[5] was exploited thanks to the ability of O_2 to convert the reduced form Ce (III) back to Ce (IV).

An example of this aerobic oxidative catalytic cycle was reported by Jung and co-workers in 2003 and described the oxidation of benzylic and allylic alcohols to aldehydes promoted by a combination of CAN and 2,2,6,6-tetramethylpiperidinyl-1-oxyl (**TEMPO**), in aerobic conditions.[5] As mentioned above, the oxoammonium salt (**TEMPO$^+$**), which is formed *in situ* by oxidation of its precursor **TEMPO**, promotes the oxidation of the alcohol, providing the corresponding aldehyde or ketone and forming **TEMPOH** as by-product. Thanks to the presence of CAN as co-oxidant, **TEMPOH** is re-oxidized to the corresponding **TEMPO$^+$**, and re-introduced into the catalytic cycle. At this point, Ce (IV) is recovered from Ce (III) by action of the oxygen present in solution, giving rise to the catalytic cycle shown in **Scheme 5.4**.

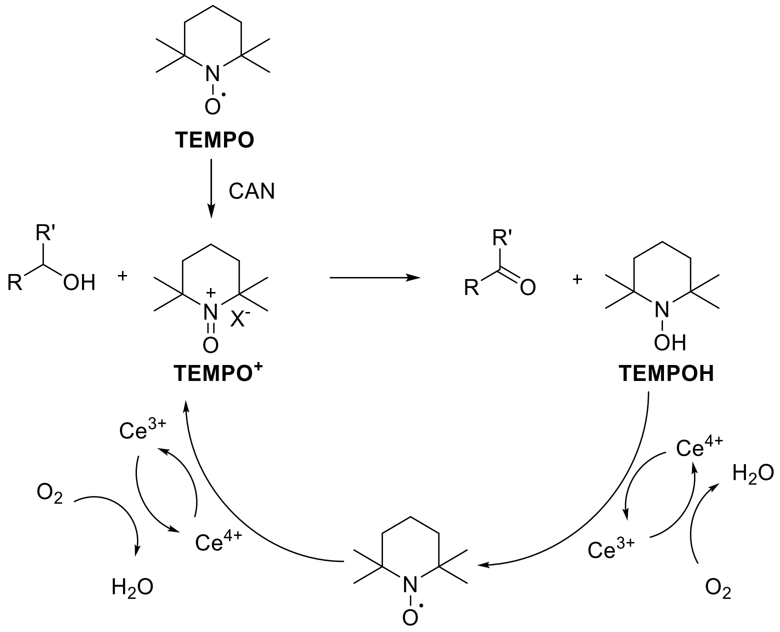

Scheme 5.4. Catalytic cycle of the aerobic oxidation of alcohols promoted by CAN and **TEMPO** radical.

These conditions have been employed for the oxidation of a wide range of alcohols, reporting more than satisfactory results.

The majority of the studies concerning aerobic catalytic oxidations under these conditions are limited to the use of **TEMPO$^+$** and some of its derivatives.[5] However, other oxoammonium-based substrates could display a better oxidative ability, enhancing the efficiency of these reactions. Our research group recently reported the synthesis of a new radical macrocycle based on a crown ether structure including a pyrrolidine-oxyl unit (*cis*-**1**, **Figure 5.1**).[10] This compound presented interesting chemical properties, such as high resistance against hydrogen addition by ascorbate (10 times higher than that of radical **TEMPO**), solubility in water and stability (**Chapter 3**).

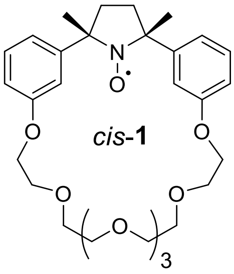

Figure 5.1. Structure of paramagnetic macrocycle *cis*-**1.**

Such properties have encouraged us to investigate the possible use of this compound as catalyst for the aerobic oxidation of alcohols in the presence of CAN, with the aim of evaluating its efficiency compared to previously reported substrates.

5.2 THE AEROBIC OXIDATION OF ALCOHOLS PROMOTED BY A NOVEL PARAMAGNETIC MACROCYCLE

In the first part of this work, the use of macrocycle *cis*-**1** for promoting the catalytic oxidation of 4-methoxybenzyl alcohol to 4-methoxybenzaldehyde in the presence of CAN and oxygen as co-catalysts was investigated (**Scheme 5.5**).

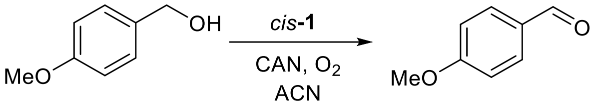

Scheme 5.5. Oxidation of 4-methoxybenzyl alcohol to 4-methoxybenzyl aldehyde**.**

The purpose was to clarify the contribute of every reactant involved in the process, in order to verify the catalytic mechanism assumed (**Scheme 5.6**), which was similar to the one described for **TEMPO** radical in **Paragraph 5.1**.

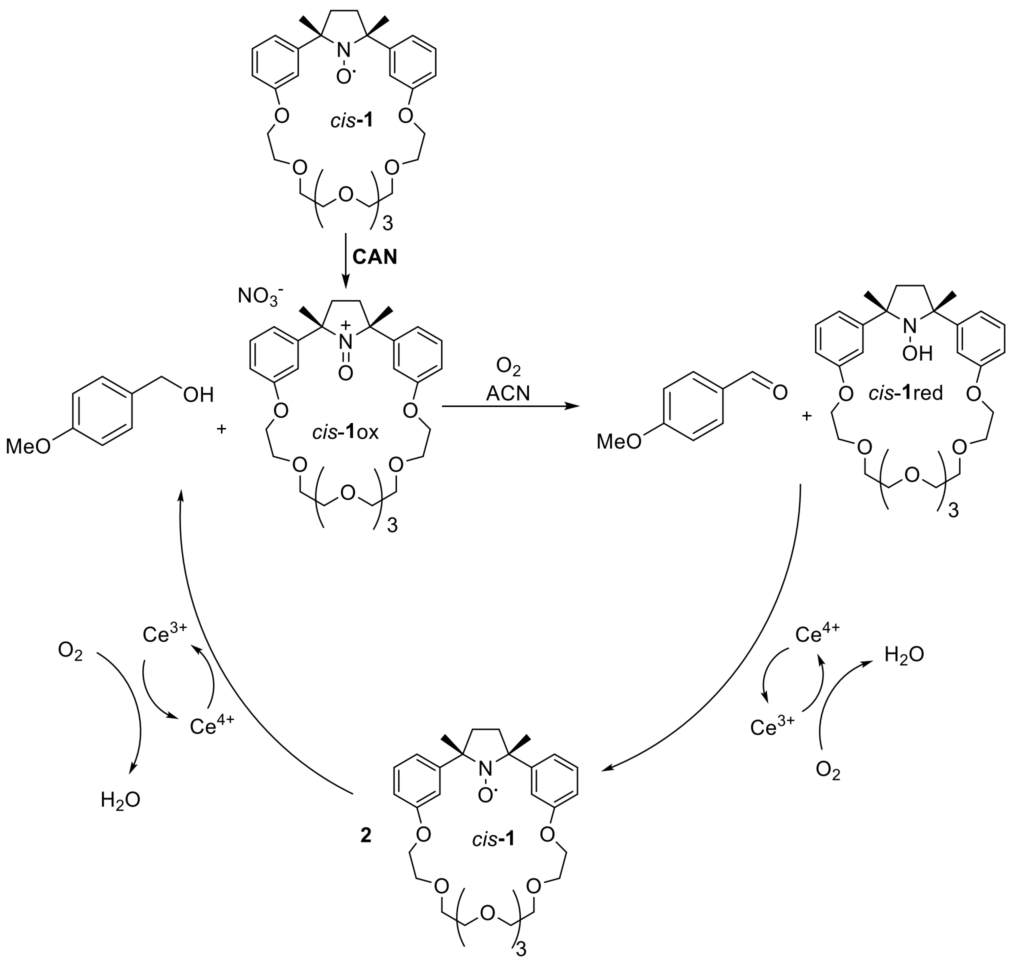

Scheme 5.6. Catalytic cycle of the oxidation of 4-methoxybenzyl alcohol promoted by nitroxide *cis*-**1** and CAN, in presence of oxygen. The oxoammonium cation *cis*-**1**ox, formed *in situ* by oxidation of *cis*-**1**, catalysed the oxidation of 4-methoxybenzyl alcohol to 4-methoxybenzyl aldehyde, forming the corresponding hydroxylamine *cis*-**1**red. This was re-oxidized to *cis*-**1**ox thanks to two equivalents of CAN, which in turn was continuously regenerated by oxygen.

Initially, the best conditions to *in situ* generate *cis*-**1**ox from *cis*-**1** were checked by employing EPR and NMR spectroscopies. The *in situ* oxidation of compound *cis*-**1** was performed adding 5 eq. of CAN directly in the EPR tube containing *cis*-**1** and observing the progressive decrease of the EPR signal of the nitroxide until complete disappearance. Successively, the formation of oxoammonium *cis*-**1**ox was verified by NMR analysis (**Figure 5.2**).

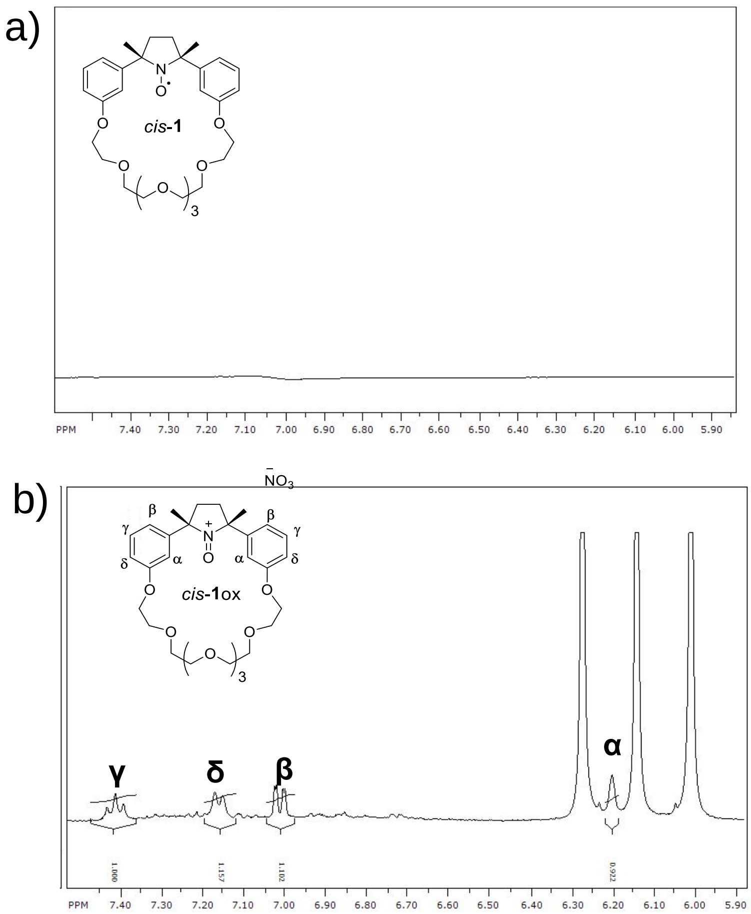

Figure 5.2. Partial NMR spectra (5.9-7.5 ppm) of: a) Macrocycle *cis*-**1**; b) Macrocycle *cis*-**1**ox 20 minutes after addition of 5 equivalents of CAN directly in the NMR tube, in deuterated ACN at 298 K.

After having found the best conditions for the formation of catalyst *cis*-**1**ox, GC-MS experiments were performed on solutions containing 4-methoxybenzyl alcohol, catalytic amounts of nitroxide and CAN, under oxygen-saturated atmosphere. By observing the evolution of the GC-MS chromatograms over time, it was possible to monitor the gradual disappearance of the chromatographic peak corresponding to the alcohol (4.11 min), and the appearance of the peak associated to the aldehyde (4.00 min) (example in **Figure 5.3**).

Secondly, it was possible to calculate the conversions in different reaction conditions (see below) by comparing the peak integrals with an internal standard.

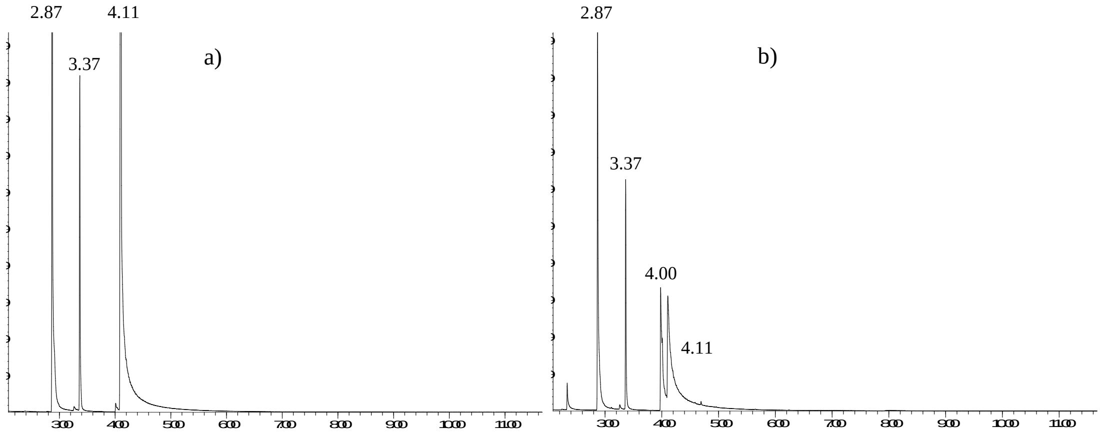

Figure 5.3. GC-MS chromatograms of a mixture containing 4-methoxybenzyl alcohol (10^{-2} M), 1,2-dichlorobenzene ($3*10^{-3}$ M), **TEMPO** (10^{-3} M) and CAN ($2*10^{-3}$ M) in ACN before (**a**) and after (**b**) 3 hours of reaction. Retention times: 2.87 min (1,2-dichlorobenzene, internal standard), 3.37 min (**TEMPO**), 4.00 min (4-methoxybenzaldehyde), 4.11 min (4-methoxybenzyl alcohol).

Preliminary GC-MS experiments were performed using **TEMPO** as catalyst and different amounts of CAN (20% or 40% of the initial alcohol concentration). Since CAN is directly involved in the recovery of the oxoammonium catalyst, the cycle of oxidation was strongly favoured increasing the concentration of CAN, leading to higher conversions, as confirmed by the results reported in **Table 5.1**. The same effect was obtained augmenting the reaction time.

Table 5.1. Conversions calculated by GC-MS experiments performed on solutions containing 4-methoxybenzyl alcohol (10^{-2} M), **TEMPO** (10^{-3} M) and different concentrations of CAN, in ACN.

Experiment	[CAN] (M)	Time (h)	Conversion (%)
1	0.002	1	40%
2	0.002	3	60%
3	0.004	3	85%

In addition, in order to verify the role of oxygen in the catalytic cycle, the same experiments were carried out under inert atmosphere. In this case, the conversions obtained were significantly lower (**Table 5.2**). Since Ce (IV) could not be regenerated from Ce (III) in absence of oxygen, the catalytic cycle stopped once that all the available Ce (IV) was consumed, strongly penalizing the efficiency of the reaction.

Table 5.2. Conversions calculated by GC-MS experiments performed in absence of O_2 on solutions containing 4-methoxybenzyl alcohol (10^{-2} M), **TEMPO** (10^{-3} M) and different concentrations of CAN, in ACN.

Experiment	**[CAN] (M)**	**Time (h)**	**Conversion (%)**
1	0.002	3	10%
2	0.004	3	40%

Successively, the performance of *cis*-**1** catalyst was explored, reproducing the same reaction conditions optimized in the case of **TEMPO** radical. Similarly, the reaction conversion was influenced by the amount of CAN employed. Conversion grew up to 99% in the presence of CAN 0.004 M, and more than satisfactory results were also achieved using the same oxidant in lower amounts (**Table 5.3**). These results evidenced that *cis*-**1** catalyst led to better results in terms of reaction efficiency, if compared to radical **TEMPO**.

Table 5.3. Conversions calculated by GC-MS experiments performed on solutions containing 4-methoxybenzyl alcohol (10^{-2} M), *cis*-**1** (10^{-3} M) and different concentrations of CAN, in ACN.

Experiment	**[CAN] (M)**	**Time (h)**	**Conversion (%)**
1	0.001	3	60%
2	0.002	3	80%
3	0.004	3	99%

Finally, in order to verify that CAN was not directly involved in the oxidation of the alcohol, further GC-MS studies were executed in absence of the macrocycle *cis*-**1** (**Table 5.4**).

Table 5.4. Conversions calculated by GC-MS experiments performed on solutions containing 4-methoxybenzyl alcohol (10^{-2} M) and different concentrations of CAN, in ACN.

Experiment	[CAN] (M)	Time (h)	Conversion (%)
1	0.001	3	8%
2	0.004	3	25%

The results evidenced significantly low conversions, indicating that CAN was not responsible of the selective oxidation of the alcohol to aldehyde, which was formed only in the presence of *cis*-**1**ox**.** On the contrary, CAN promoted prevalently the full oxidation of 4-methoxybenzyl alcohol to the corresponding acid, whose peak was observed in the GC-MS chromatogram (consult **Chapter 7** for more details).

In conclusion, we believe that the novel macrocycle *cis*-**1** can be used as efficient catalyst for the aerobic oxidation of alcohols in the presence of CAN and oxygen. The hypothesised catalytic mechanism was verified, and the target compound gave more than satisfactory results, even better than those obtained with **TEMPO** radical.

5.3 FIRST EXPERIMENTS ON THE AEROBIC OXIDATION OF ALCOHOLS PROMOTED BY A PARAMAGNETIC MOLECULAR MACHINE

The study of catalytic cycle of alcohol oxidation promoted by macrocycle *cis*-**1** was extended to the bistable rotaxane **R1·(PF$_6$)$_2$** shown in **Scheme 5.7**, [10] in which *cis*-**1** represents the ring component. In this molecular machine, the ring shuttling over the dumbbell could be promoted by oxidation of the nitroxide unit to oxoammonium cation.

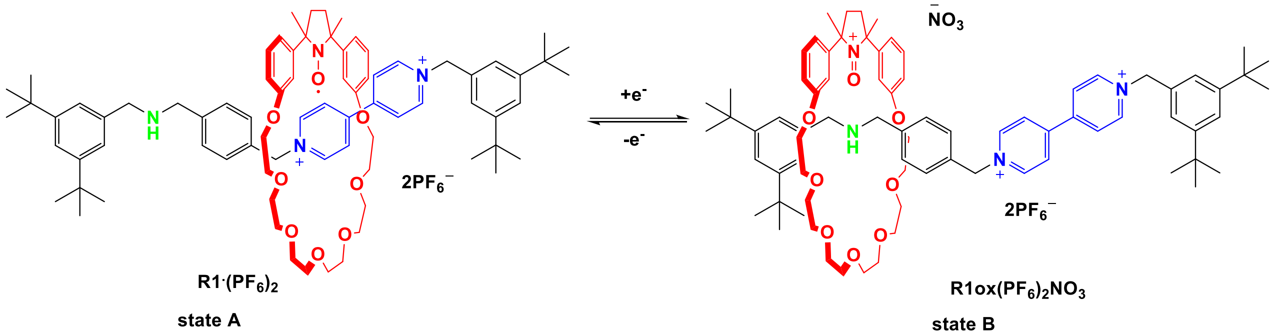

Scheme 5.7. Redox-induced switching of rotaxane **R1·(PF$_6$)$_2$**.

In particular, after oxidation of the nitroxide group, the macrocycle is forced to move from the bipyridinium (**BPY**$^{2+}$) to the electron rich amine (**NH**) station (**state B**), because of the repulsion between bis-pyridinium and oxoammonium cations. Reduction of **R1ox(PF$_6$)$_2$NO$_3$** leads back to the starting **state A**, where the paramagnetic wheel is positioned on the **BPY**$^{2+}$ group.

Based on the results described in **Paragraph 5.2,** the reaction of rotaxane **R1·(PF$_6$)$_2$** with 4-methoxybenzyl alcohol in the presence of CAN under aerobic conditions, could give rise to the catalytic cycle shown in **Scheme 5.8,** analogous to that described for *cis*-**1** (**Scheme 5.6**).

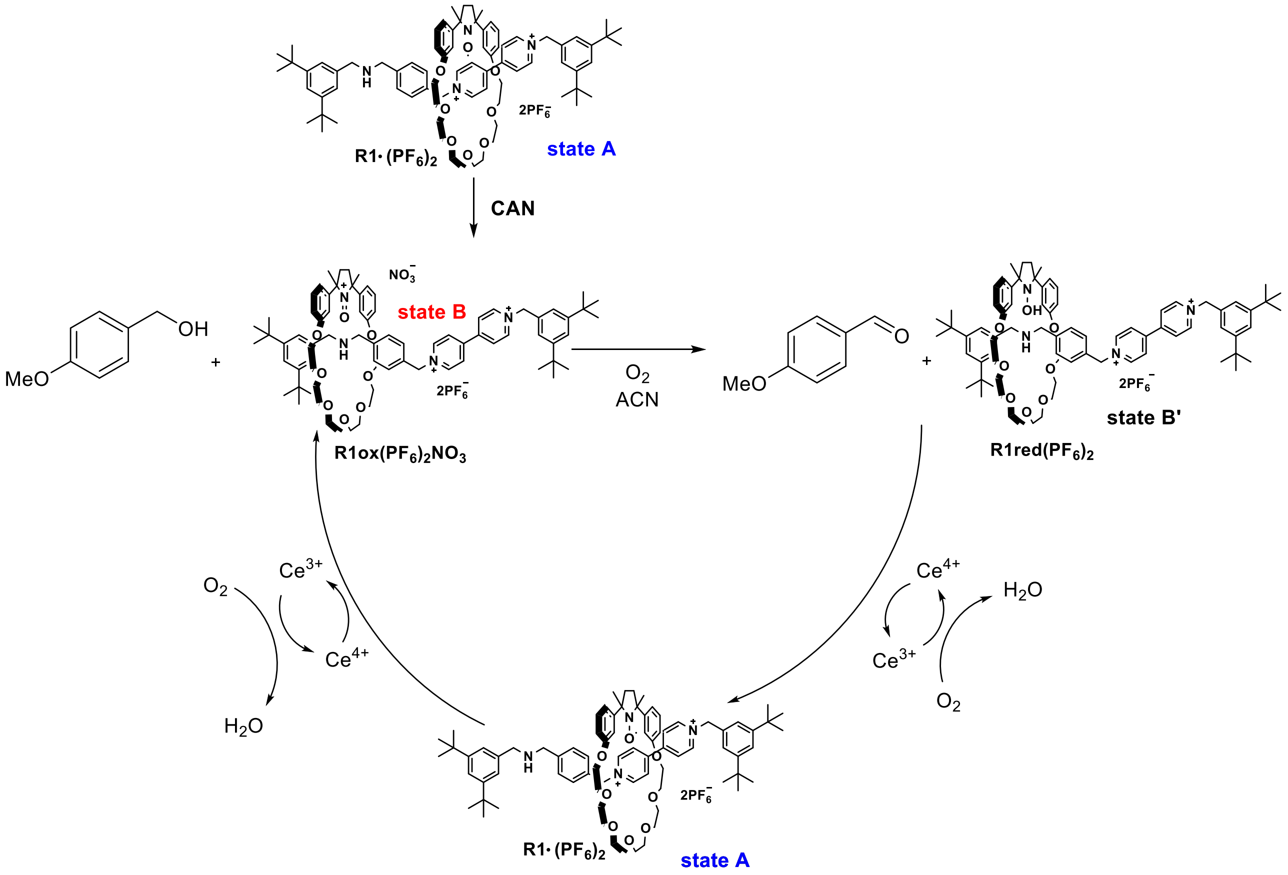

Scheme 5.8. Catalytic cycle of the oxidation of 4-methoxybenzyl alcohol promoted by rotaxane **R1·(PF$_6$)$_2$** and CAN in presence of oxygen.

In details, rotaxane **R1·(PF$_6$)$_2$** in the **state A,** obtained *in situ* by basic treatment with di-isopropyl ethylamine (DIPEA) of the protonated form **R1H·(PF$_6$)$_3$**,[10] is oxidized with CAN to **R1ox(PF$_6$)$_2$NO$_3$** (**state B**). Successively, **R1ox(PF$_6$)$_2$NO$_3$** promotes the alcohol oxidation, forming the hydroxylamine adduct (**state B'**), which can successively re-form rotaxane **R1·(PF$_6$)$_2$** by oxidation with CAN, leading the ring back to the original position on the **BPY^{2+}** station (**state A**). A second equivalent of CAN restores **state B** starting again the catalytic cycle. At the same time, CAN is regenerated by oxygen in continuity.

Unfortunately, the first results obtained using **R1·(PF$_6$)$_2$** as catalyst in the oxidation of 4-methoxybenzyl-alcohol were not satisfactory. GC-MS analyses showed low conversion of the starting alcohol under the same conditions employed with *cis*-**1**.

In order to overcome the inhibiting effect presumably deriving from the base employed for the *in situ* deprotonation of rotaxane **R1H·(PF$_6$)$_3$**, the design of an efficient methodology for the preventive isolation of deprotonated rotaxane **R1·(PF$_6$)$_2$** is still under investigation**.**

5.4 CONCLUSIONS

In this project, the oxidative catalytic cycle of 4-methoxybenzyl alcohol promoted by an oxoammonium salt, *cis*-**1**ox, and CAN under aerobic conditions, was studied. EPR spectroscopy and GC-MS studies were employed for monitoring and verifying the contribute of all the reagents involved in the process, and enabled to determine the optimal reaction conditions. Macrocycle *cis*-**1** displayed an interesting catalytic efficiency, if compared with the one obtained for other reported catalysts, such as **TEMPO** radical.

The investigation of the aerobic catalytic cycle of 4-methoxbenzyl alcohol using a bistable rotaxane based on the paramagnetic macrocycle *cis*-**1** is still in progress.

REFERENCES

[1] J. M. Bobbitt, C. Brùckner and N. Merbouh, *Org. React.,* vol. 74, p. 106–424, 2009.

[2] G. I. Likhtenshtein, J. Yamauchi, S. Nakatsuji, S. Smirnov and R. Tamura, Nitroxides: Applications in Chemistry, Biomedicine and Materials Science, Winnehim: Wiley-VCH, 2008.

[3] T. Studer and A. Vogler, *Synthesis,* p. 1979–1993, 2008.

[4] S. D. Burke and R. L. Danheiser, Handbook of Reagents for Organic Synthesis: Oxidizing and Reducing Agents, New York: John Wiley & Sons, 1999.

[5] S. S. Jung and H. C. Kim, *Synthesis,* p. 2135–2137, 2003.

[6] N. Wang, R. Liu, J. Chen and X. Liang, *Chem. Commun.,* p. 5322–5324, 2005.

[7] F. Minisci, F. Recupero, G. F. Pedulli and M. Lucarini, *J. Mol. Catal. A: Chem.,* p. 204–205, 2003.

[8] N. Ragauskas and A. J. Jiang, *Org. Lett.,* vol. 7, p. 3689–3692, 2005.

[9] N. J. Hill, J. M. Hoover and S. S. Stahl, *J. Chem. Educ. ,* vol. 90, p. 102−105, 2013.

[10] V. Bleve, P. Franchi, E. Konstanteli, G. L., S. M. Goldup, E. Mezzina and M. Lucarini, *Chem. Eur. J.,* vol. 24, pp. 1198-1201, 2018.

CHAPTER 6: SYNTHESIS AND EPR INVESTIGATION OF A NOVEL PARAMAGNETIC CROWN-ETHER MACROCYCLE

6.1 INTRODUCTION

Macrocycles based on aza-crown ethers present an interesting biological activity due to their unique ability to incorporate cations of different size into their cavity and transport them across cell membranes.[1] Due to their suitability for biochemical applications, the investigation of the inclusion properties of different substrates belonging to this class of molecules has found a lot of interest among the scientific community.[2][3] Thanks to the ability of nitroxide groups (N-O$^{\bullet}$) to perform halogen, hydrogen bonds and other non-covalent interactions,[4][5] their covalent incorporation in crown ether structures could be a powerful tool for the preparation of novel multi-featured ionophores, opening to a *plethora* of possible applications in the fields of bio-chemistry, metal sensing and radical molecular machinery. In these cases, EPR spectroscopy acquires a key role in the detection and monitoring of the binding events, association/dissociation processes, conformational and dynamic motions affecting the substrates, thanks to its high sensitivity for the chemical environment surrounding the paramagnetic units (**Paragraph 1.2.1**). However, there are only few examples in the literature concerning the synthesis of spin labelled crown ether macrocycles employed as molecular hosts and the use of EPR spectroscopy as monitoring technique for the study of the target substrates.[6][7] Thus, this work aimed to design, synthetize and study a novel type of crown ether macrocycle containing a nitroxide unit (**AC7O$^{\bullet}$**) (**Figure 6.1**). The incorporation of the paramagnetic centre in an aliphatic crown ether structure enables its high exposition to non-covalent interactions with included guests, potentially enhancing the complexing ability of the compound. EPR spectroscopy was employed for studying the host properties of the target substrate and for calculating its complexation equilibrium constants (K_a) toward different types of inorganic and organic cationic guests.

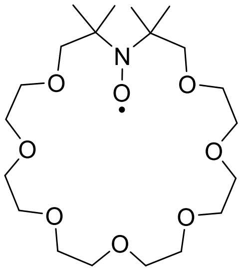

Figure 6.1. Structure of paramagnetic macrocycle **AC7O$^\bullet$.**

6.2 SYNTHESIS AND EPR INVESTIGATION OF A NOVEL PARAMAGNETIC CROWN-ETHER MACROCYCLE

6.2.1 Synthesis and characterization

A methodology for the synthesis of aza-crown ethers reported by Lai and co-workers in 1985 was adapted in order to afford the desired compound (**Scheme 6.1**).[8] The optimized synthetic pathway involved a first formation of the morfolinone **2’’** in basic conditions and a second reduction with lithium aluminium hydride to give precursor **3’’**. Successively, the cyclization step was promoted by sodium *tert*-butoxyde base in the presence of a bis-tosylated glycol chain. Finally, oxidation of the amine **AC7** to nitroxide was performed using 3-chloroperbenzoic acid (*m*-CPBA), affording the final aza-crown oxyl macrocycle (**AC7O$^\bullet$**) in 30 % yield.

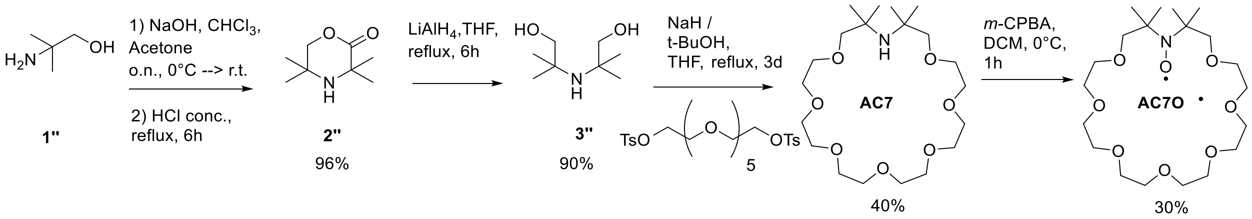

Scheme 6.1. Synthetic pathway affording macrocycle **AC7O$^\bullet$.**

The critical steps of this synthesis were the cyclization forming compound **AC7** and its oxidation to nitroxide **AC7O$^\bullet$**. The first one led to low yields due to the competitive formation of non-cyclized by-products. Concerning the last oxidation step, the difficulty was related to the formation of a ring-opened bright blue by-product due to the over-oxidation of the cyclic nitroxide to the nitroso-derivative reported in **Figure 6.2**, which was detected by ESI-MS analysis.

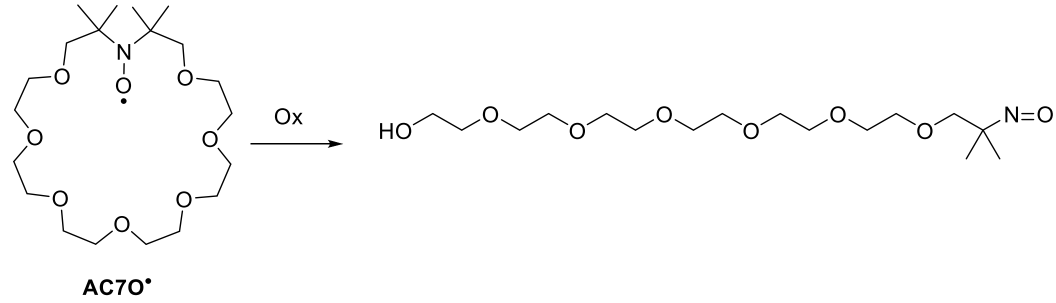

Figure 6.2. Structure of nitroso by-product deriving from the over-oxidation of nitroxide **AC7O$^\bullet$.**

In order to minimize the nitroso formation, a smaller amount of acid (0.7 eq.) was employed and the progressive formation of nitroxide **AC7O$^\bullet$** was followed by EPR, monitoring the signal intensity of the radical until a *plateau*. The reaction was then quenched by addition of 1 equivalent of $Ba(OH)_2$ and purified by chromatography column, affording the desired macrocyclic nitroxide up to 30% yields.

6.2.2 EPR studies

The host properties of **AC7O$^\bullet$** were investigated by observing the EPR spectral response of the compound in the presence of different cationic guests in solution. If the radical moiety is involved directly in the interaction with the guest, a significant variation of the EPR spectral parameters occurs after complexation. In particular, a variation of the hyperfine coupling constant (a_N) was observed in the EPR spectrum of **AC7O$^\bullet$** after addition of Ca^{2+}, Ba^{2+} and Sr^{2+} salts (**Figure 6.3b,c,e**). This effect was attributed to a variation of the spin density on the nitrogen atom of the nitroxide moiety, occurring in the presence of a non-covalent interaction between the N-O$^\bullet$ group and the included guest (**Paragraph 1.2.1**). In the case of complexation of metal cations presenting non-zero nuclear spins (I) (*i.e.* $^{133}Cs^+$, $^{23}Na^+$ and $^7Li^+$), the EPR spectrum of macrocycle **AC7O$^\bullet$** presented a further line splitting into multiplets after addition of the guests, deriving from the coupling of the unpaired electron with the complexed spin active nuclei (**Figure 6.3d,f,g**), according to the relationship $N_{lines}=(2n_AI_A+1)(2n_BI_B+1)\ldots(2n_NI_N+1)$ (**Paragraph 1.2.1**). Furthermore, the complexation of metal cations that are presents in different isotopic forms in a significant percentage of relative abundance, as in the case of $^{85}Rb^+$ and $^{87}Rb^+$, resulted in an EPR spectrum reflecting the interaction of the unpaired electron with both isotopomers (**Figure 6.3h**).

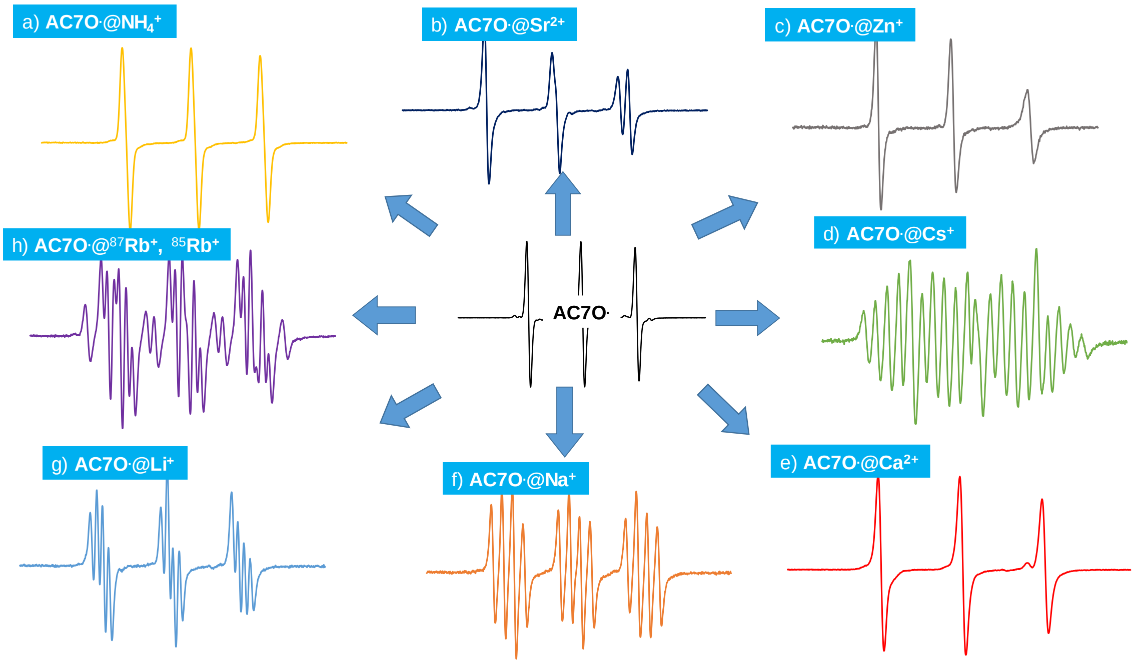

Figure 6.3. Comparison between EPR spectra of free **AC7O**$^\bullet$ (centre) and **AC7O**$^\bullet$ after addition of: a) NH_4PF_6; b) $Sr(Picr)_2$; c) $ZnClO_4$; d) Cs(Picr); e) $Ca(Picr)_2$; f) $Na(ClO_4)$; g) $Li(ClO_4)$; h) $Rb(ClO_4)$ in ACN at 298K.

Differently, no significant spectral variations between complexed and non-complexed form of **AC7O**$^\bullet$ were observed after addition of K$^+$. However, it was plausible to assume that the inclusion of K$^+$ occurred without direct involvement of the nitroxide function. Thus, EPR titrations were performed adding a K$^+$ salt to samples containing macrocycle **AC7O**$^\bullet$ already complexed with cation Ca^{2+}. The spectral response recorded after addition of K$^+$ indicated the progressive exit of Ca^{2+} cation from the host system, evidenced by the observance a EPR spectrum similar to that of free **AC7O**$^\bullet$. This effect was attributed to the competitive complexation with K$^+$, confirming the formation of AC7O·@K$^+$ complex.

Later on, the complexing behaviour of **AC7O**$^\bullet$ in the presence of organic guests, such as dibenzylammonium cation (DBA), which is representative of many linear components employed for the preparation of rotaxanes,[7] was evaluated in order to investigate possible applications in the field of radical MIMs. In the presence of DBA salt, the EPR spectrum of **AC7O**$^\bullet$ showed a significant increase of the a_N constant (from 15.28 to 16.16 G) (**Figure 6.4**), indicating a strong affinity also with organic species.

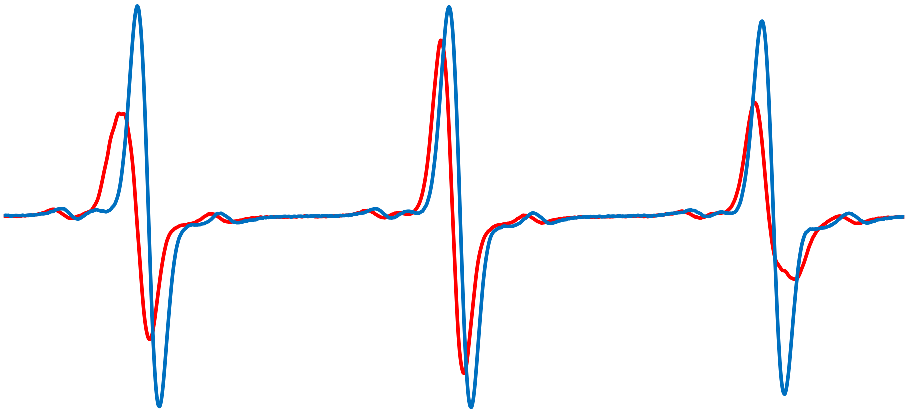

Figure 6.4. Comparison of the EPR spectra of **AC7O$^\bullet$** (blue line) and **AC7O$^\bullet$** after addition of excess of DBA (red line), indicating the hosting of the organic cation.

Thanks to these spectral variations, it was possible to calculate the complexation equilibrium constants (K_a) by using EPR spectroscopy and computer simulations.[9]

The analysis was conducted using constant concentrations of **AC7O$^\bullet$** in the presence of variable amounts of each guest and extrapolating the ratios between the concentrations of complexed and non-complexed form of **AC7O$^\bullet$** ($\frac{[AC7O{\cdot}@M^+]}{[AC7O{\cdot}]}$) by using EPR spectra simulations. The K_a values were obtained considering the angular coefficients of the linear regression plots reporting the calculated values of $\frac{[AC7O{\cdot}@M^+]}{[AC7O{\cdot}]}$ as a function of guest concentration. In the presence of a large excess of guest, the value of K_a was approximated according to the following equation:

$$K_a = \frac{[AC7O{\cdot}@M^+]}{[AC7O{\cdot}][M^+]} = \frac{[AC7O{\cdot}@M^+]}{[AC7O{\cdot}]_0[M^+]_0}$$

Alternatively, when using concentrations of guest comparable to those of **AC7O$^\bullet$**, the K_a were obtained considering the complete mathematical treatment:

$$K_a = \frac{[AC7O{\cdot}@M^+]}{[AC7O{\cdot}][M^+]} =$$

$$= \frac{[AC7O{\cdot}@M^+]}{([AC7O{\cdot}]_0 - [AC7O{\cdot}@M^+])([M^+]_0 - [AC7O{\cdot}@M^+])}$$

If $[AC7O{\cdot}@M^+] = x$, K_a becomes:

$$K_a = \frac{x}{([AC7O\cdot]_0 - x)([M^+]_0 - x)}$$

Concerning the complexation of cation K$^+$, for which no spectral variations were observed, the K_{K^+} was indirectly calculated thanks to competitive titrations with cation Ca^{2+}, performed by adding 4 or 5 different concentrations of a K$^+$ salt to samples containing macrocycle **AC7O$^\bullet$** complexed with cation Ca^{2+}. The corresponding K_{K^+} was estimated by considering the following equation:

$$\frac{[AC7O\cdot@\mathrm{Ca}^{2+}]}{[AC7O\cdot@\mathrm{K}^+]} = \frac{K_{\mathrm{Ca}^{2+}}}{K_{\mathrm{K}^+}}\frac{[\mathrm{Ca}^{2+}]}{[\mathrm{K}^+]}$$

Here, $\frac{[AC7O\cdot@\mathrm{Ca}^{2+}]}{[AC7O\cdot@\mathrm{K}^+]}$ was obtained by EPR spectra simulation, $K_{\mathrm{Ca}^{2+}}$was known from the previous titrations, $[\mathrm{Ca}^{2+}]$ was kept constant, while $[\mathrm{K}^+]$ was approximated to $[\mathrm{K}^+]_0$. A linear regression plot was extrapolated by plotting $\frac{[AC7O\cdot@\mathrm{Ca}^{2+}]}{[AC7O\cdot@\mathrm{K}^+]}$ value as a function of $[\mathrm{K}^+]_0$ for obtaining the accurate value of K_{K^+}. All the calculated K_a values are reported in **Table 6.1**.

Table 6.1. Calculated K_a for the complexation between **AC7O$^\bullet$** and different guests in ACN and acetone (^{a}). The hyperfine coupling constant (a_N) of **AC7O$^\bullet$** is 15.24 G in ACN and 15.06 G in acetone.

Salt	**Cation**	**K_a/M^{-1}(T=294K)**	**a_N/G**	**Ionic radius (Å)**	**Cation nuclear spin (*I*)**
$LiClO_4$	Li^+	536	16.05	0.76	3/2
$NaClO_4$	Na^+	3200	15.45	1.02	3/2
Na(Picr)	Na^+	3200	15.46	1.02	3/2
K(Picr)	K^+	30050	15.52	1.38	0
$RbClO_4$	Rb^+	Non determined (not soluble)	15.65 (^{85}Rb) 15.59 (^{87}Rb)	1.52	3/2 5/2
Cs(Picr)	Cs^+	5042	15.75	1.67	7/2
$Ca(Picr)_2$	Ca^{2+}	59600	16.75	0.99	0
$Sr(Picr)_2$	Sr^{2+}	100000	16.50	0.112	0
NH_4PF_6	NH_4^+	12334	15.88	1.4	0
$(PhCH_2)_2NH_2PF_6$	$(PhCH_2)_2NH_2^+$	117	16.01		0
Na(Picr)^a	Na^+	612.5	15.27	1.02	3/2
Cs(Picr)^a	Cs^+	1569.8	15.76	1.67	7/2
$Ca(Picr)_2$^{a}	Ca^{2+}	61.0	16.53	0.99	0
$(PhCH_2)_2NH_2PF_6$^{a}	$(PhCH_2)_2NH_2^+$	20.6	16.04		0

The data reported in **Table 6.1** show that the affinity of **AC7O$^\bullet$** increased exponentially with the ionic radius of the guest (*i.e.* Li^+ *vs* Na^+ *vs* Cs^+) and with the entity of the charge (*i.e.* Ca^{2+} *vs* Na^+). However, an exception was noticed for K^+ cation, for which the corresponding K_{K^+} was estimated over 5 times greater than K_{Cs^+}. In addition, the affinity for organic DBA cation was significantly much lower than that obtained for the inorganic ones.

In order to complete the analysis of the complexation of alkaline and alkaline-earth metal salts, which were not soluble in pure ACN (*i.e.* $MgCl_2$, $Ba(CH_3COO)_2$, NaCl and $CaCl_2$), supplementary experiments in ACN/H_2O 99/1 were performed (**Table 6.2**).

Table 6.2. Calculated K_a for the complexation between **AC7O•** and different guests in ACN/H_2O 99/1. In the same solvent the hyperfine coupling constant (a_N) of **AC7O•** is 15.34 G.

Salt	**Cation**	**K_a/M^{-1} (T=294K)**	**a_N/G**	**Ionic radius (Å)**
NaCl	Na^+	570.5	15.49	1.02
RbCl	$^{85}Rb^+$ (72.12%)	6373.5	15.65	1.52
	$^{87}Rb^+$ (27.83%)		15.66	
$CaCl_2$	Ca^{2+}	9609	16.70	0.99
$Ba(CH_3COO)_2$	Ba^{2+}	2404.8	16.28	1.35
$MgCl_2$	Mg^{2+}	620.7	16.48	0.72

Once again, the results confirmed that the ion size played a decisive role in favouring the host-guest complex formation, as evident from comparison between the values of $K_{Ca^{2+}}$ and $K_{Mg^{2+}}$ and between K_{Na^+} and K_{Rb^+}. However, an exception was noticed for Ba^{2+} (ionic radius 1.35 Å), whose affinity was not higher than that found for the smaller Ca^{2+}. This result was plausibly attributed to the high solvation of Ba^{2+} ion by H_2O molecules present in 1% in the mixture, thus, preventing the formation of AC7O·@Ba^{2+} complex. As last, the effect of increasing percentages of H_2O on the complexation properties of **AC7O·** in the presence of NaCl or $CaCl_2$ salts (**Table 6.3**) was checked. Inspection of **Table 6.3** shows that the affinity for Na^+ cation decreased proportionally to the water amount present in the solvent mixture. This behaviour was even enhanced for Ca^{2+} cation, for which the hydration shell around the cation strongly limited the establishment of effective chelating interactions with host macrocycle. This inhibiting effect of water should be considered when comparing data obtained in different experimental conditions.

Table 6.3. Complexation ability of **AC7O·** towards Na^+ and Ca^{2+} guests in different ACN/H_2O mixtures.

Salt	**Mixture ACN/H_2O**	**K_a/M^{-1}(T=294K)**	**a_N/G (free)**	**a_N/G (bound)**
NaCl	99.5/0.5	690.6	15.31	15.46
NaCl	99/1	570.5	15.34	15.49
NaCl	98/2	342.3	15.42	15.56
NaCl	96/4	193.2	15.44	15.63
NaCl	92/8	64.5	15.56	15.91
$CaCl_2$	99/1	9609	15.35	16.70
$CaCl_2$	98/2	742.7	15.43	16.80

6.3 CONCLUSIONS

In these preliminary experiments, the inclusion properties of a novel paramagnetic crown ether macrocycle, **AC7O$^\bullet$**, toward alkali, earth-alkali metals and few organic guests were tested. Evidence of the complexation was given by significant variations in the spectral parameters (multiplicity and hyperfine constants) between the EPR spectra of the complexed and non-complexed form of **AC7O$^\bullet$**. Thanks to these spectroscopic features, the complexation equilibrium constants (K_a) were easily determined by theoretical simulation of the EPR spectra. The novel macrocycle **AC7O$^\bullet$** showed a good affinity towards a variety of guests, showing complexation equilibrium constants up to 160000 M^{-1}. For this reason, it will be further investigated for possible applications in metal sensing.

REFERENCES

[1] M. Nakatsuji and Y. Okahara, Biomimetic and Bioorganic Chemistry, New York: Springer Verlag, 1985.

[2] K. Marsalek and V. Sindelar, *Org. Lett.* , vol. 22, no. 4, p. 1633–1637, 2020.

[3] R. A. Schultz, E. Schlegel, D. M. Dishong and G. Gokel, *J. Chem. Soc. Chem. Comm.,* vol. 4, pp. 242-243, 1982.

[4] P. L. M. Franchi, P. Pedrielli and G. F. Pedulli, *ChemPhysChem,* vol. 3, pp. 789-793, 2002.

[5] L. Gualandi, E. Mezzina, P. Franchi and M. Lucarini, *Chem. Eur. J.,* vol. 22, pp. 16017-16021, 2016.

[6] L. Gualandi, P. Franchi, A. Credi, E. Mezzina and M. Lucarini, *Phys. Chem. Chem. Phys.*, vol. 21, p. 3558, 2019.

[7] V. Bleve, P. Franchi, E. Konstanteli, L. Gualandi, S. Goldup, E. Mezzina and M. Lucarini, *Chem. Eur. J.*, vol. 24, p. 1198, 2018.

[8] J. T. Lai, *J. Org. Chem.,* vol. 50, p. 1329, 1985.

[9] M. Lucarini, B. Luppi, G. F. Pedulli and B. P. Roberts, *Chem.Eur. J.,* vol. 5, pp. 2048-2055, 1999.

CHAPTER 7: EXPERIMENTAL

7.1 GENERAL INFORMATION

EPR spectra have been recorded on a Bruker-ELEXYS spectrometer by using the following instrument settings: microwave power 0.79 mW, modulation amplitude 0.04 mT, modulation frequency 100 kHz, scan time 180 s, 2K data points.[1]

^{1}H NMR and ^{13}C-NMR spectra of the target compounds and their precursors were recorded at 298 K on a Varian Mercury spectrometer operating at 400 MHz or 600MHz in CD_3CN, CD_3COCD_3, CD_3SOCD_3 and $CDCl_3$ solutions using the solvent peak as internal standard (1.94, 2.05, 2.50 and 7.26 ppm). Chemical shifts are reported in parts per million (δ scale).

ESI-MS spectra were recorded on a Waters Micromass ZQ 4000 spectrometer using the following instrumental settings: positive ions; desolvation temperature: 200° C; capillary voltage: 3.54 kV; cone voltage: 113 V.

HRMS spectra were recorded on a Waters Xevo G2-XS QTof mass spectrometer with an ESI-APCI type source and direct sample infusion system.

UV spectra were registered on a JASCO V-550 spectrophotometer operating at a constant temperature of 25 °C, recording within a wavelength range between 200 nm and 600 nm.

All starting reagents were used without further purification and were commercially available. Dry solvents were bought dry and used directly.

7.2 CHAPTER 3

7.2.1 Synthesis

Synthesis of compounds **7** and *cis*-**1** was performed according to the literature procedure.[2]

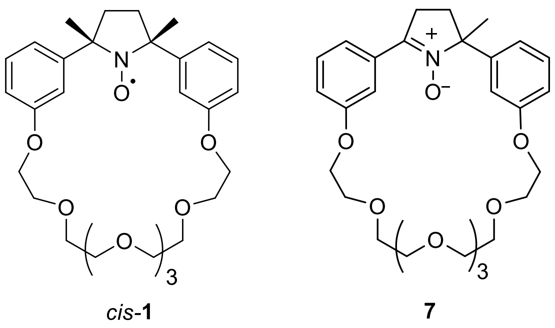

Scheme 7.1. Molecular structures of compounds **7** and *cis*-**1.**

*Synthesis of cis-***2:**

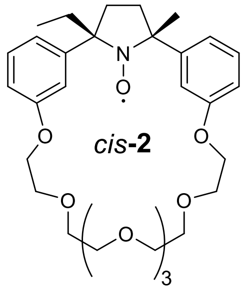

cis-**2**

Ethyl-lithium 1.5 M in diethyl ether (0.5 mL) was added at -78 °C to a stirred solution of nitrone **7**[2] (0.030 g, 0.0565 mmol) in THF (3 mL). After 30 minutes the reaction was quenched with saturated aqueous NH_4Cl. The aqueous layer was successively extracted with CH_2Cl_2, dried ($MgSO_4$), concentrated and treated for 12 hours with $Cu(OAc)_2$ (cat. amount) in methanol (7 ml). The resulting mixture was quenched with a saturated solution of $NaHCO_3$ and extracted with $CHCl_3$. The organic layer was concentrated and then purified by column chromatography on SiO_2 using CH_2Cl_2/MeOH 95:5 as eluent mixture (R_f= 0.55), providing nitroxide *cis*-**2** as orange oil in overall quantitative yield.

ESI-MS: *m/z* 581 ($M+Na^+$).

^1H NMR (400 MHz, Acetonitrile-d_3) δ 7.74 (broad, s.), 3.57 (m).

EPR (H_2O) a_N = 15.28 G, g_{factor} = 2.00575.

Oxidation with $Ce(NH_4)_2(NO_3)_6$ of the NMR sample containing the nitroxide gave the corresponding *cis*-oxoammonium salt after 5 minutes (see **Chapter 3**): ^1H NMR (400 MHz, Acetonitrile-d_3) δ 7.48 (t, *J* = 8.1 Hz, 1H), 7.35 (t, *J* = 8.1 Hz, 1H), 7.16 (m, 2H), 7.08 (d, *J* = 8.1 Hz, 1H), 6.93 (d, *J* = 8.1 Hz, 1H), 6.59 (s, 1H), 5.73 (s, 1H), 4.12 – 3.37 (m, 24H), 3.13 (dd, *J* = 13.3, 7.5 Hz, 2H), 2.51 (dd, *J* = 13.9, 7.3 Hz, 2H), 2.28 – 2.14 (m, 2H), 2.05 (s, 3H), 0.84 (t, *J* = 7.3 Hz, 3H).

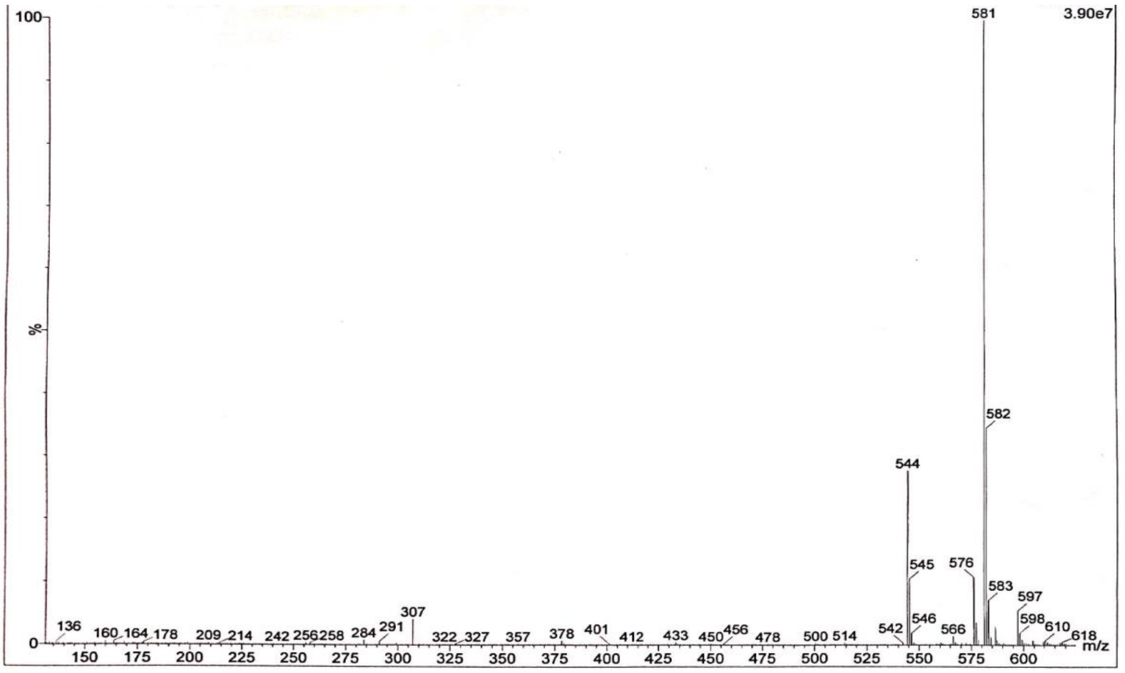

Figure 7.1. ESI-MS spectrum of *cis*-**2** in MeOH at room temperature.

7.2.2 Kinetic studies

EPR kinetic studies were performed according to the literature procedure.[3] In a typical experiment, stock solutions containing glutathione (50 mM) and nitroxide *cis*-**1** or *cis*-**2** (0.3 mM) in 50 mM sodium phosphate buffer (pH 7.4) were prepared. All the stock solutions were purged with nitrogen, then, the necessary aliquots of ascorbate were added and the evolution of the EPR peak height as a function of time immediately recorded (**Figure 7.1** to **7.6**). The k_{EPR} values were calculated as the angular coefficient of the linear regression plot reporting the $ln\frac{[nitroxide]_0}{[nitroxide]_t}$ as a function of time for different concentrations of ascorbate (from 30mM to 111mM). The rate constants k were extrapolated as slope of the dependence of the k_{EPR} value as a function of the concentration of ascorbate, as described in **Chapter 3**.

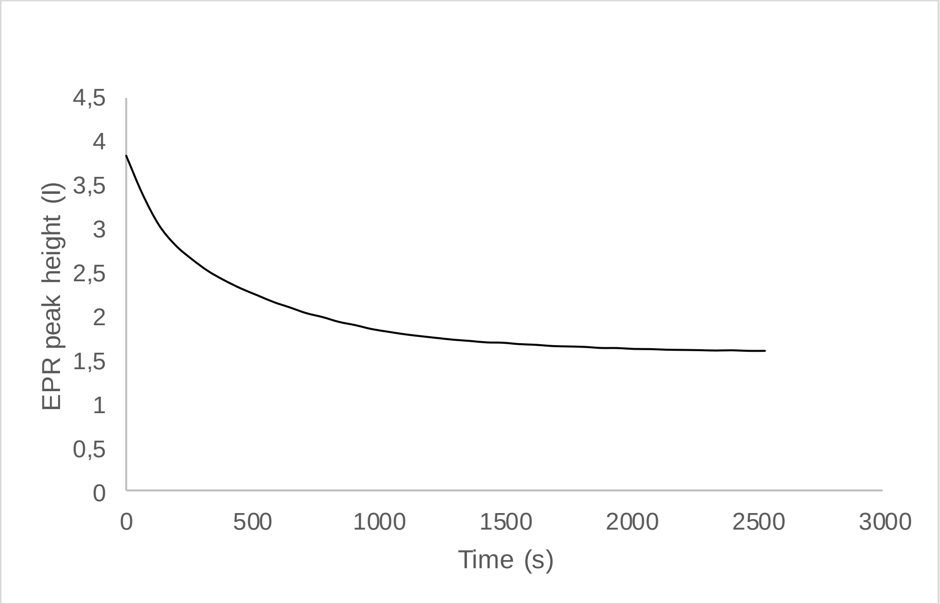

Figure 7.2. Evolution of the EPR peak height as a function of time of a solution of *cis*-**1** (0.3 mM) after addition of ascorbate (30 mM) in a phosphate buffer containing glutathione (50 mM) at pH 7.4.

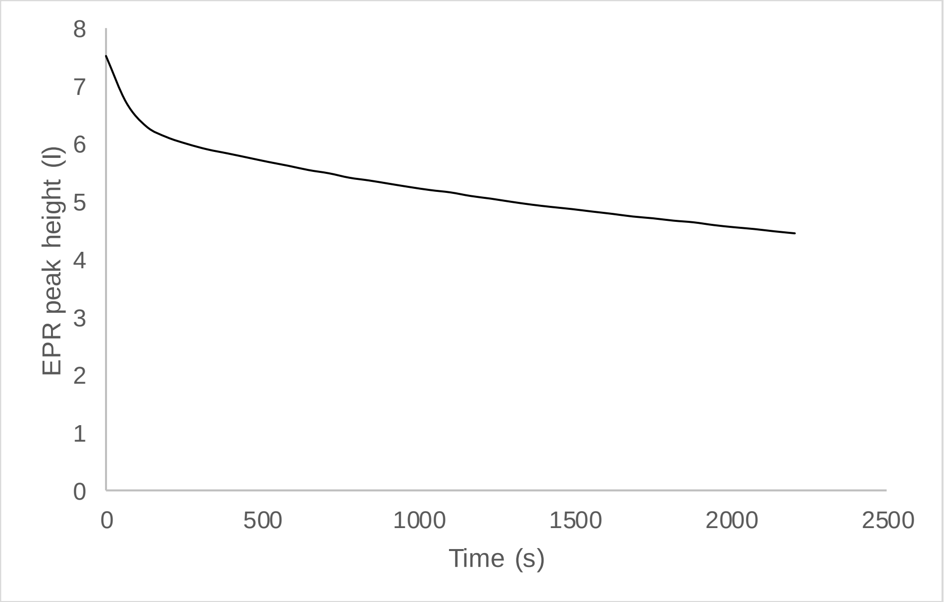

Figure 7.3. Evolution of the EPR peak height as a function of time of a solution of *cis*-**1** (0.3 mM) after addition of ascorbate (66 mM) in a phosphate buffer containing glutathione (50 mM), at pH 7.4.

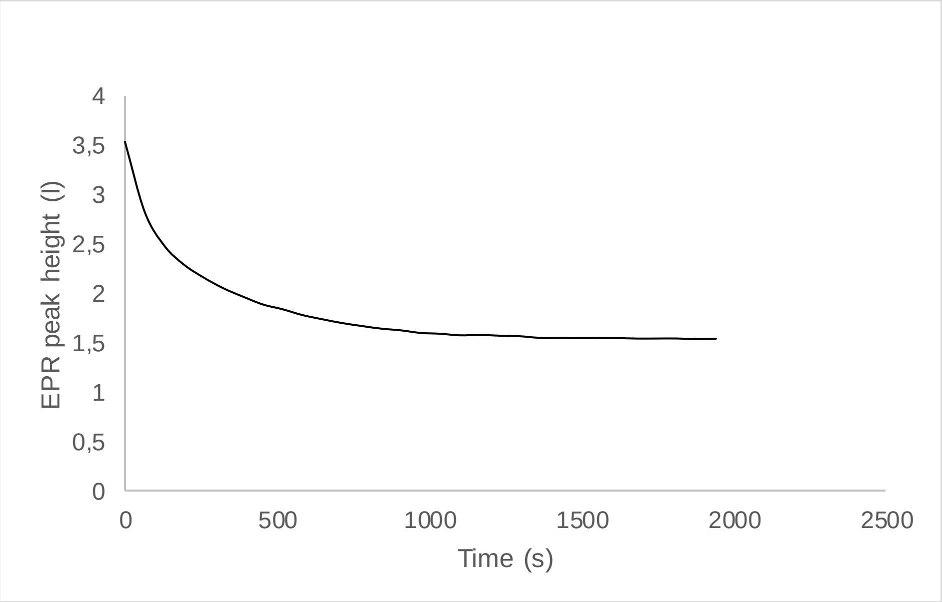

Figure 7.4. Evolution of the EPR peak height as a function of time of a solution of *cis*-**1** (0.3 mM) after addition of ascorbate (111 mM) in a phosphate buffer containing glutathione (50 mM), at pH 7.4.

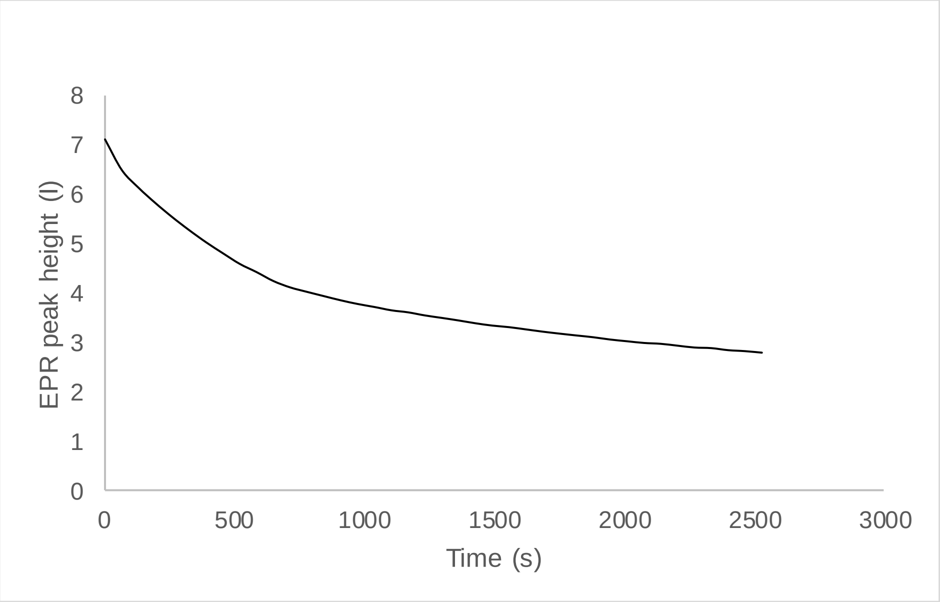

Figure 7.5. Evolution of the EPR peak height as a function of time of a solution of *cis*-**2** (0.3 mM) after addition of ascorbate (30 mM) in a phosphate buffer containing glutathione (50 mM), at pH 7.4.

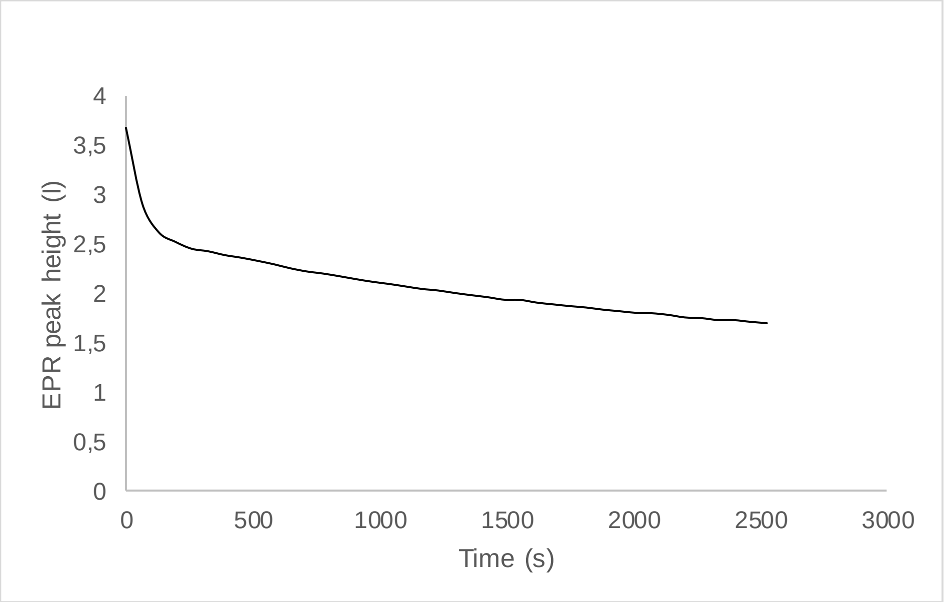

Figure 7.6. Evolution of the EPR peak height as a function of time of a solution of *cis*-**2** (0.3 mM) after addition of ascorbate (66 mM) in a phosphate buffer containing glutathione (50 mM), at pH 7.4.

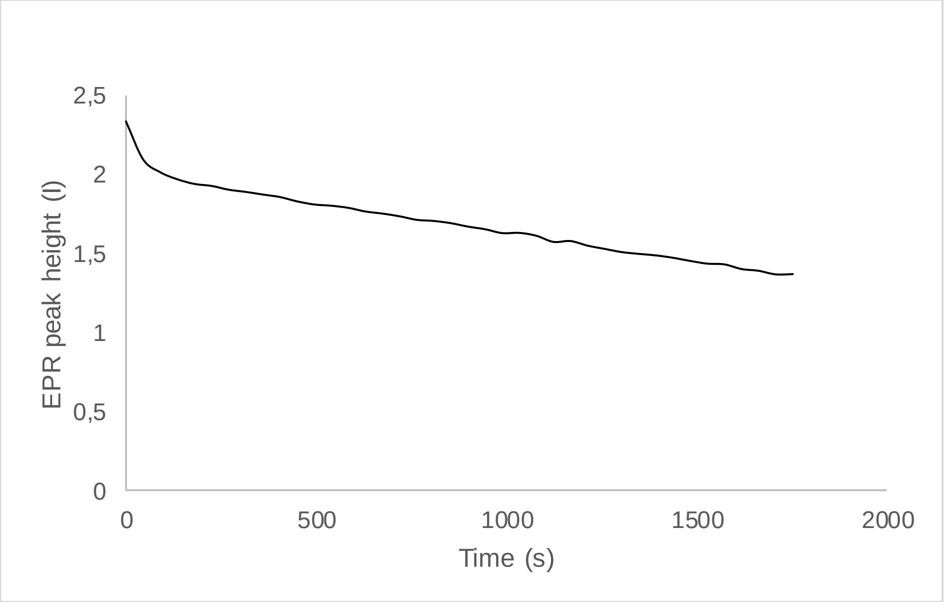

Figure 7.7. Evolution of the EPR peak height as a function of time of a solution of *cis*-**2** (0.3 mM) after addition of ascorbate (111 mM) in a phosphate buffer containing glutathione (50 mM), at pH 7.4.

7.3 CHAPTER 4

7.3.1 Synthesis

Compound **R1H•(PF$_6$)$_3$** and acids **1’, 3’, 4’** and **5’** were prepared following the procedures reported in the literature.[2][4]

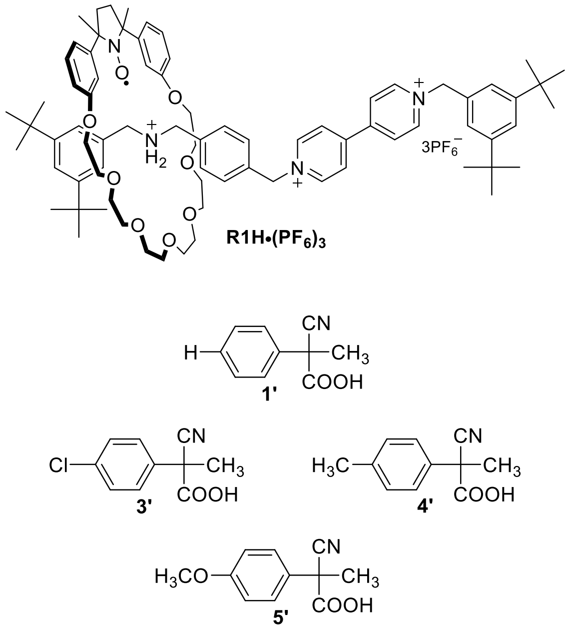

Scheme 7.2. Molecular structures of compound **R1H•(PF$_6$)$_3$** and acids **1’, 3’, 4’** and **5’.**

7.3.2 EPR kinetic studies for the fuel-driven reversible cycle

A solution of **R1H•(PF$_6$)$_3$** (0.1 mM) and diisopropylethylamine amine (0.1 mM) was introduced (ca. 50 µL) into a capillary tube with the internal diameter of ca. 1.85 mm. An EPR spectrum was recorded to verify the complete deprotonation of **R1H•(PF$_6$)$_3$** to **R1•(PF$_6$)$_2$**. Subsequently, 1 mol. eq. of the proper fuel (**1’, 3’, 4’** or **5’**) was added and EPR spectra were registered at regular time intervals. Oxygen consumption studies were performed by a similar procedure. In this case, the sample was closed by introducing into the sample tube a second capillary tube (external diameter of 1.60 mm) sealed at one end and leaving very little dead volume space. The decrease of the nitroxide concentration and the oxygen uptake was followed by EPR spectroscopy.

7.4 CHAPTER 5

7.4.1 Synthesis

Compounds *cis*-**1** and **R1H•(PF$_6$)$_3$** (see **Schemes 7.1** and **7.2**) were prepared following the procedure reported in the literature.[2]

7.4.2 EPR analysis of the in situ formation of oxoammonium salts

A solution of nitroxide (**TEMPO**, *cis*-**1, R1H•(PF$_6$)$_3$**) (0.1 mM) in ACN was treated with an excess of CAN (5 mol. eq.) and then introduced (ca. 50 µL) into a capillary tube with the internal diameter of ca. 1.85 mm. An EPR spectrum was recorded and compared to that of the starting radical to verify the complete oxidation of nitroxide to oxoammonium salt.

7.4.3 GC-MS analysis

The GC-MS analysis were conducted using a Network GC-system 6890N (Agilent technologies) with a time delay of 2.00 minutes, flow rate of 2 ml/s, starting from an initial temperature of 50 °C up to 270 °C, through a speed ramp of 30 °C/min. A solution of 4-methoxybenzyl-alcohol (0.01 M) and nitroxide **TEMPO**, *cis*-**1** or **R1•(PF$_6$)$_2$** (0.001 M) in ACN was prepared and fluxed with oxygen. Then, the necessary aliquots of CAN (0.002 M or 0.004 M) were added and the mixtures refluxed while stirring and fluxed by pure oxygen for all the time of reaction. Stock samples of the mixture were collected at regular time intervals performing GC-MS analysis for following the reaction. In the reactions conducted under inert atmosphere the mixture was fluxed with nitrogen.

The conversions were calculated by comparing the integrals of the chromatographic peaks related to alcohol and aldehyde, in the presence of an internal standard (1,2-dichlorobenzene, DCB, 0.003 M).

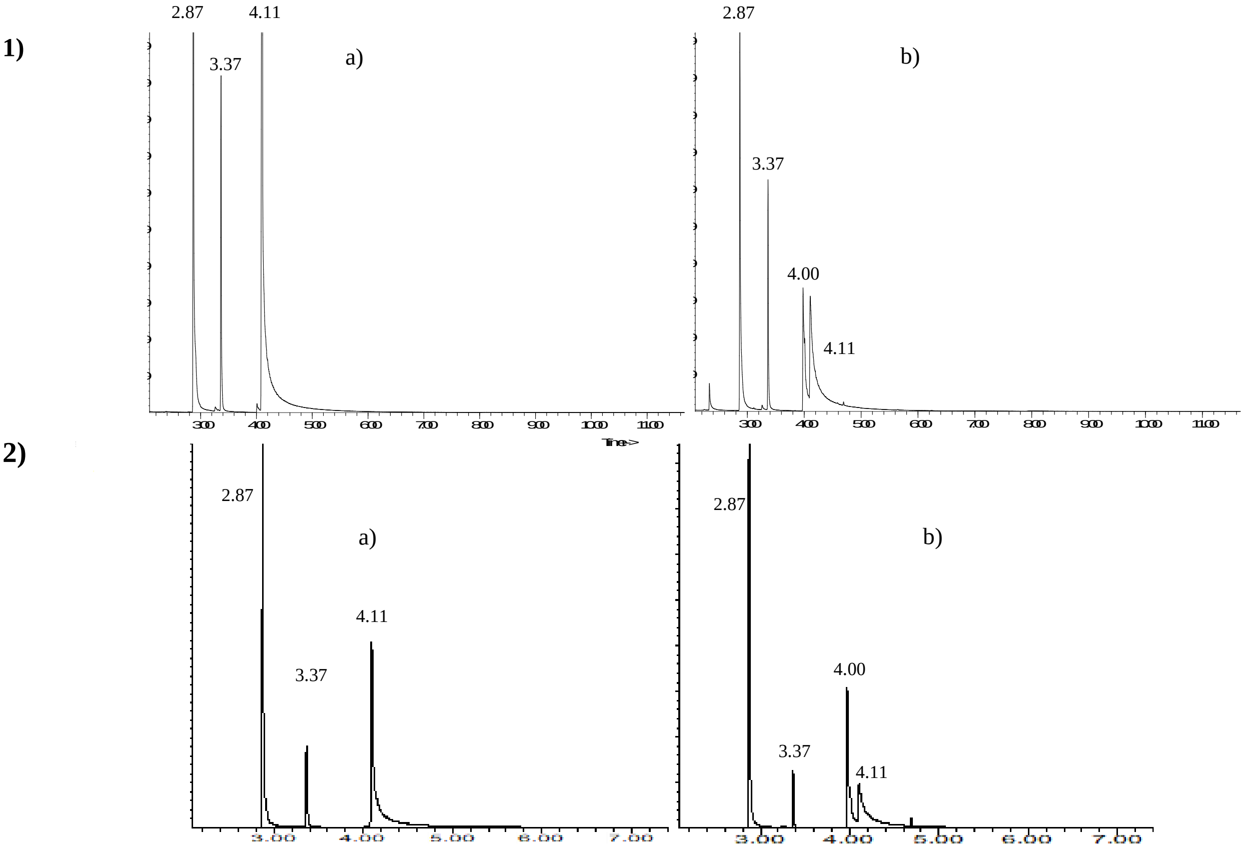

Figure 7.8. 1) GC-MS chromatograms of a mixture containing 4-methoxybenzyl alcohol (10^{-2} M), DCB ($3x10^{-3}$ M), **TEMPO** (10^{-3} M) and CAN ($2x10^{-3}$ M) in ACN before (**a**) and after (**b**) 3 hours of reaction. **2)** GC-MS chromatograms of a mixture containing 4-methoxybenzyl alcohol (10^{-2} M), DCB ($3x10^{-3}$ M), **TEMPO** (10^{-3} M) and CAN ($4x10^{-3}$ M) in ACN before (**a**) and after (**b**) 3 hours of reaction.

Retention times: 2.87 min (1,2-dichlorobenzene, internal standard), 3.37 min (**TEMPO**), 4.00 min (4-methoxybenzaldehyde), 4.11 min (4-methoxybenzyl alcohol).

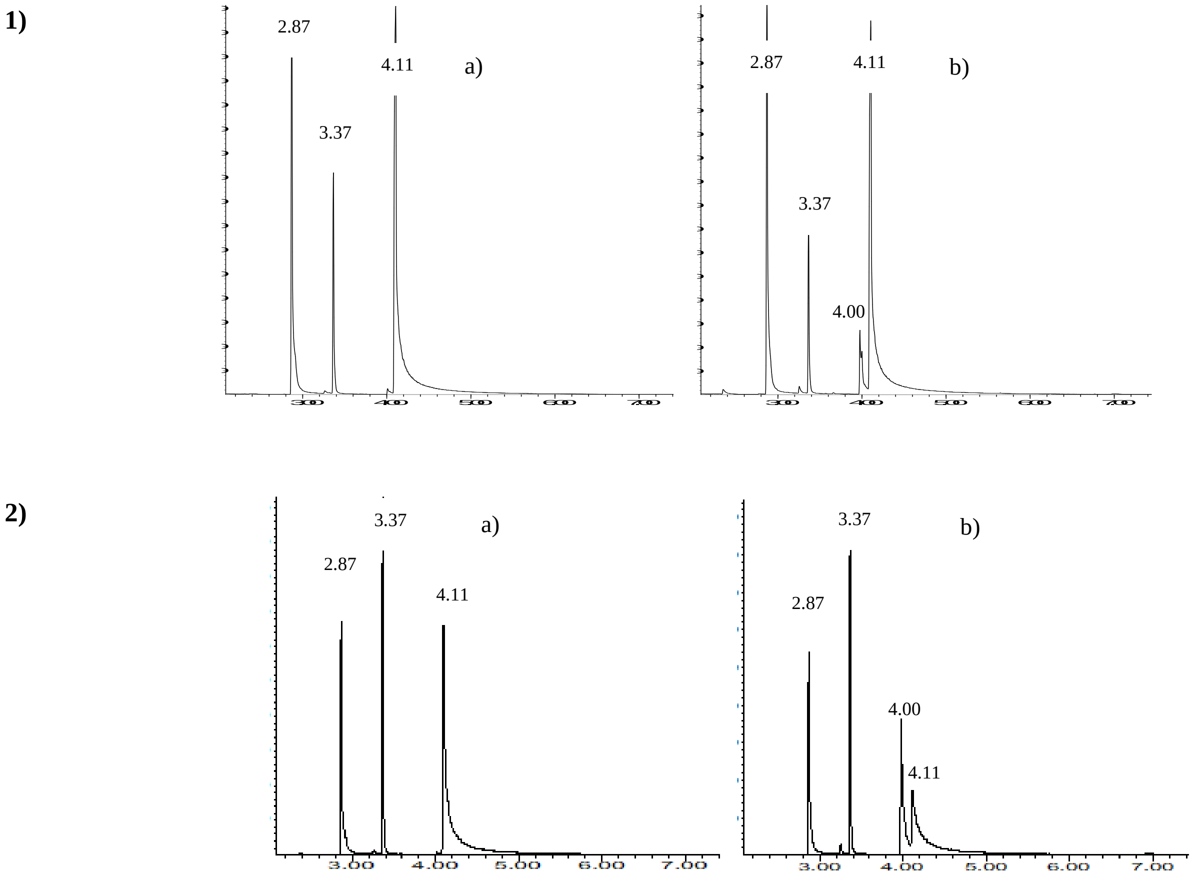

Figure 7.9. 1) GC-MS chromatograms of a mixture containing 4-methoxybenzyl alcohol (10^{-2} M), DCB ($3x10^{-3}$ M), **TEMPO** (10^{-3} M) and CAN ($1x10^{-3}$ M) in ACN before (**a**) and after (**b**) 3 hours of reaction under inert atmosphere. **2)** GC-MS chromatograms of a mixture containing 4-methoxybenzyl alcohol (10^{-2} M), DCB ($3x10^{-3}$ M), **TEMPO** (10^{-3} M) and CAN ($4x10^{-3}$ M) in ACN before (**a**) and after (**b**) 3 hours of reaction under inert atmosphere.

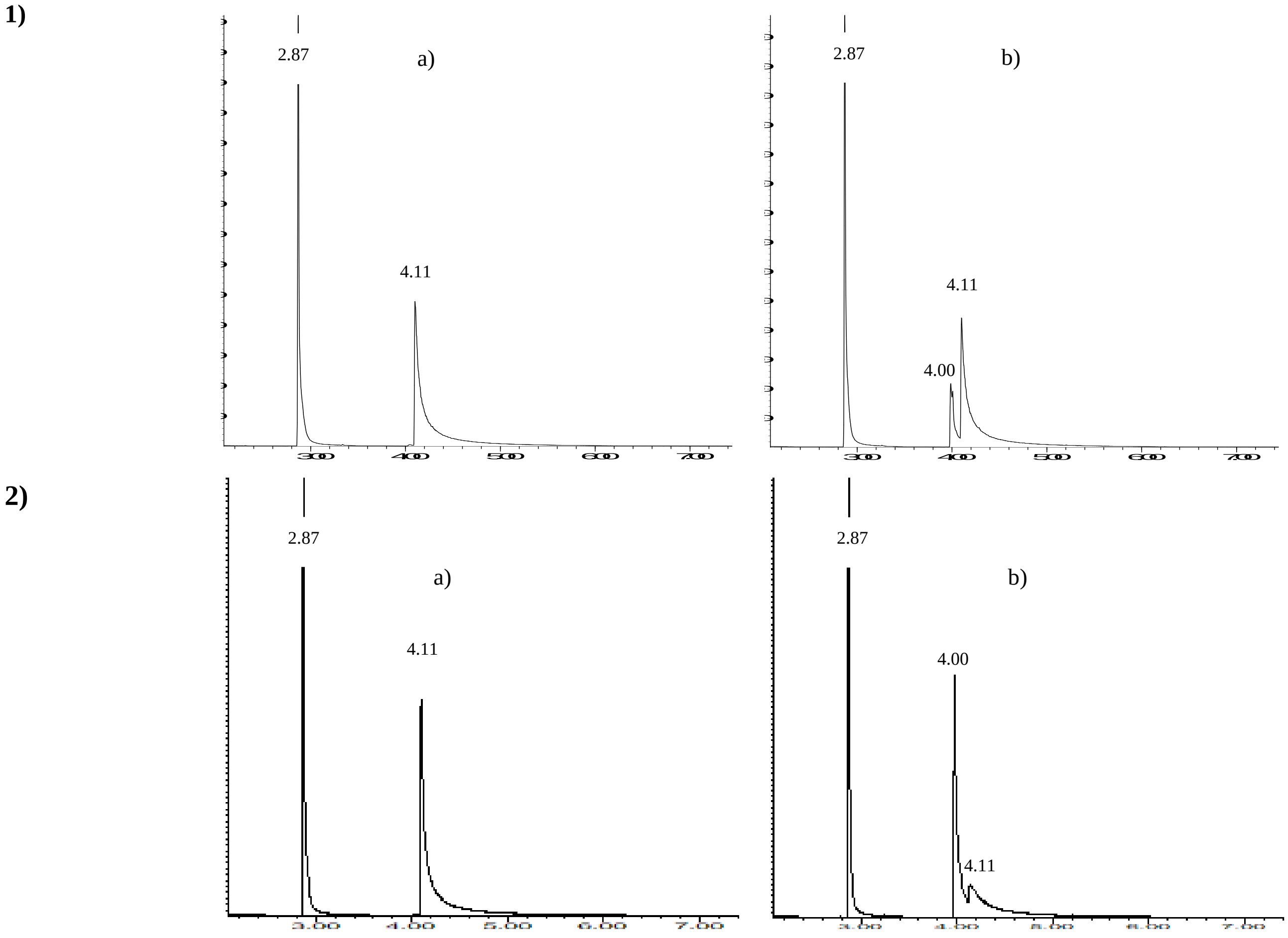

Figure 7.10. 1) GC-MS chromatograms of a mixture containing 4-methoxybenzyl alcohol (10^{-2} M), DCB ($3x10^{-3}$ M), *cis*-**1** (10^{-3} M) and CAN ($1x10^{-3}$ M) in ACN before (**a**) and after (**b**) 3 hours of reaction. **2)** GC-MS chromatograms of a mixture containing 4-methoxybenzyl alcohol (10^{-2} M), DCB ($3x10^{-3}$ M), *cis*-**1** (10^{-3} M) and CAN ($4x10^{-3}$ M) in ACN before (**a**) and after (**b**) 3 hours of reaction.

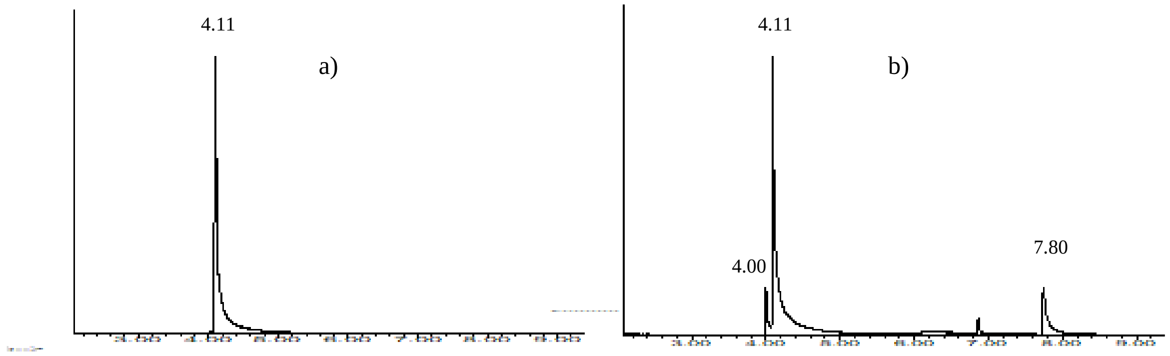

Figure 7.11. GC-MS chromatograms of a mixture containing 4-methoxybenzyl alcohol (10^{-2} M), DCB ($3x10^{-3}$ M) and CAN ($4x10^{-3}$ M) in ACN before (**a**) and after (**b**) 3 hours of reaction. Retention times: 7.87 min (4-methoxybenzoic acid).

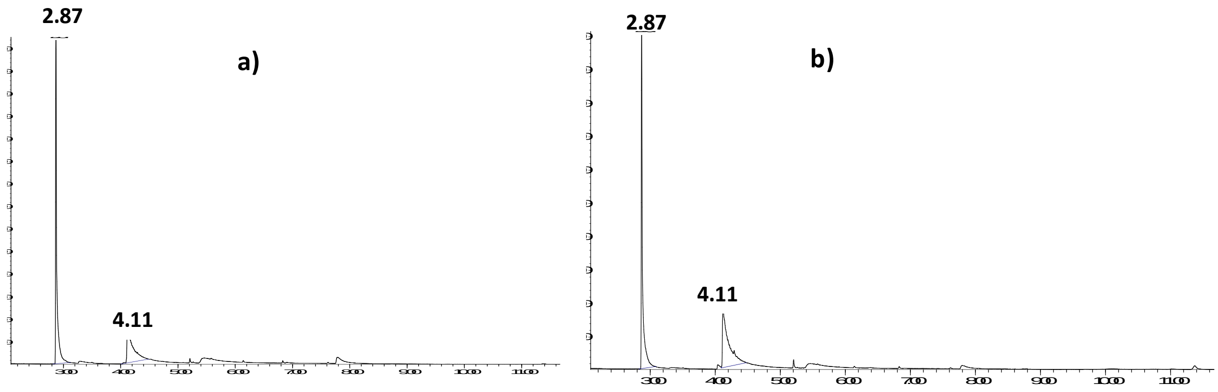

Figure 7.12. GC-MS chromatograms of a mixture containing 4-methoxybenzyl alcohol (10^{-2} M), DCB ($3x10^{-3}$ M), **R1H·(PF$_6$)$_3$** (10^{-3} M), DIPEA ($5x10^{-3}$ M) and CAN ($4x10^{-3}$ M) in ACN before (**a**) and after (**b**) 3 hours of reaction.

7.5 CHAPTER 6

7.5.1 Synthesis

The synthesis of **2”** and **3”** was performed according to the literature procedure.[5]

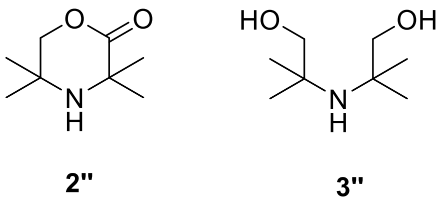

Scheme 7.3. Molecular structures of compounds **2”** and **3”.**

Synthesis of **AC7**

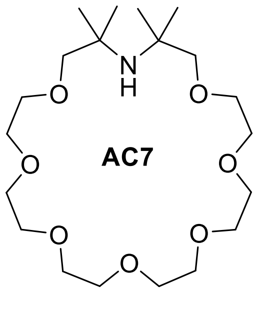

In a 250 mL three-necked round bottom flask fitted with a reflux condenser and flashed with N_2, was added *t*-BuOH (0.183 g, 2.48 mmol) and dissolved in 20 mL of THF. NaH (0.100 g, 2.48 mmol) was added portion-wise to the mixture over a period of 30 minutes. The mixture was left under stirring for 2 h at room temperature. After this period a mixture of **3”** (0.200 g, 1.24 mmol) in THF (20 mL) was added dropwise and left reacting for 20 minutes. Then, a solution of ditosylate (0.731 g, 1.24 mmol) in 40 mL of THF was added dropwise to the reaction mixture and left stirring under reflux (65 °C) for 3 days. The solvent was evaporated *in vacuo* and then water was added (100 mL), extracting the organic phases with CH_2Cl_2. The collected extracts were dried over $MgSO_4$ and evaporated *in vacuo*. The crude was purified by chromatography over a SiO_2 column (from CH_2Cl_2:MeOH 9:1 to 7:3 as eluent), obtaining **AC7** as a pale yellow oil (0.100 g, 20 % yield).

^{1}H NMR (400 MHz, $CDCl_3$) δ: 3.76 – 3.49 (m, 24H), 3.18 (s, 4H), 1.12 (s, 12H)

^{13}C NMR (100 MHz, $CDCl_3$) δ: 81.68, 71.19, 70.94, 70.80, 70.76, 70.69, 70.48, 54.10, 27.34.

ESI-MS: *m/z* 408 $(M+H)^+$, 430 $(M+Na)^+$

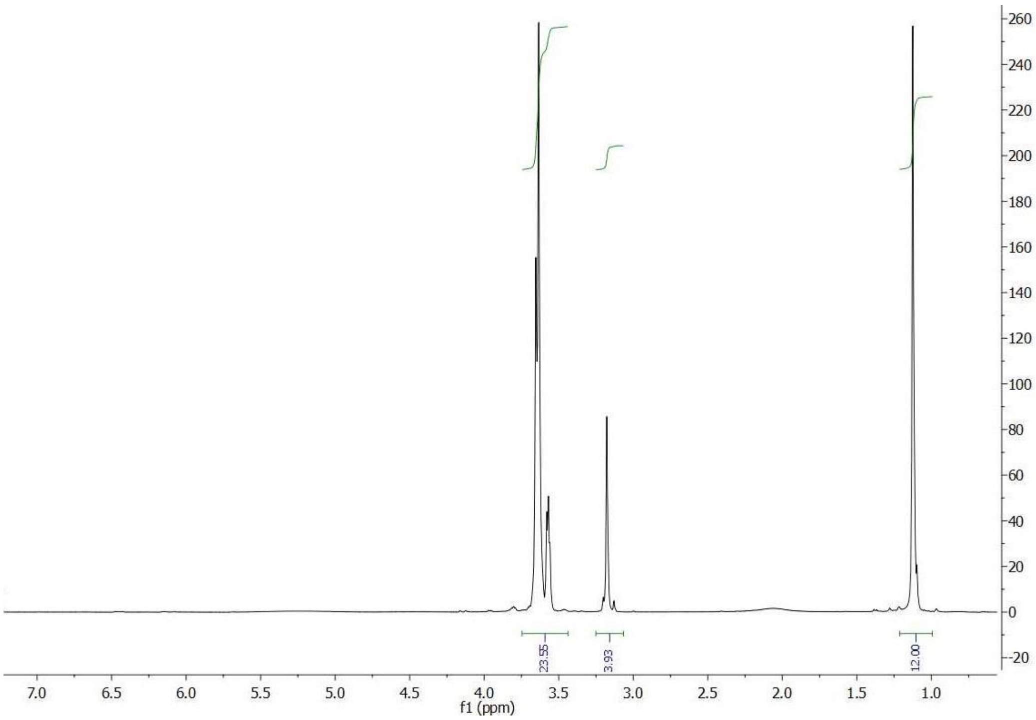

Figure 7.13. ^{1}H NMR spectrum of **AC7** in $CDCl_3$ at room temperature, 400 MHz.

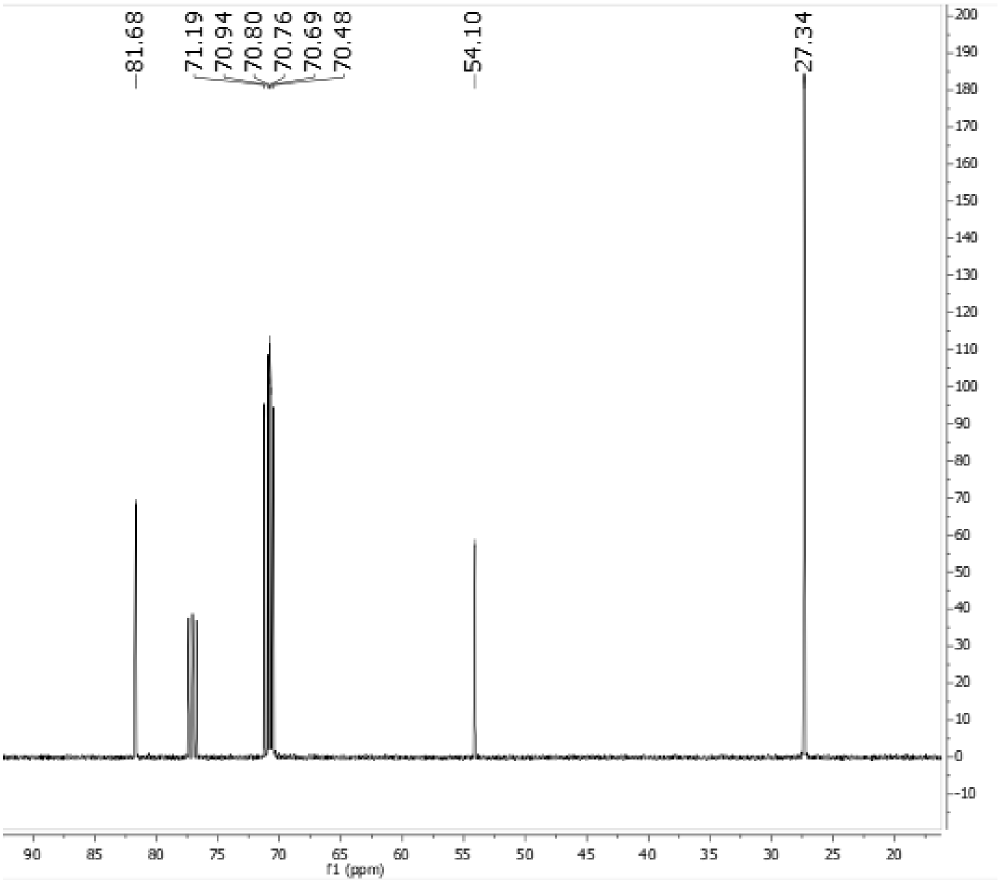

Figure 7.14. ^{13}C NMR spectrum of **AC7** in $CDCl_3$ at room temperature, 100 MHz.

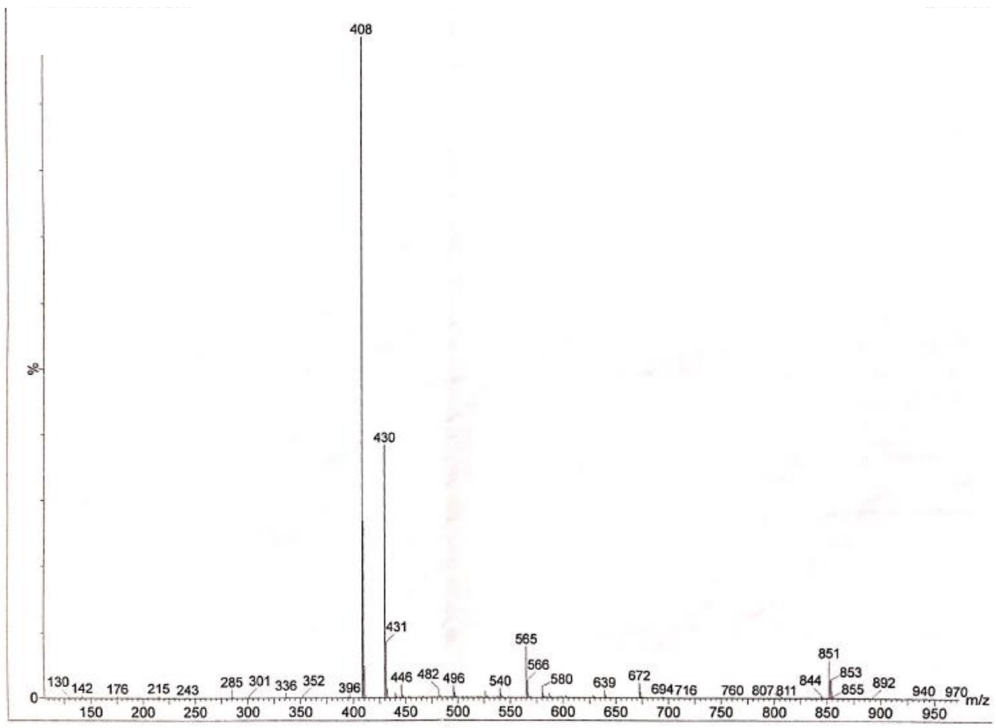

Figure 7.15. ESI-MS spectrum of **AC7** in MeOH at room temperature.

Synthesis of **AC7O·**

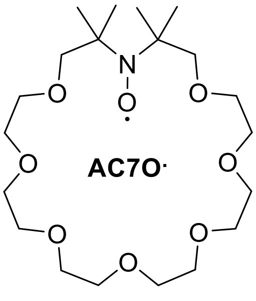

In a 50 mL three-necked round bottom flask, a solution of *m*-CPBA (0.0183 g, 0.0992 mmol) in 6 mL of anhydrous DCM was added to a mixture of **AC7** (0.100 g, 0.124 mmol) in 30 mL of DCM using a syringe pump, over a period of 1 h. The mixture was then treated with a saturated solution of $Ba(OH)_2$, extracted three times with 100 mL of DCM, dried over $MgSO_4$ and evaporated *in vacuo*. The crude was then purified by chromatography over SiO_2 (DCM:MeOH from 97:3 to 95:5), obtaining **AC7O·** as an orange oil in 30% yield.

EPR in ACN: a_N = 15.09 G, g_{factor} = 2.00584.

UV-visible: ε=760 M^{-1} cm^{-1}, λ_{max}=239 nm, ACN, rt.

HRMS: calcd. (%) for $C_{20}H_{40}NO_8$ 422.2743, obs. 422.2673.

Figure 7.16. EPR spectrum of **AC7O**$^{\cdot}$ in Acetonitrile at room temperature.

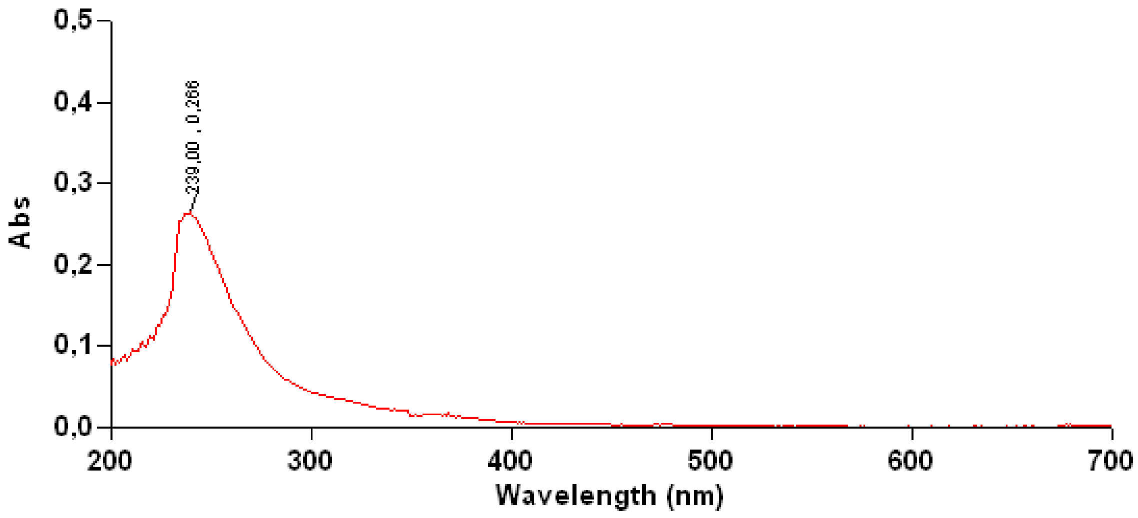

Figure 7.17. UV-visible spectrum of a solution of **AC7O**$^{\cdot}$ in Acetonitrile at room temperature.

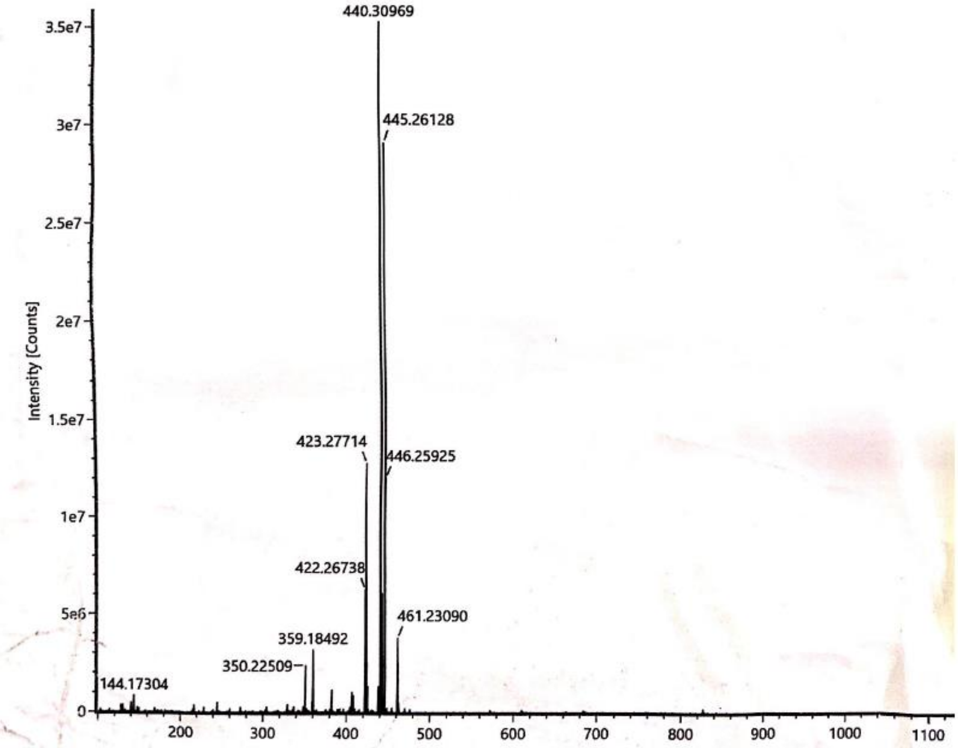

Figure 7.18. HRMS spectrum of **AC7O**$^{\cdot}$ in MeOH at room temperature.

7.5.2 EPR complexation studies

The exact concentration of **AC7O**$^{\cdot}$ was accurately determined by comparing the integral of the experimental EPR spectrum of **AC7O**$^{\cdot}$ and the integral of the spectrum originating from a standard solution of **TEMPO**. The K_a were calculated employing the mathematical equations described in **Paragraph 6.2**. The EPR simulated spectra were obtained using well-established procedures based on the density matrix theory[1] and assuming a two-jump model.

Acetonitrile

Salt	Cation	K_a/M^{-1}	a_N/G	[Host](10^{-5} M)	[Guest](10^{-3} M)	Method
$LiClO_4$	Li^+	536	16.05	4.9	0.4 - 9.0	Linear
$NaClO_4$	Na^+	3200	15.45	10.0	0.04 – 8.19	Non linear
Na(Picr)	Na^+	3200	15.46	5.9	0.036 – 6.4	Non linear
K(Picr)	K^+	30050	15.52	3.7	0.036 – 6.4	Linear
$RbClO_4$	Rb^+	Non determ.	15.65 15.59	5.0	//	Qualitative
Cs(Picr)	Cs^+	5042	15.75	4.9	0.144 – 1.296	Linear
$Ca(Picr)_2$	Ca^{2+}	59600	16.75	//	//	Non linear
$Sr(Picr)_2$	Sr^{2+}	100000	16.50	5.2	0.005 – 0-125	Non linear
NH_4PF_6	NH_4^+	12334	15.88	//	//	Non linear
$(PhCH_2)_2NH_2PF_6$	$(PhCH_2)_2NH_2^+$	117	16.01	//	//	Linear

1) $LiClO_4$

Figure 7.19a. AC7O· in the presence of $LiClO_4$ 2 mM in ACN.

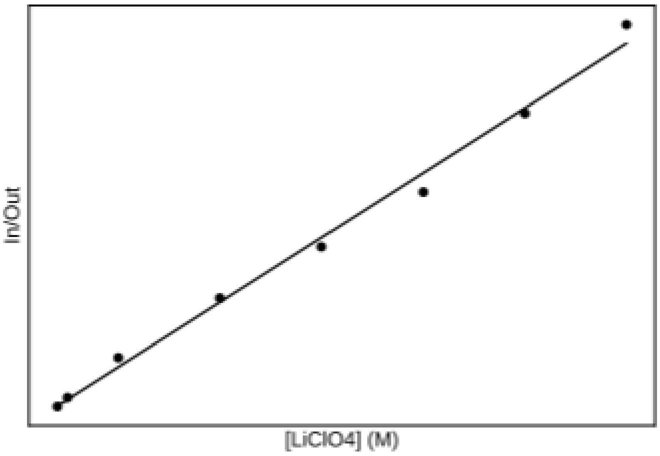

Figure 7.19b. Regression plot reporting the in/out ratio ([**AC7O·@Li⁺**]/[**AC7O·**]) as function of guest concentration.

2) $NaClO_4$

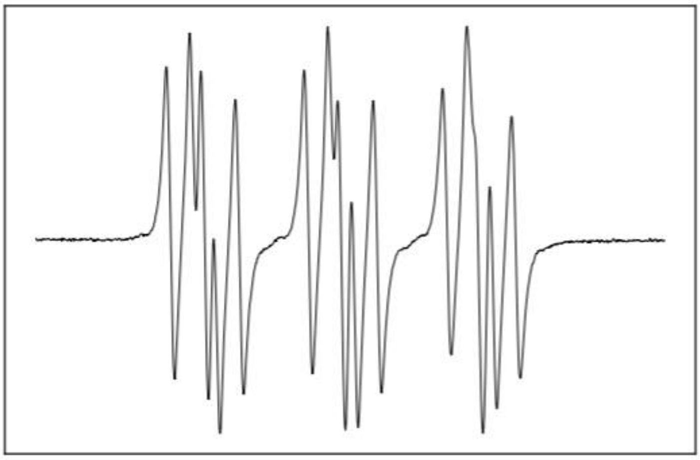

Figure 7.20. AC7O· in the presence of $NaClO_4$ 0.33 mM in ACN. Non-linear regression plot.

3) Na(Picr)

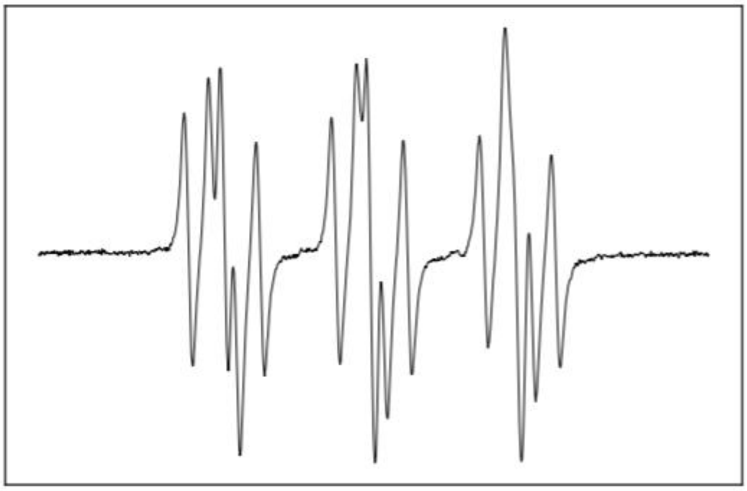

Figure 7.21. AC7O· in the presence of Na(Picr) 0.36 mM in ACN. Non linear regression.

4) Cs(Picr)

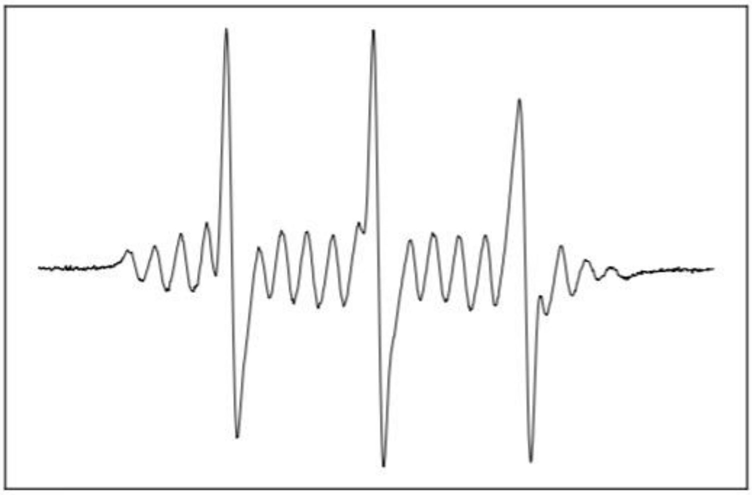

Figure 7.22a. AC7O$^{\cdot}$ in the presence of Cs(Picr) 0.288 mM in ACN.

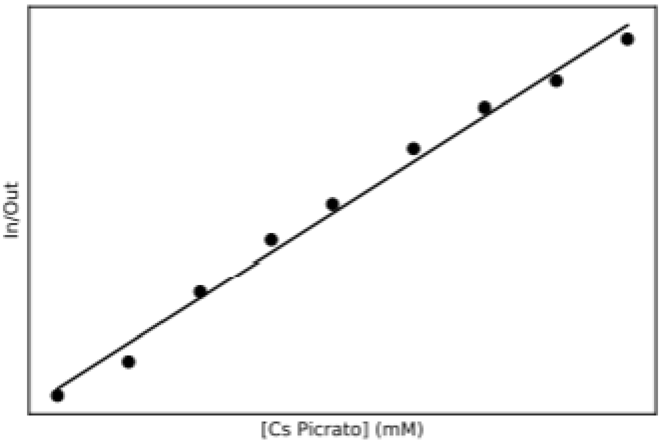

Figure 7.22b. Regression plot reporting the in/out ratio ([**AC7O$^{\cdot}$@Cs^{2+}**]/[**AC7O$^{\cdot}$**]) as function of guest concentration.

5) $Ca(Picr)_2$

Figure 7.23. AC7O$^{\cdot}$ in the presence of $Ca(Picr)_2$ 0.058 mM in ACN. Non linear regression.

6) $Sr(Picr)_2$

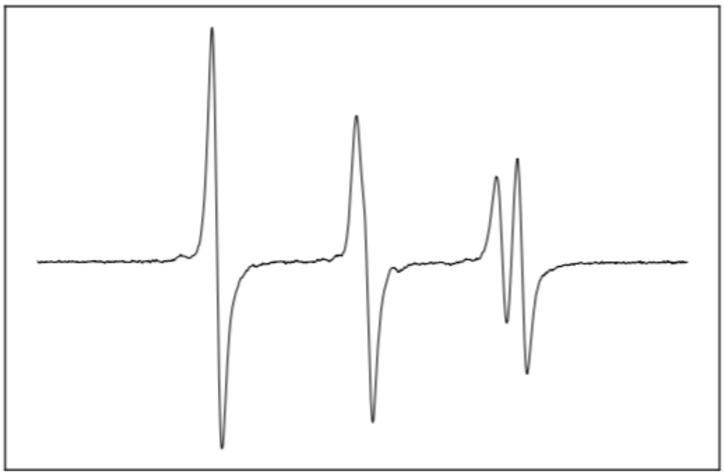

Figure 7.24. AC7O$^{\cdot}$ in the presence of $Sr(Picr)_2$ 0.0625 mM in ACN. Non linear regression plot.

7) NH_4PF_6

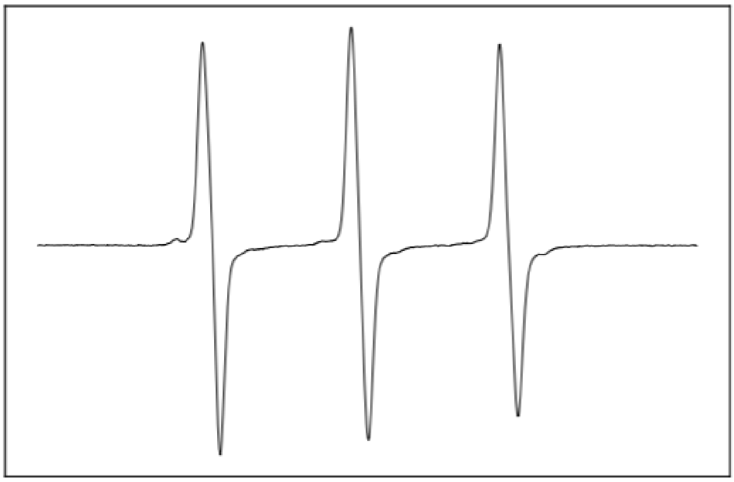

Figure 7.25. AC7O· in the presence of NH_4PF_6 0.0625 mM in ACN. Non linear regression plot.

8) $(PhCH_2)_2NH_2PF_6$

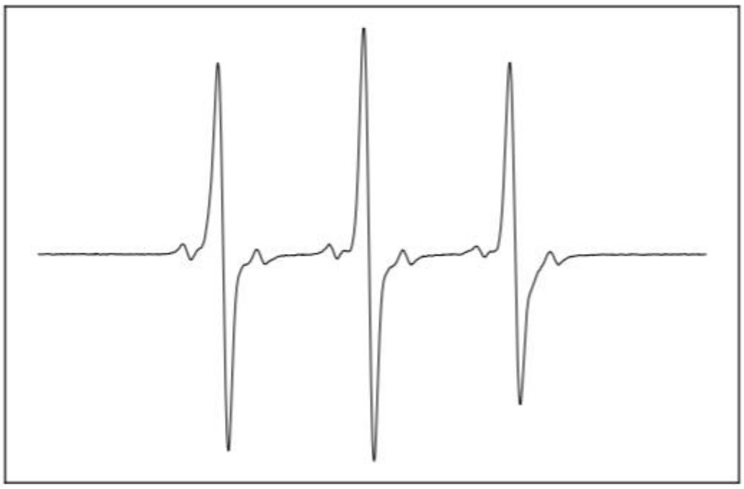

Figure 7.26a. AC7O· in the presence of DBA 1.2 mM in ACN.

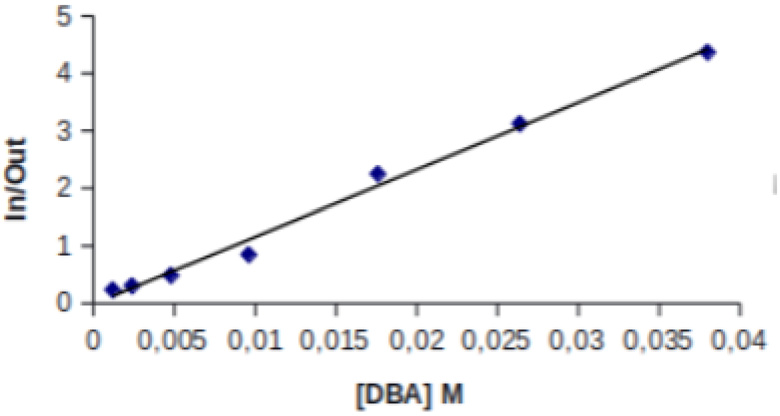

Figure 7.26b. Regression plot reporting the in/out ratio ([**AC7O$^{\cdot}$@DBA**]/[**AC7O$^{\cdot}$**]) as function of guest concentration.

Acetone

Salt	Cation	K_a/M^{-1}	a_N/G	[Host](10^{-5} M)	[Guest](10^{-3} M)	Method
Na(Picr)	Na^+	612.45	15.27	10.7	0.75 - 16	Linear
Cs(Picr)	Cs^+	1569.8	15.75	//	0.25 - 3.66	Linear
$Ca(Picr)_2$	Ca^{2+}	61.0	16.53	//	0.66 – 29.70	Linear
$(PhCH_2)_2NH_2PF_6$	$(PhCH_2)_2NH_2^+$	20.6	16.04	//	1.0 – 250.0	Linear

1) Na(Picr)

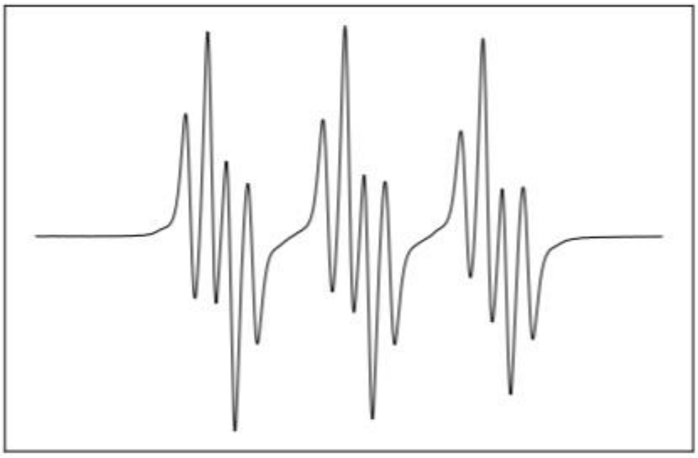

Figure 7.27a. AC7O$^{\cdot}$ in the presence of Na(Picr) 14 mM in Acetone.

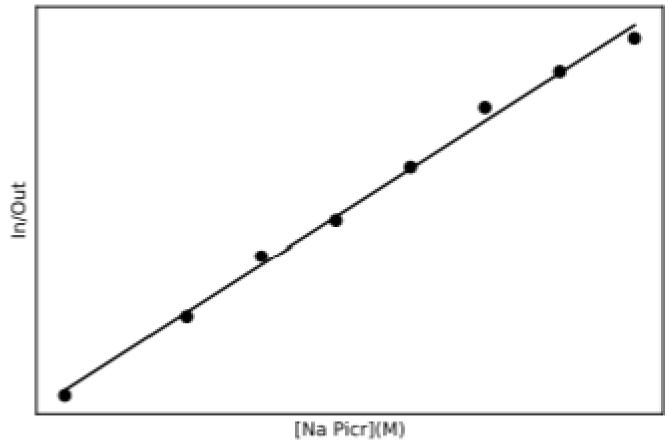

Figure 7.27b. Regression plot reporting the in/out ratio ([**AC7O**·@**Na**$^+$]/[**AC7O**·]) as function of guest concentration.

2) Ca(Picr)$_2$

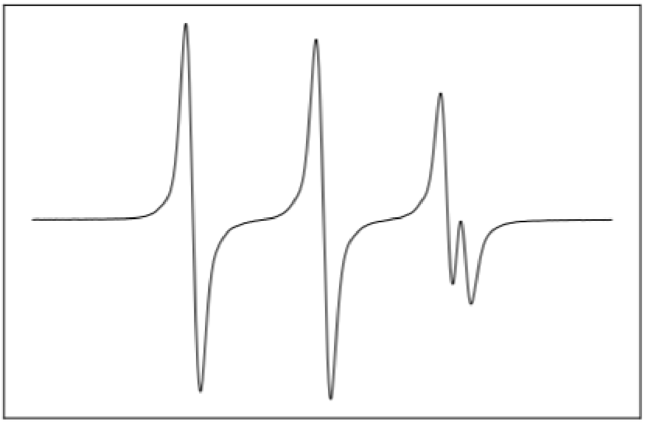

Figure 7.28a. AC7O· in the presence of Ca(Picr)$_2$ 0.058 mM in Acetone.

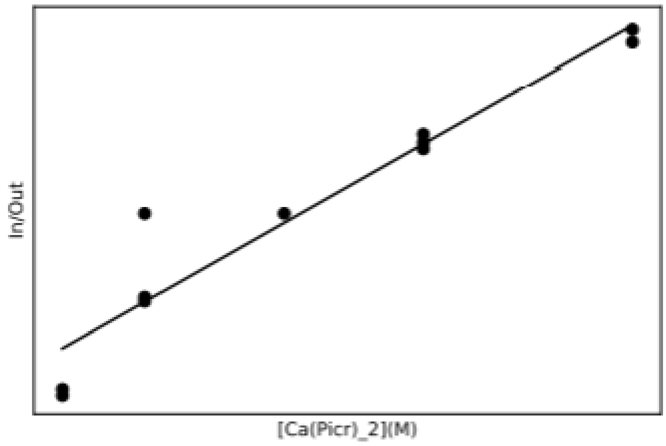

Figure 7.28b. Regression plot reporting the in/out ratio ([**AC7O**·@**Ca**$^{2+}$]/[**AC7O**·]) as function of guest concentration.

3) Cs(Picr)

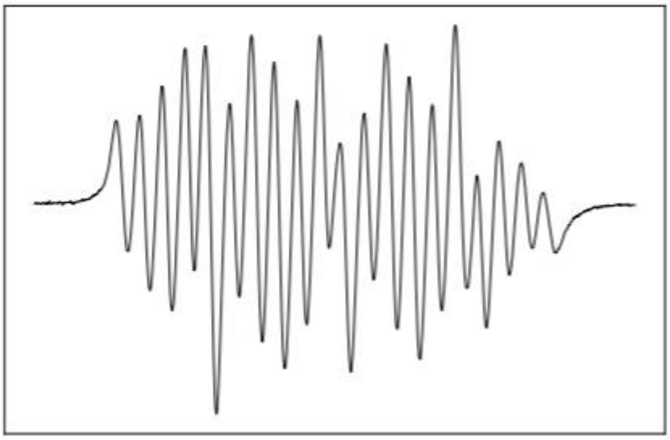

Figure 7.29a. AC7O$^{\cdot}$ in the presence of Cs(Picr) 3.66 mM in Acetone.

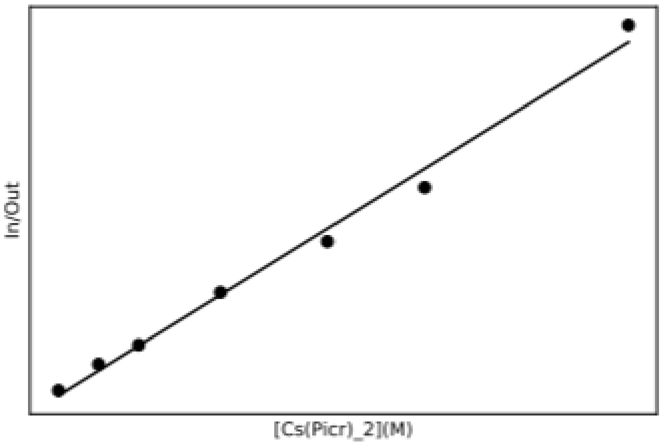

Figure 7.29b. Regression plot reporting the in/out ratio ([**AC7O**$^{\cdot}$@**Cs**$^{+}$]/[**AC7O**$^{\cdot}$]) as function of guest concentration.

REFERENCES

[1] M. Lucarini, B. Luppi, G. F. Pedulli and B. P. Roberts, *Chem.Eur. J.,* vol. 5, pp. 2048-2055, 1999.

[2] V. Bleve, P. Franchi, E. Konstanteli, G. L., S. M. Goldup, E. Mezzina and M. Lucarini, *Chem. Eur. J.,* vol. 24, pp. 1198-1201, 2018.

[3] S. A. Dobrynin, Y. I. Glazachev, Y. V. Gatilov, E. I. Chernyak and G. E. Salnikov, *J. Org. Chem.*, vol. 83, p. 5392−5397, 2018.

[4] C. Biagini, S. Albano, R. Caruso, L. Mandolini, J. A. Berrocal and S. Di Stefano, *Chem. Sci.,* vol. 9, pp. 181-188, 2018.

[5] C. He and M. J. Gaunt, *Angew. Chem. Int. Ed.,* vol. 54, p. 15840, 2015.

ACKNOWLEDGMENTS

My deepest acknowledgments are addressed to Prof. Marco Lucarini, supervisor of this thesis, Prof. Elisabetta Mezzina, co-supervisor, and Prof. Paola Franchi, for the support and the indispensable help provided for the realization of these projects and for the availability always demonstrated during the three years of doctorate. The supervision and the responsibilities I was given, have been chosen in perfect combination for encouraging my personal and professional growth at the best. I would also like to thank Dr. Lorenzo Gualandi for the immense support and for transmitting to me his enthusiasm for chemistry and research. A part of my award are then reserved to the researchers I had the pleasure to work with: in particular Fabio Mollica, who was my research partner at the beginning of my PhD and whose support was fundamental also in the next years, Dr. Olivier Ouari and all his research group, who gave me the opportunity not only to perform part of my research abroad, but also provided me the best personal and professional environment to work in. Lastly, I would like to give special thanks to the University of Bologna for giving me the opportunity and the indispensable materials to accomplish this path.